

# **Molecular Tools for Probing Signaling Networks of the EGFR Protein Kinase**

A thesis submitted in partial fulfilment of the requirements for the degree of

**Master of Research**

by

**Ivan de Jesus Salazar Estrada**

**BSc (Chemistry)**

Department of Chemistry and Biomolecular Sciences  
Macquarie University  
Sydney, Australia

October 2015



## Table of contents

Abstract	iii
Declaration	v
Acknowledgements	vii
Abbreviations	ix
List of Figures	xiii
List of Schemes	xv
List of Tables	xv
1. INTRODUCTION	1
1.1 Protein kinases	1
1.1.1 Small-molecule protein kinase inhibitors	2
1.2 Epidermal growth factor receptor (EGFR)	6
1.2.1 EGFR inhibitors	12
1.3 Chemical probes	15
1.3.1 Chemical probes for PKs	16
1.3.2 Chemical probes for EGFR	17
1.4 Objectives	18
2. EXPERIMENTAL SECTION	20
2.1 General information	20
2.2 Synthesis and characterization	21
2.2.1 Synthesis of compounds <b>4a–4c</b>	21
2.2.2 Synthesis of compounds <b>5a–5c</b>	22
2.2.3 Synthesis of compounds <b>6a–6c</b>	23
2.2.4 Synthesis of compounds <b>7a–7c</b>	25
2.2.5 Synthesis of probes <b>1a–1c</b>	26
2.3 Purification of chemical probes	28
2.4 KINOMEscan <sup>TM</sup> binding assay	28
3. RESULTS AND DISCUSSION	30
3.1 EGFR Probes design	30
3.2 Probes synthesis	33
3.2.1 Synthesis of 4-anilinoquinazoline binding groups	33

3.2.2 Linker attachment at the C6 position	36
3.2.3 Attachment of the biotin affinity tag	36
3.3 Probes purification and characterization	37
3.4 Binding assays	38
 4. CONCLUSIONS AND FUTURE DIRECTIONS	 42
 REFERENCES	 44
APPENDICES	A1

## Abstract

The epidermal growth factor receptor (EGFR) is one of the first and most extensively studied receptor tyrosine protein kinases and a validated drug target. Through protein phosphorylation, EGFR orchestrates several signaling pathways that regulate cell growth and proliferation, and aberrant EGFR signaling has been reported in numerous cancer types. Several FDA-approved drugs target the ATP site of EGFR, and new therapeutics are in development that target the signaling partners of oncogenic EGFR. However, resistance is a challenge to overcome, and other EGFR-associated signaling proteins have been shown to confer resistance. Chemical probes may aid the elucidation of EGFR signaling networks for finding improved combination therapies. Here we report the synthesis of first-generation biotinylated chemical probes **1a–1c** targeting EGFR. These probes are based on the 4-anilinoquinazoline core structure of gefitinib and erlotinib, two FDA-approved EGFR-targeting drugs. The probes **1a–1c** exhibit excellent binding affinities for EGFR ( $K_d = 23 - 41$  nM). These probes are expected to serve as the basis for future development of next-generation multifunctional probes for understand endogenous EGFR signaling networks.



### **Declaration**

I certify that the work in this title entitled “Molecular Tools for Probing Signaling Networks of the EGFR Protein Kinase” has not been previously submitted as part of requirements for a degree to any other university or institution other than Macquarie University. I also certify that the thesis is an original piece of research and it has been written by me. Any help and assistance that I have received in my research work and the preparation of the thesis itself have been appropriately acknowledged. Finally, I certify that all information sources and literature used are indicated in the thesis.





## **Acknowledgments**

I would like to acknowledge the following people, without whom this thesis would have not been possible:

My supervisor, Dr. Fei Liu, for entrusting me this fascinating project and guiding me in my first steps as a graduate student. Thanks for your professional and personal encouragement.

My fellow lab mates: Damian, Harry, Ryan, Sviatoslav and Umesh, for their help in setting up my work place, advice in experimental techniques, and encouragement.

CBMS staff and fellow students involved in my methods training: Ryan Kenny (NMR), Tony Wang (HPLC), Jason Smith and Kavita Ragini (LC-MS), Mark Tran (FT-IR) and Bhumika Shah (PyMOL).

The Jamie, Karuso, Try and Piggot research groups in CBMS department, for assistance in materials supply and instrumental operations.

Macquarie University for a research scholarship.

My lovely family: Jose, Charis and Iris. For your unconditional love and support. Thanks for allowing me to fulfil my dreams. Gracias, los amo.

Finally, thanks God for all your blessings. Thanks for writing life with Chemistry.



## Abbreviations

°C	degrees celsius
4Å-MS	4 angstrom molecular sieves
ABL	abelson tyrosine kinase
ABP	activity based probe
Ac	acetyl
AcO	acetate
AfBP	affinity based probe
AKT	protein kinase B
ALK	anaplastic lymphoma kinase
Aq.	aqueous
ATP	adenosine 5'-triphosphate
AXL	receptor tyrosine protein kinase UFO
BC	breast cancer
BODIPY	boron-dypyrromethane
br	broad
BTC	betacellulin
BTK	brutons's tyrosine kinase
Cbl	casita B-lineage lymphoma ubiquitin protein ligase
CDK	cyclin-dependant kinase
CLL	chronic lymphocytic leukaemia
cm <sup>-1</sup>	wavenumber
CML	chronic myelogenous leukaemia
CNS	central nervous system
CRC	colorectal cancer
δ	NMR chemical shift in parts per million
d	doublet
<i>d</i> <sub>6</sub>	hexadeuterated
dd	doublet of doublets
DFG	Asp-Phe-Gly motif
DMF	<i>N,N</i> -dimethylformamide
DMSO	DMSO
EDC	1-ethyl-3-(3-dimethylaminopropyl)carbodiimide

EGF	epidermal growth factor
EGFR	epidermal growth factor receptor
EGN	epigen
EPR	epiregulin
ErbB	epidermal growth factor receptor family of proteins
ErbB2/3/4	human epidermal growth factor receptor 2/3/4
ERK	extracellular-signal regulated kinase
ESI	electrospray ionisation
Et	ethyl
FDA	United States Food and Drug Administration
g	gram
GIST	gastrointestinal stromal tumor
Grb2	growth factor receptor-bound protein 2
h	hour
HB-EGF	heparin-binding EGF-like receptor
HGF	hepatocyte growth factor
HPLC	high-performance liquid chromatography
HSQC	heteronuclear single bond correlation spectroscopy
Hz	hertz
IGF-1	insulin-like growth factor 1
IMF	idiopathic myelofibrosis
IPF	idiopathic pulmonary fibrosis
<i>i</i> -Pr	isopropyl
IR	infrared spectroscopy
<i>J</i>	coupling constant
JAK1/2/3	janus kinase 1/2/3
$K_d$	dissociation constant
KIT	stem cell factor receptor
LC-MS	liquid chromatography-mass spectrometry
LRIG1	leucine-rich repeats and immunoglobulin-like domains-1
$\mu$	micro
m	multiplet (NMR), medium (IR)
$\mu$ M	micromolar
<i>m/z</i>	mass to charge ratio
MAPK	mitogen-activated protein kinase

MCL	mantle cell lymphoma
Me	methyl
MEK	mitogen activated protein kinase
MET	hepatocyte growth factor receptor
mg	milligram
MHz	megahertz
MIG-6	mitogen-inducible gene-6
min	minute
mmol	milimole
MTC	medullary thyroid cancer
NBD	nitrobensoxadiazole
NGF	nerve growth factor
NHS	<i>N</i> -hydroxysuccinimide
nM	nanomolar
NMR	Nuclear magnetic resonance spectroscopy
NRG	neuregulin
NRTK	non-receptor tyrosine kinase
NSCLC	non-small-cell lung cancer
PC	pancreatic cancer
PDK1	phosphoinositide-dependent protein kinase 1
PEG	polyethylene glycol
PI3K	phosphoinositide 3-kinase
PIP3	Phosphatidylinositol-3,4,5-triphosphate
PKC	protein kinase C
PKs	protein kinases
PLC	phospholipase C
ppm	parts per million
PTB	phosphotyrosine binding domain
PTEN	phosphatase and tensin homolog protein
PTM	post-translational modification
r.t.	room temperature
RA	rheumatoid arthritis
RAF	RAF serine/threonine protein kinase family
RALT	receptor-associated late transducer

RAS	rat sarcoma GTPase family
RCC	renal cell cancer
RNA	ribonucleic acid
RNAi's	small interfering RNAs
RTPK	receptor tyrosine protein kinase
s	singlet (NMR), strong (IR)
SAR	structure activity relationship
SH2	Src homology 2 domain
Shc	SH2-containing transforming protein 1
SHP	SH2-containing phosphatase
S <sub>N</sub> 2	bimolecular nucleophilic substitution
S <sub>N</sub> Ar	nucleophilic aromatic substitution
SOS	son of sevenless protein
SPRY	sprouty adaptor protein
Src	sarcoma family kinases
STAT	signal transducer and activator of transcription protein
STPKs	serine/threonine protein kinases
t	triplet
TAMRA	5-(6-)carboxytetramethyl rhodamine
TC	thyroid cancer
TGA- $\alpha$	transforming growth factor alpha
TKI	tyrosine kinase inhibitor
TLC	thin layer chromatography
TPKs	tyrosine protein kinases
UV	ultraviolet
VEGFR	vascular endothelial growth factor receptor
w	weak
WT	wild type

## List of Figures

Fig. 1.1	Schematic representation of PK in the active and some inactive conformation.	2
Fig. 1.2	Types of small-molecule kinase inhibitors according to their binding mode.	3
Fig. 1.3	FDA-approved small-molecule kinase inhibitors (up to April 2015).	4
Fig. 1.4	Schematic representation of the domain structure of the ErbB family proteins.	6
Fig. 1.5	Schematic model of ligand-induced activation of ErbB proteins.	8
Fig. 1.6	Major signaling proteins recruited and signaling pathways activated by ErbBs.	9
Fig. 1.7	Schematic representation of the ErbB signaling network.	10
Fig. 1.8	EGFR inhibitors based on the 4-anilinoquinazoline core.	13
Fig. 1.9	General structure of a chemical probe and some typical components.	15
Fig. 1.10	Structure of selected chemical probes for protein kinases.	17
Fig. 1.11	Structures of representative EGFR chemical probes.	18
Fig. 3.1	Crystal structures of gefitinib and erlotinib bound to the EGFR ATP site.	30
Fig. 3.2	<sup>1</sup> H NMR spectrum of compound <b>5a</b> and its corresponding quinazolonium salt.	34
Fig. 3.3	<sup>1</sup> H, <sup>13</sup> C and HSQC NMR spectra of compound <b>5c</b> .	35
Fig. 3.4	Selected regions of <sup>1</sup> H and <sup>13</sup> C NMR spectra of probe <b>1c</b> showing characteristic signals of the biotin tag.	38
Fig. 3.5	A representative chromatogram from compound <b>1b</b> purification.	38
Fig. 3.6	Schematic representation of the KINOMEscan <sup>TM</sup> binding assays.	39
Fig. 3.7	Structure of some recently reported dual EGFR inhibitors.	41
Fig. 4.1	Schematic representation of potential second-generation EGFR chemical probes.	43





### List of Schemes

Scheme 3.1	Design and retrosynthetic analysis of first-generation EGFR probes <b>1a–1c</b> .	32
Scheme 3.2	Synthesis of 4-anilinoquinazoline binding groups.	33
Scheme 3.3	Attachment of the heptanoate linker to the C6 position of the 4-anilinoquinazoline core.	36
Scheme 3.4	Attachment of biotin tag to carboxylate salts <b>7a–7c</b> .	37

### List of Tables

Table 3.1	SAR studies of previously reported EGFR probes.	31
Table 3.2	Binding affinity of chemical probes <b>1a–1c</b> and selected reference compounds against EGFR.	40



# 1. INTRODUCTION

## 1.1 Protein kinases

Protein kinases (PKs) are one of the largest protein families and in the human genome constitute about 2% of coded proteins.<sup>1</sup> PKs catalyse the transfer of the  $\gamma$ -phosphate group of ATP to the hydroxyl group of a serine, threonine or tyrosine residue of the substrate protein. According to their specificity for the phosphorylation residue, PKs are classified into two main classes: serine/threonine protein kinases (STPKs) or tyrosine protein kinases (TPKs). The STPK family comprises 388 proteins, while the TPK family includes 90 proteins.<sup>2</sup> The addition of the highly charged phosphate group profoundly changes conformation, activity, protein-protein interactions, or the order/disorder state of the substrate protein.<sup>3,4</sup> Phosphorylation is acknowledged as the most abundant type of cellular post-translational modification (PTM), lying at the heart of signal transduction and regulating virtually every cellular process, such as growth, differentiation, survival, metabolism, membrane transport, motility, gene transcription and cell cycle progression among others.<sup>4,5</sup> Due to their critical role in cell signaling, the activity of PKs is tightly regulated through several mechanisms including gene transcription, PTMs, interaction with regulatory partners, cellular localization and protein degradation.<sup>6,7</sup>

The dynamic nature of PKs is a key factor behind their regulation. PKs adopt many different conformations between the active and inactive state, a term known as conformational plasticity.<sup>8-10</sup> This dynamism is partly embedded in the structure of the kinase domain,<sup>11-13</sup> which consists of a small, mostly  $\beta$ -stranded N-terminal lobe and a large,  $\alpha$ -helical C-terminal lobe. These two lobes are connected by a hinge region that facilitates movement of the lobes relative to each other. The active conformation of the kinase may require PTM, such as phosphorylation, for accessibility.<sup>14</sup>

The small molecule substrate, ATP, binds in a deep cleft between the two lobes making hydrogen bonds to the hinge region as well as hydrophobic and electrostatic interactions. Regulatory elements that define the active/inactive state of the kinase include a conserved catalytic lysine, the  $\alpha$ C-helix, and a conserved glutamate contained in the  $\alpha$ C-helix from the N-lobe, as well as the activation loop and the conserved Asp-Phe-Gly (DFG) motif at the N-terminus of the activation loop from the C-lobe (Fig. 1.1).<sup>3</sup> In the active conformation, which is similar in most kinases, the aspartate from the DFG motif and the  $\alpha$ C-helix are oriented into the catalytic site. This orientation allows the coordination of a  $Mg^{2+}$  ion and the

formation of a salt bridge between the catalytic lysine and the conserved glutamate from the  $\alpha$ C-helix. These electrostatic interactions are required for the correct alignment of ATP and the protein substrate for phosphoryl transfer. Inactive conformations, with less chemical constraints required for catalysis, is more diverse among different PKs.<sup>8, 10</sup> However, inactive conformations fall into two clusters, arising from the rotation of the  $\alpha$ C-helix (Src/CDK-like inactive) or the DFG motif (DFG-out inactive) away from the active site.<sup>10</sup> The relative stability of the different conformational states of a PK changes in response to PTMs and binding of regulatory proteins, substrates and ligands. Thus, PKs are considered molecular switches in response to specific biological cues, which in turn are often initiated in response to an extracellular event.<sup>11</sup>

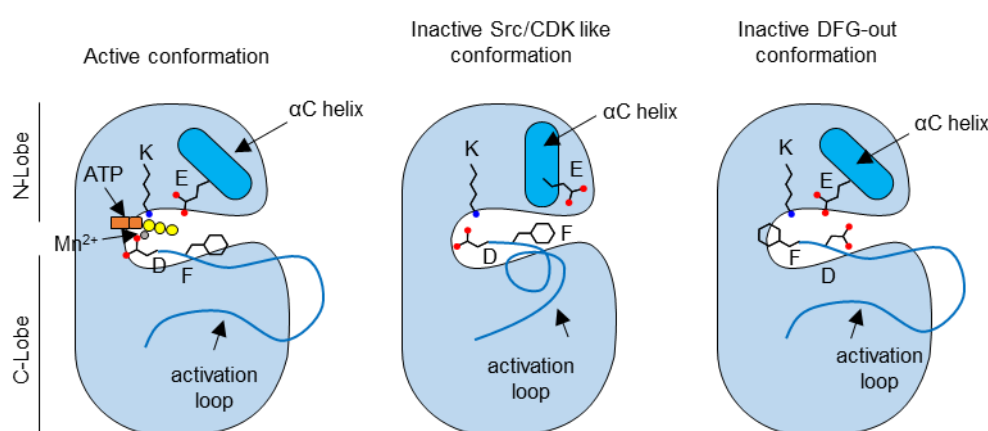


**Fig. 1.1** Schematic representation of PK in the active and some inactive conformation.

### 1.1.1 Small-molecule protein kinase inhibitors

Deregulation of PK activity is known to play a crucial role in the development of a number of diseases including cancer,<sup>15, 16</sup> inflammatory diseases,<sup>17</sup> CNS disorders<sup>18, 19</sup> and cardiovascular disorders.<sup>20</sup> For this reason, PKs are considered an important class of validated drug targets and subject of intense research.<sup>21-23</sup> Although strategies such as monoclonal antibodies, protein products, vaccines and small interfering RNAs (RNAi's) have been developed, most of the kinase inhibitors discovered to date are based on small molecules.<sup>24-27</sup>

According to their binding mode, these small molecules inhibitors are grouped into two categories: irreversible and reversible.<sup>24, 28</sup> Irreversible or covalent inhibitors possess a “warhead” that typically reacts with a nucleophilic cysteine residue proximal to the ATP site and thus impedes ATP binding.<sup>28</sup> Reversible inhibitors are further classified into five categories: type I–V (Fig. 1.2).<sup>24, 29</sup> Type I inhibitors are ATP-competitive and typically bind

to the active form of kinases with the DFG-in conformation. They frequently occupy the adenine pocket of the ATP site making one to three hydrogen bonds to residues in the hinge region. For these inhibitors, target selectivity is achieved by making use of a hydrophobic pocket adjacent to the ATP site that often shows structural variability among different PKs.<sup>29-31</sup> The size and ease of access to this pocket is controlled by the so called “gatekeeper” residue near the hinge region.<sup>32</sup> Type II inhibitors are also ATP-competitive, but bind to the kinase in the inactive DFG-out conformation. The outward displacement of the DFG motif allows for inhibitor access to extra hydrophobic (allosteric) pockets for binding.<sup>33, 34</sup> Type III and IV inhibitors bind to an allosteric pocket either adjacent to (Type III) or remote from (Type IV) the ATP site.<sup>24, 35, 36</sup> Some inhibitors, such as bisubstrate and bivalent inhibitors (Type V), exhibit more than one of these aforementioned binding modes.<sup>37</sup>

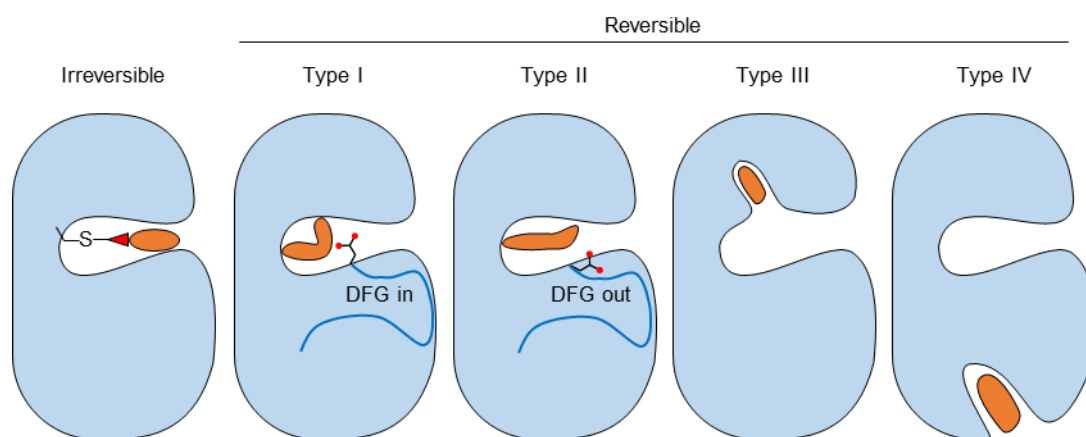
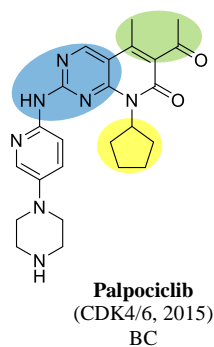
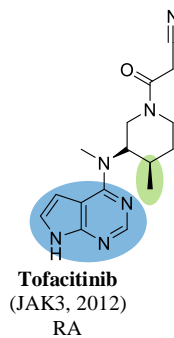
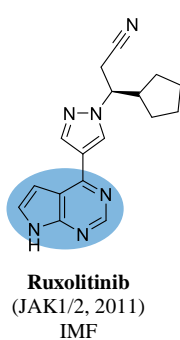
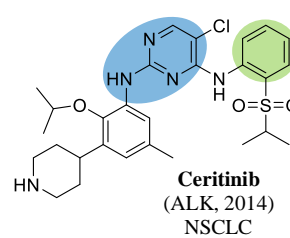
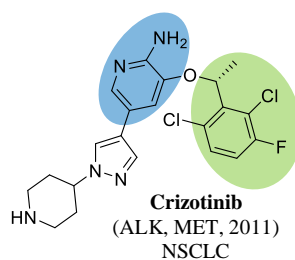
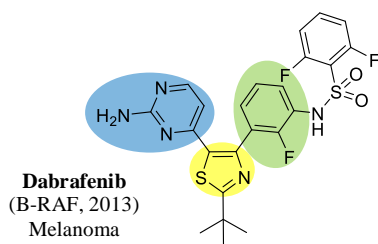
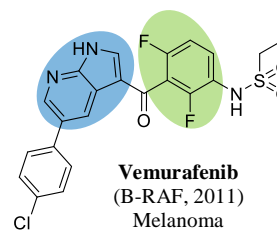
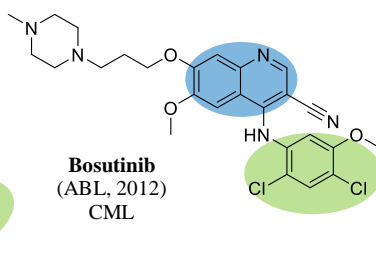
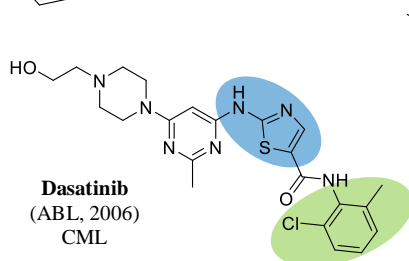
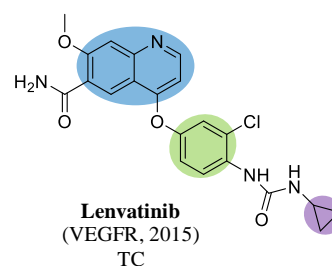
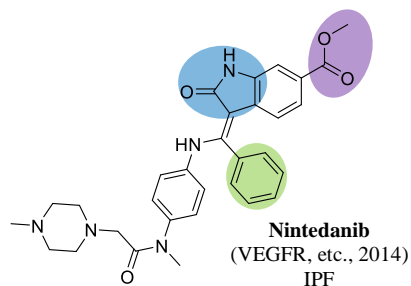
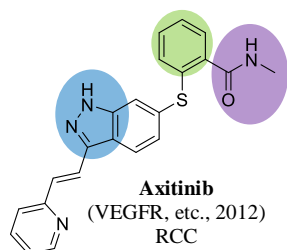
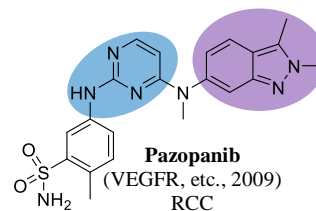
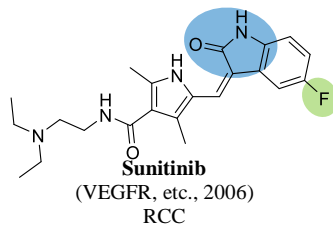
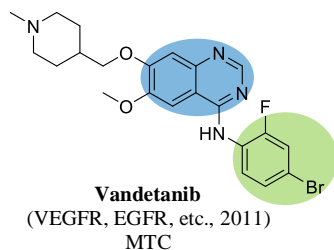
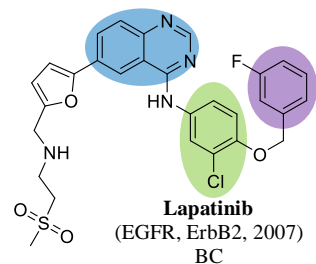
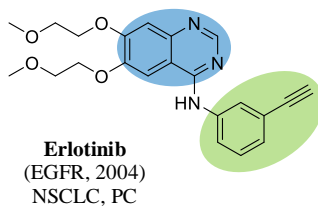
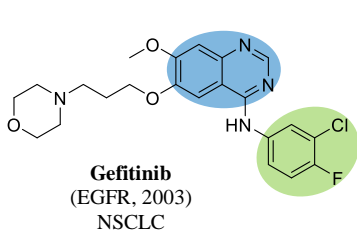


**Fig. 1.2** Types of small-molecule kinase inhibitors according to their binding mode.

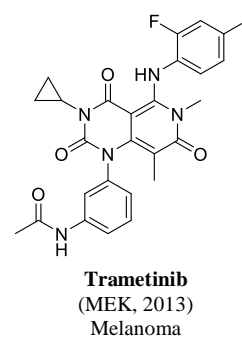
The approval of the first rationally developed small-molecule PK inhibitor, imatinib (Glivec®), by the FDA in 2001 marked a breakthrough in drug development and targeted therapy for PKs.<sup>38</sup> Since this milestone event, the interest and progress in the development of PK inhibitors has increased considerably, making PK one of the most pursued family of drug targets, especially for cancer treatment.<sup>23, 25, 39</sup> This tendency is reflected in the number small-molecule kinase inhibitors that have received FDA approval since 2001, which increased to 28 by April 2015 (Fig. 1.3), as well as numerous candidates currently in clinical trials.<sup>23, 25, 39, 40</sup>

Several factors have contributed to the clinical success of small-molecule kinase inhibitors for cancer treatment.<sup>24</sup> Many of these inhibitors have taken advantage on the fact that some cancer cells are highly dependent on the activity of a few mutated kinases in an early stage

## Type I



## Type III



Continues on next page

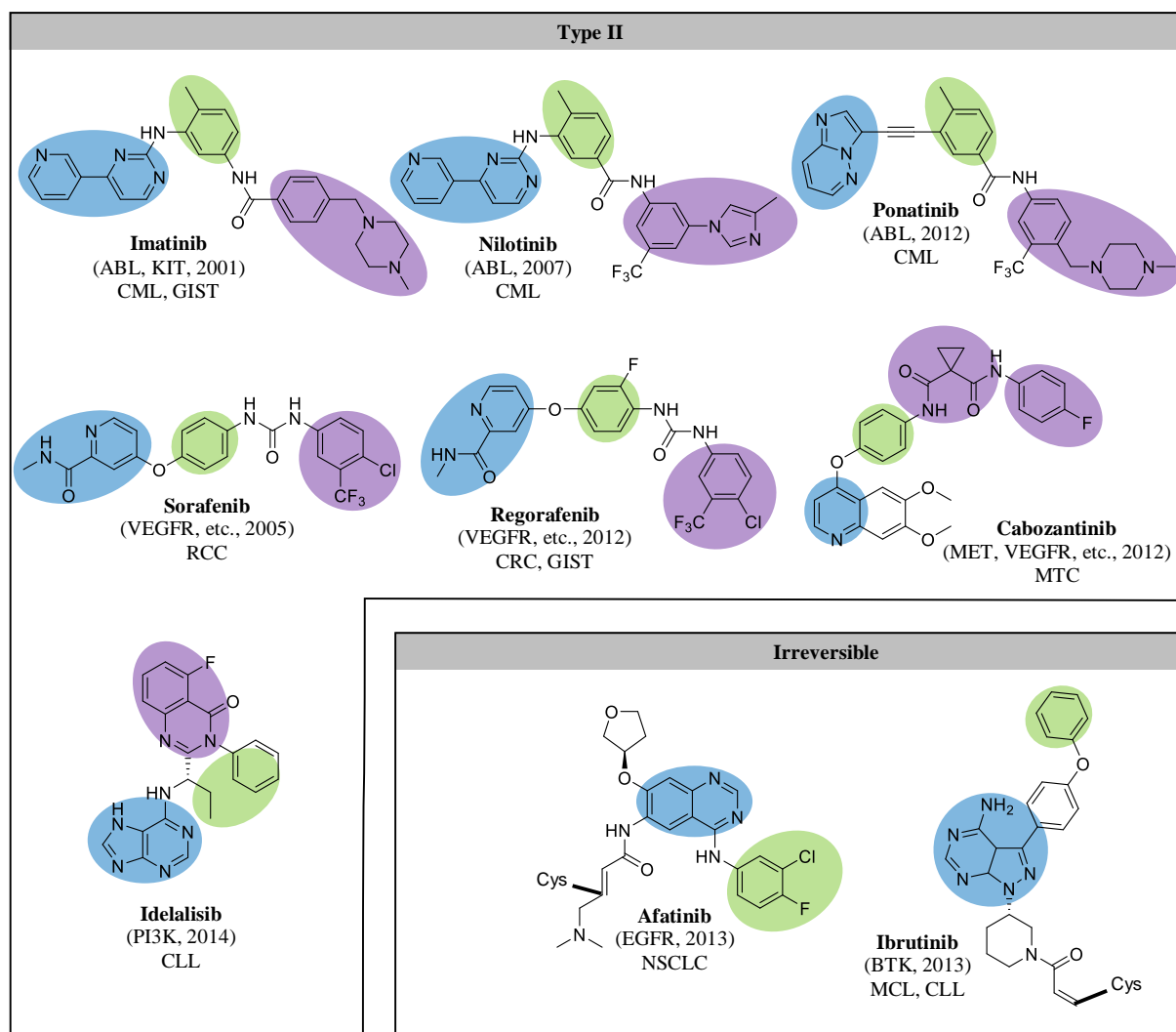


**Fig. 1.3** FDA-approved small-molecule kinase inhibitors (up to April 2015).

BC, breast cancer; CLL, chronic lymphocytic leukaemia; CML, chronic myelogenous leukaemia; CRC, colorectal cancer; GIST, gastrointestinal stromal tumor; IMF, idiopathic myelofibrosis; IPF, idiopathic pulmonary fibrosis; MCL, mantle cell lymphoma; MTC, medullary thyroid cancer; NSCLC, non-small-cell lung cancer; PC, pancreatic cancer; RA, rheumatoid arthritis; RCC, renal cell cancer; TC, thyroid cancer.

of the disease (oncogene addiction), which render them susceptible to the appropriate inhibitor.<sup>41, 42</sup> However, a number of significant challenges remain to be addressed, such as the emergence of drug resistance, selectivity issues, limited understanding of the disease dependence on a target kinase, as well as the complex chemistry behind how signal transduction is reprogrammed in response to oncogenic events and in the presence of inhibitors.<sup>24, 27, 40</sup>

## 1.2 Epidermal growth factor receptor (EGFR)

The epidermal growth factor receptor (EGFR) is one of the first and most extensively studied receptor tyrosine protein kinases (RTPKs) and a validated drug target.<sup>43-45</sup> EGFR is expressed in tissues of epithelial, mesenchymal and neuronal origin, where it regulates cellular processes required for normal development and function. Aberrant EGFR activities, due to mutation, overexpression or autocrine ligand production, are associated with the development of numerous types of cancer.<sup>46-48</sup>

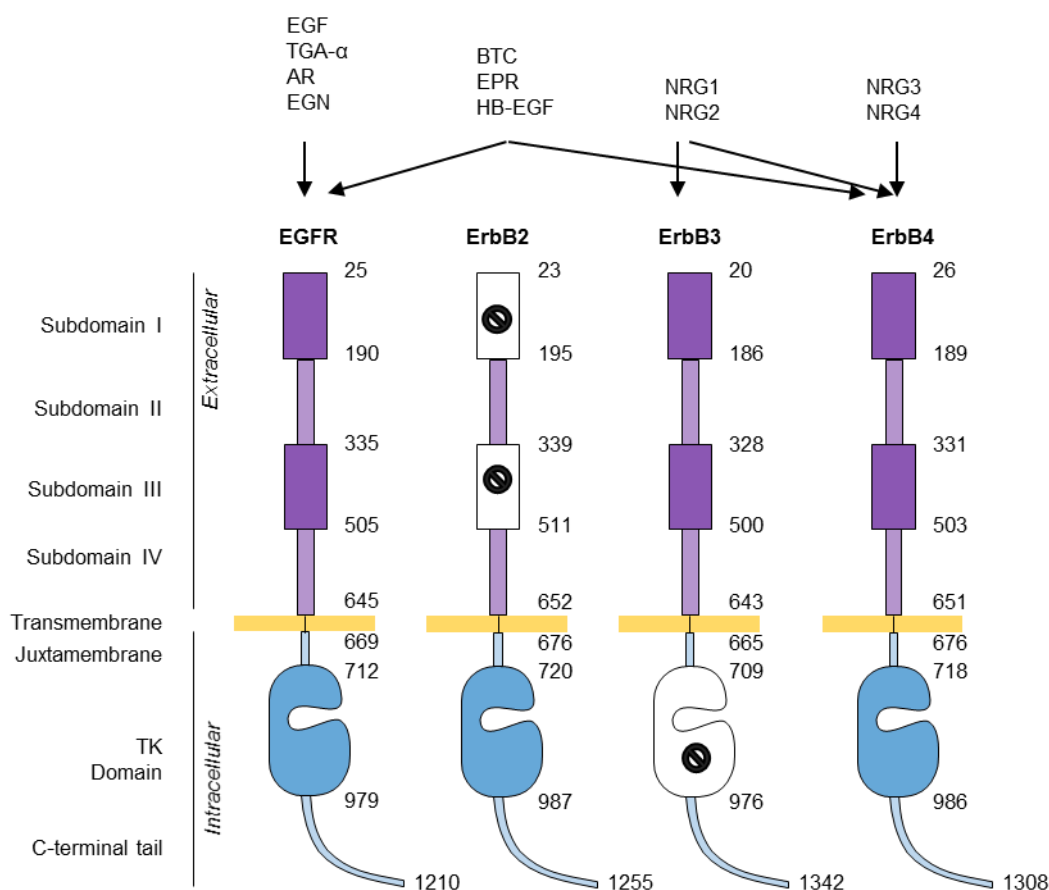


**Fig. 1.4** Schematic representation of the domain structure of the ErbB family proteins.

EGFR is one of the four members of the ErbB (from viral erythroblastoma gene) family of RTPKs, which includes EGFR itself (EGFR/ErbB1/HER1), ErbB2 (neu, HER2), ErbB3 (HER3) and ErbB4 (HER4). The structure of ErbB proteins consist of approximately 1200 residues distributed into an extracellular ligand binding domain, a single helix transmembrane domain, and an intracellular tyrosine kinase domain flanked by an intracellular juxtamembrane segment and C-terminal tail (Fig. 1.4). The extracellular domain contains four subdomains. Subdomains I and III are involved in ligand binding, while subdomains II and IV participate in dimer formation. In the kinase domain of ErbB3, two conserved residues involved in catalysis are mutated: the glutamate in the  $\alpha$ C-helix involved



in ATP binding and an aspartate base thought to deprotonate the substrate hydroxyl group. Consequently, ErbB3 exhibits weak kinase activity and is generally considered a pseudokinase.<sup>49</sup>

At least eleven different ligands are known to bind the ErbB receptors, and they are usually classified into three groups according to their specificity for the different ErbB members (Fig. 1.4).<sup>50, 51</sup> The first group includes epidermal growth factor (EGF), transforming growth factor  $\alpha$  (TGF- $\alpha$ ), amphiregulin (AR) and epigen (EGN), all of which bind exclusively to EGFR. The second group binds to either EGFR or ErbB4, including betacellulin (BTC), epiregulin (EPR) and heparin-binding EGF-like growth factor (HB-EGF). The last group consists of the neuregulins (NRGs), which bind to ErbB3 and ErbB4. All these ligands contain an EGF-like domain responsible for receptor binding, and they are produced as membrane-bound precursor proteins that are cleaved to yield active growth factors. No known ligands have been identified to bind to the extracellular domain of ErbB2.

A general paradigm for RPTK activation involves ligand binding first, followed by receptor dimerization or reorganization of constitutive dimers.<sup>43, 52-54</sup> However, in the absence of structural information, a precise mechanism for EGFR activation remained a mystery for many years. Even though a complete picture of endogenous EGFR function in its natural context is still absent, much structural and functional understanding of its activation has accumulated in the last 13 years.<sup>7, 55-57</sup>

In the absence of ligand, EGFR is largely monomeric and inactive (Fig. 1.5). The extracellular domain presents a tethered conformation which buries a dimerization arm in subdomain II and dimerization interfaces in subdomain IV through intramolecular interactions.<sup>58, 59</sup> A similar set of domain interactions is seen in ErbB3 and ErbB4,<sup>60, 61</sup> but ErbB2 is locked in a conformation that prevents its homo-dimerization such that ErbB2 becomes the preferred hetero-dimerization partner for the other ErbB members.<sup>62</sup>

The kinase domain of EGFR presents a Src/CDK like inactive conformation<sup>63</sup> and is docked against the membrane through electrostatic interactions, which obstructs its active site.<sup>64, 65</sup> A helical segment at the N-terminus of the intracellular juxtamembrane is also docked against the membrane through hydrophobic interactions.<sup>64, 65</sup> Ligand binding to subdomains I and III draw these subdomains together,<sup>66, 67</sup> extending the extracellular domain into a conformation that exposes the dimerization interfaces in subdomains II and IV required for

dimerization (Fig. 1.5).<sup>59, 68</sup> Dimerization of the extracellular domains II and IV brings the two transmembrane domains into close proximity. This conformation facilitates the association of the transmembrane domains through N-terminal GxxxG like motifs, which are classical transmembrane dimerization motifs.<sup>64, 65</sup> The transmembrane domain dimer of EGFR in turn facilitates the dissociation of the juxtamembrane and the kinase domain from the membrane.<sup>64, 69</sup> Free from membrane retention, the kinase domains form an asymmetric dimer, in which the C-lobe of the activator kinase docks onto the N-lobe of the receiver kinase through hydrophobic interactions and promotes a conformational change in the C-helix and activation loop of the latter for catalytic activation.<sup>63</sup> Formation of this asymmetric dimer is also necessary for the activation of the other ErbB homo- and heterodimers,<sup>70, 71</sup> except for ErbB3 that can only take the activator position.<sup>71</sup>

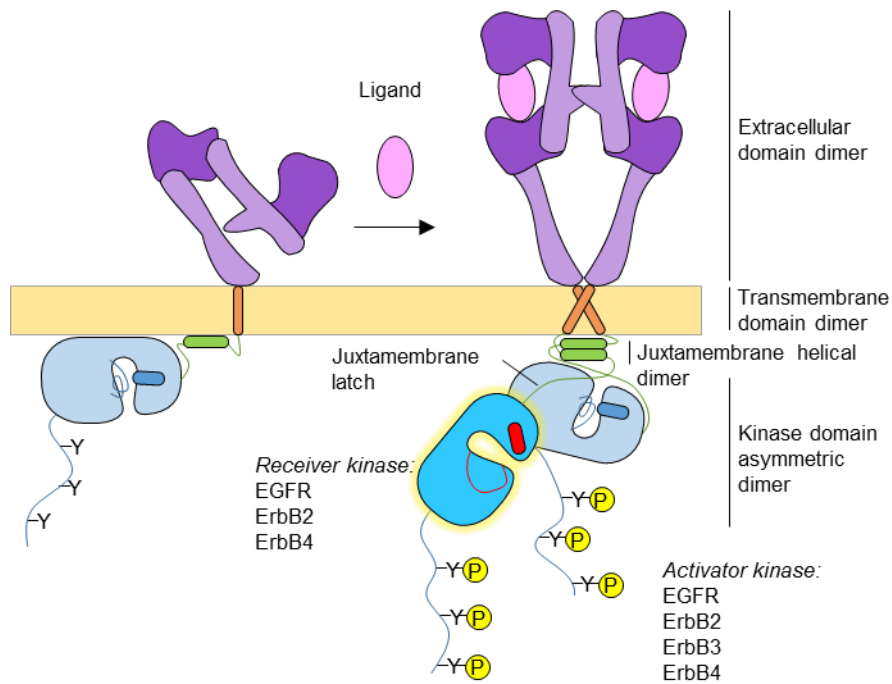


**Fig. 1.5** Schematic model of ligand-induced activation of ErbB proteins.

The asymmetric EGFR kinase domain dimer is stabilized by the juxtamembrane in two different ways: (1) the C-terminal segment of the juxtamembrane of the receiver latches the N-lobe of the receiver to the C-lobe of the activator through hydrogen bonds and hydrophobic contacts; (2) the helical N-terminal portion of the juxtamembrane in both kinases form an antiparallel dimer.<sup>72, 73</sup> These interactions of the juxtamembrane segments are required for kinase activation,<sup>72, 74</sup> and are in turn facilitated by the formation of the transmembrane dimer.<sup>64, 65</sup> The C-terminal tail is also known to have a regulatory role in the activation of EGFR, but a clear mechanism is not achieved yet.<sup>75, 76</sup> In summary, the kinase

activity of EGFR is highly dependent not only on the overall conformation of all its structural components, but also on its protein partners. EGFR constructs used in vitro may present a different catalytic profile compared to their endogenous homologs. The complexity behind EGFR activity regulation in vivo remains a challenge in developing EGFR-based therapeutics.<sup>77-79</sup>

Upon orchestration of all conformational changes described above, the activated ErbB kinase phosphorylates specific tyrosine residues in the C-tail of both receptors. Some tyrosine residues in the kinase domain can also be phosphorylated by cytoplasmic non-receptor tyrosine kinases (NRTKs). Phosphotyrosines serve as docking sites for the recruitment of a number of signaling molecules containing the Src homology 2 domain (SH2) or phosphotyrosine binding (PTB) domain, whose modular nature mediate interactions with other proteins, phospholipids or nucleic acids and allows the assembly of signaling complexes.<sup>53, 80, 81</sup> The recruited proteins include adaptors, such as Shc and Grb2; transcription factors (STAT1/5); and a variety of enzymes including kinases (PI3K, Src, Abl), phosphatases (SHP1/2), ubiquitin ligases (Cbl) and phospholipases (PLC- $\gamma$ ), among others. The different ErbB receptors present different patterns of interaction partners, and some of the most common ErbB partner proteins are shown in Fig. 1.6.<sup>82 83</sup>

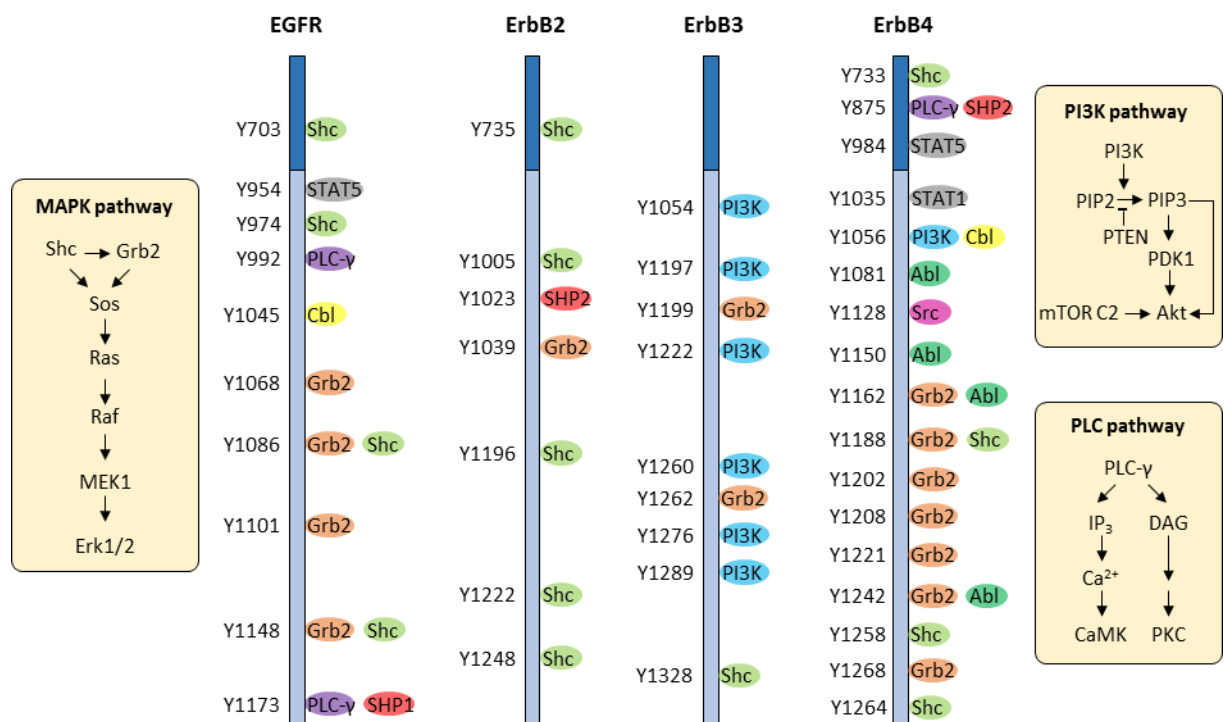


**Fig. 1.6** Major signaling proteins recruited and signaling pathways activated by ErbBs.

The signaling pathways triggered by the recruitment of signaling proteins to ErbB receptors are common to other RTPK, and eventually lead to a modification in the transcriptional activity of the cell resulting in proliferation, differentiation, apoptosis or survival (Fig. 1.6).<sup>53, 84, 85</sup> One of the most extensively studied ErbB signalling conduits is the MAPK pathway, in which the recruitment of adaptor proteins in the proximity of the membrane activates the small G-protein RAS through the guanine exchange factor SOS. RAS activates a kinase cascade in which RAF activates MEK1, which in turn activates ERK1/2. ERK1/2 is then translocated to the nucleus and regulates transcription factors leading to proliferation or differentiation. The PI3K/AKT pathway is another prominent conduit activated by ErbBs. The recruitment of PI3K by ErbB receptors activates its enzymatic activity, producing the phosphoinositide PIP3. This in turn allows AKT and PDK1 to translocate to the membrane, where AKT is activated by interactions with other proteins. AKT finally activates downstream proapoptotic proteins and transcription factors leading to survival and proliferation. Other major pathways activated involved in ErbB signaling also include the PCL- $\gamma$  and the JAK/STAT pathways that impact on phospholipid metabolism and gene transcription.

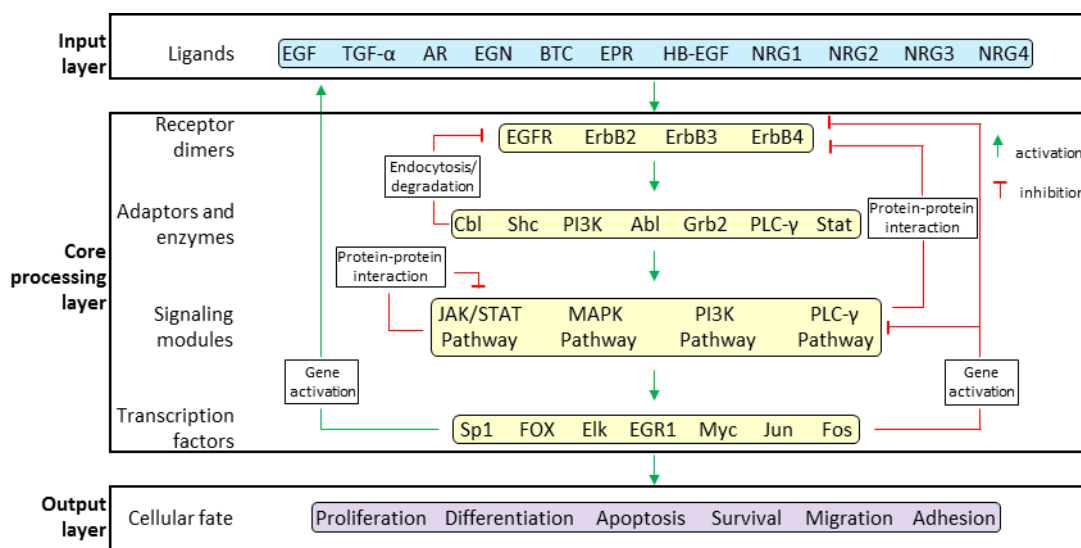


**Fig. 1.7** Schematic representation of the ErbB signaling network.

Far from being linear, the EGFR/ErbB signaling pathway comprises a highly complex multilayered signaling network of at least 211 reactions involving 322 components (Fig. 1.7).<sup>86, 87</sup> From a systems perspective, the EGFR network has a characteristic bow-tie or hourglass architecture in which diverse input and output signals are connected through a core process of relatively limited, highly redundant and interconnected set of biochemical interactions that define the basic processing modules.<sup>88</sup> Numerous positive and negative

feedback loops exist both within and between the different levels of the network, which regulate the amplitude, kinetics and frequency of signals that allow the correct processing of information and impart precision, robustness and versatility to the system.<sup>86, 89-91</sup> These feedback loops can be activated immediately after receptor activation or later in the signal transduction. Early activated loops involve pre-existing components that regulate receptor degradation and PTMs. An important example of an early loop is the receptor endocytosis coupled to degradation, which is the most effective process for signal termination.<sup>92, 93</sup> Upon activation EGFR is internalized into endosomes, where depending on several factors it is either recycled to the surface or ubiquitinated by the recruitment of Cbl for lysosomal degradation. An example of other early feedback loop is seen in the MAPK pathway, in which phosphorylation of RAF by its downstream partner ERK disrupts the RAS/RAF interaction, desensitizing it from further stimulation.<sup>94</sup> On the other hand, the late group of feedback loops require the synthesis of new proteins, which can have either activating or inhibitory effects on signaling. The activation of the MAPK pathway, for example, can induce the production of the EGFR ligands TGF- $\alpha$ , HB-EGF and AR, inducing an autocrine loop.<sup>95</sup> Some newly synthesized proteins that negatively regulate EGFR signaling include SPRY, LRIG1 and MIG-6 (RALT), which attenuate the signal through distinct mechanisms involving, for example, inhibition of signaling enzymes or enhanced receptor degradation.<sup>96-99</sup>

The final output triggered by EGFR activation is highly context dependent and controlled by numerous factors such as the nature of the ligand, composition of the receptor dimer, recruited protein partners, and expression levels of ligands, receptors and signaling proteins.<sup>100</sup> However, the true heart of signaling specificity seems to lie on the dynamic organization in space and time of the multiple regulatory elements and mechanisms of the signaling network.<sup>101, 102</sup> For example, stimulation of rat pheochromocytoma PC-12 cells with EGF induces transient activation of ERK in the MAPK pathway that limits the signal duration and leads to proliferation. Exposure of the same cells to nerve growth factor (NGF) promotes a sustained activation that prolongs signal duration and leads to differentiation.<sup>103</sup> Several factors contribute to these differences in time, including positive/negative feedback loops, ERK localization and compartmentalization, phosphorylation of transcription factors and crosstalk with the PI3K/AKT pathway.<sup>104, 105</sup>

The etiology of a number of cancers can be traced back to the manipulation of the different components of the ErbB network, which are then able to bypass or modify the normal

regulatory processes and rewire the signaling network to sustain the malignancy.<sup>106, 107</sup> For example, mutant forms of EGFR in lung cancer are constitutively activated in a ligand-independent manner and have been associated with enhanced kinase activity, increased cell survival, and impairment of downregulation compared to their wild type homologs.<sup>108-110</sup> The robustness of the network can also be harnessed to produce drug resistance, as the inhibition of an element of the system can release upstream elements from negative feedback regulation and thus reactivate the signal or activate alternative signaling pathways.<sup>111</sup>

The increasing understanding of the importance of signaling networks, such as the one centred around EGFR, has prompted a shift in the paradigm of drug development from the classical, single-target approach to a network-based approach, known as network pharmacology.<sup>112</sup> Aiming to understand the specific mechanisms or perturbations in the network of a particular disease (network rewiring), this new paradigm seems promising for facilitating the identification of new drug targets, predicting drug sensitivity, and reducing drug resistance and side effects.<sup>113, 114</sup> However, the elucidation of these signaling networks is a complex challenge that requires a multidisciplinary approach and relies on the development of novel molecular tools, many of which are derived from EGFR inhibitors as discussed below.

### 1.2.1 EGFR inhibitors

EGFR inhibitors with the highest potency and selectivity known to date are based on the 4-anilinoquinazoline scaffold (indicated in blue in Fig. 1.8).<sup>115, 116</sup> From the structure-activity relationship (SAR) studies it is known that electron-donating substituents at position C6 and C7 of the quinazoline and a small lipophilic electron-withdrawing substituent at the *meta* position of the aniline are required to modulate binding affinity.<sup>117, 118</sup> Crystal structures show that these inhibitors bind to the active kinase domain of EGFR with a DFG-in conformation (Type I).<sup>119-122</sup> In general, the nitrogen at position N1 of the quinazoline forms a hydrogen bond the backbone of Met793 in the hinge region and the substituents at C6 and C7 are directed towards the solvent-exposed region, while the anilino group is directed to a hydrophobic pocket in the gatekeeper region.

Gefitinib and erlotinib, the first EGFR inhibitors to receive FDA approval, are currently approved for the treatment of non-small cell lung cancer (NSCLC) harboring EGFR with exon 19 deletions or exon 21 (L858R) mutations. Lapatinib, which has a dual activity against EGFR and ErbB2, is approved for the treatment of breast cancer overexpressing ErbB2. The

sensitivity of NSCLC cells with mutant forms of EGFR to these first generation inhibitors has been attributed to a higher affinity for the inhibitors and lower affinity for ATP compared to wild type EGFR,<sup>123</sup> as well as oncogenic addiction to the mutant forms.<sup>124</sup> However, the clinical efficacy of tyrosine kinase inhibitors (TKI) in general is limited by resistance, which may be intrinsically present (*de novo* or primary resistance) or developed after initial successful treatment (acquired resistance). Several mechanisms underlying resistance to EGFR inhibitors and other TKI have been identified.<sup>78, 125</sup> Most of the cases with resistance to EGFR inhibitors fall into one of two categories: secondary mutations in EGFR or bypass of EGFR control/dependence.

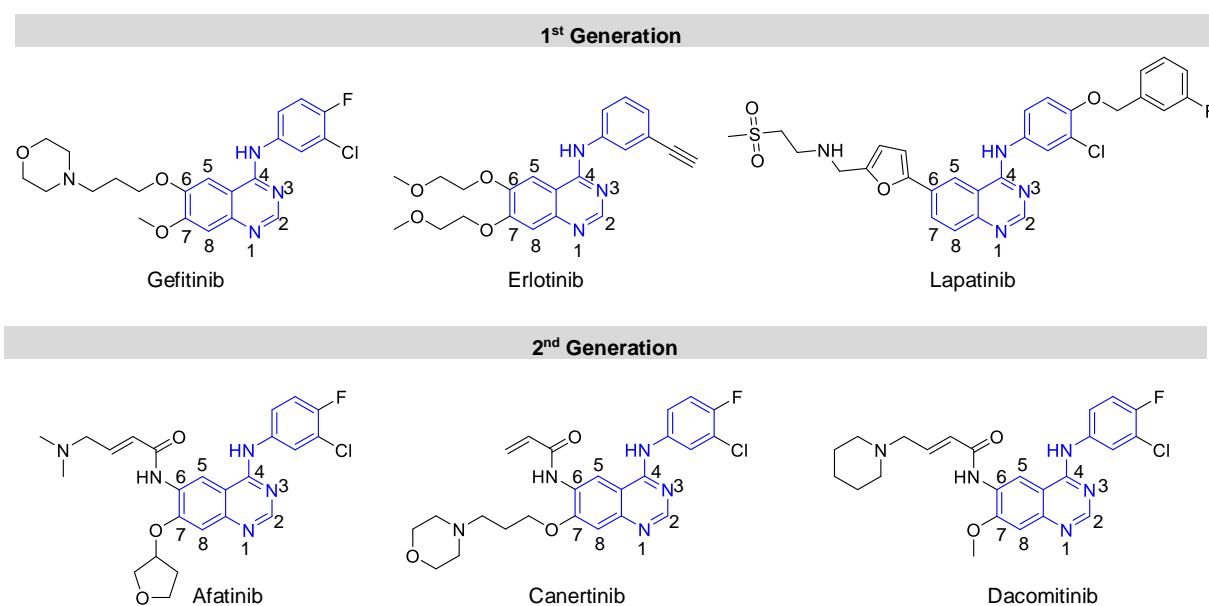


**Fig. 1.8** EGFR inhibitors based on the 4-anilinoquinazoline core (shown in blue).

Approximately 50% of the cases of acquired resistance to gefitinib or erlotinib in NSCLC arises from a second mutation in the gatekeeper residue (T790M), which restores the mutant's affinity for ATP.<sup>126-129</sup> In an effort to overcome this resistance mechanism, second-generation irreversible inhibitors based on the same 4-anilinoquinazoline scaffold, such as afatinib, canertinib and dacomitinib, have been developed (Fig. 1.8).<sup>130</sup> Although some of these inhibitors retain the capacity to inhibit this resistant mutant form, they do so at concentrations too prohibitively high for clinical use.<sup>131</sup> Afatinib is currently approved for the treatment of NSCLC wild type (WT) EGFR resistance.<sup>132</sup> Third generation inhibitors are being developed to target specifically the resistant T790M EGFR while sparing WT EGFR, and some of them are currently under clinical trials.<sup>133</sup>

Other resistance mechanisms arise from the (re)activation or maintenance of signaling pathways downstream of EGFR despite adequate inhibition of the latter, which has been termed bypass resistance or kinome reprogramming.<sup>134</sup> In these cases, the redundant and robust characteristics of the EGFR signaling network allows the activation of signaling pathways in several ways. The reprogramming includes mutations of downstream signaling proteins, use of other RTPKs and disruption of negative feedback loops. One of the first cases of this reprogramming was identified in resistant cases of NSCLC with amplification of the gene encoding for the RTPK hepatocyte growth factor receptor (MET).<sup>135, 136</sup> In these cases, MET promoted resistance by restoring the PI3K/AKT pathway, which in some cell lines required ErbB3. Further studies demonstrated that activation of MET by its ligand, hepatocyte growth factor (HGF), renders NSCLC cells resistant to EGFR inhibition albeit through an ErbB3 independent activation of the PI3K/AKT pathway.<sup>137, 138</sup> In both cases, the combination of EGFR and MET inhibitors was effective in blocking downstream signaling and induced marked tumor regression.

In a similar way, other RTPKs including ErbB2,<sup>139</sup> IGF-1<sup>140, 141</sup> and AXL<sup>142, 143</sup> have been shown to mediate bypass resistance to EGFR inhibitors in several types of cancer, and inhibition of these RTPKs usually restores sensitivity to EGFR inhibitors. In a different bypass mechanism, the overexpression or mutation of a component of a pathway downstream to EGFR may reduce the dependence of this pathway on EGFR. Several signaling proteins including PIK3CA, PTEN, KRAS, BRAF and MEK have been shown to be mutated or overexpressed in cancers resistant to EGFR inhibition.<sup>144-148</sup> In yet another bypass mechanism, EGFR may be activated in response to the inhibition of downstream signaling proteins as a consequence of disruption in a negative feedback loop. For example, in some colorectal cancers, inhibition of BRAF was shown to be ineffective for blocking the MAPK pathway due to the activation of EGFR.<sup>149, 150</sup> Combining BRAF and EGFR inhibitors blocked the reactivation of the MAPK pathway and resulted in regression. These examples of bypass mechanism of resistance highlight the potential of combination therapies in reducing escape routes from EGFR inhibition, as well as the need of understanding the changes in the signaling network in response to a specific therapeutic approach. As discussed next, the use of small-molecule probes combined with mass spectrometry is a valuable tool for the elucidation of these adaptive changes, leading to the identification of potential targets and optimal target combination.



Chemical probes are small molecules designed to modulate the function of a biomacromolecule (often a protein) for interrogating the role of that target in a specific biological system or context.<sup>151</sup> This chemical approach is complementary to biological tools (such as RNA interference), as the rapid and conditional perturbation of individual functions of a protein, rather than its complete knockout, allows for temporal control and differentiation between scaffold and catalytic effects.<sup>152, 153</sup> Chemical probes have been successfully applied in target validation and drug discovery,<sup>154</sup> elucidation of signaling pathways,<sup>155</sup> bioimaging,<sup>156</sup> and have in general led to advances in our understanding of diverse aspects of biology.<sup>155</sup>



15

based” probe (ABP), otherwise it is termed an “affinity based” (A/BP) probe.<sup>158</sup> The main function of the linker is to provide enough space between the binding group and the tag to minimize disruption of interactions with the target. The linker usually consists of an alkyl or polyethylene glycol (PEG) chain.<sup>159</sup> An alkyl linker enhances the hydrophobic character and facilitates cell membrane permeation, while the more hydrophilic component of a PEG linker increases the solubility of the probe in water. Several other strategies can also be adopted for the linker region, such as the use of peptides or cleavable linkers.<sup>160</sup> The tag group allows the manipulation and characterization of the target protein. Some commonly used tags include radioisotopes, affinity tags (biotin or short peptides), fluorophores (fluorescein, rhodamine or BODIPY), and handles for biorthogonal or click chemistry (azides or alkynes), each of which present different scopes and limitations.<sup>161</sup>

The comprehensive characterization of chemical probes is essential to assure that the tools selected for a specific experimental system are adequate for the target. In an effort to standardize criteria for proper selection and use, some guidelines or principles on what defines high-quality chemical probes have been proposed.<sup>151, 162-164</sup> These guidelines highlight the importance of a high potency (< 100 nM in an *in vitro* biochemical assay or < 1–10  $\mu$ M in a cell-based assay) and selectivity (>10–100 fold over related targets), well-defined chemical structure and properties, well-defined mechanism of action and the context in which the probe is used. It is important to stress that these principles are not strict rules to discard any probes that do not meet these criteria. In fact, only very few reported kinase inhibitors fully fulfil these parameters<sup>165</sup> and a strict adherence to these stringent requirements would certainly overlook many compounds with therapeutic potential.<sup>166</sup> In many cases, the seminal identification of a low-quality probe for a new target may render useful information and lead to the development of new probes with improved features. For example, staurosporine is generally non-selective against PKs but has inspired the discovery of other probes, such as the staurosporine analogue UCN-01, for elucidating the role of the cell cycle regulator kinase CHK1. This in turn promoted the development of more selective inhibitors that moved onto clinical trials.<sup>163</sup> The anilino-pyrimidine scaffold, as another example, led to the discovery of imatinib, the first FDA-approved kinase inhibitor.<sup>38</sup>

### 1.3.1 Chemical probes for PKs

Several chemical probes for kinases have been developed taking advantage of the optimized small molecules that have moved into clinical applications, such as imatinib and dasatinib among others (Fig. 1.10).<sup>167-170</sup> In combination with other techniques such as mass

spectrometry, these probes have been applied for the enrichment, isolation, and identification of PKs, which have allowed the determination of selectivity profiles, identification of new targets, and elucidation of signaling events and networks in specific contexts.<sup>171</sup> For example, Yao and coworkers developed a cell-permeable photoaffinity probe based on dasatinib (a dual Src/Abl inhibitor) and a click handle (Fig. 1.10).<sup>168</sup> Using this probe in K562 and HepG2 cancer live cells and cell lysates, a total of 84 off-target proteins were identified. From these proteins, 6 STPKs were identified as dasatinib targets for the first time and validated by pull-down /immunoblotting experiments, as well as by kinase inhibition assays. This probe was also shown to be a suitable imaging probe to detect endogenous cellular activities of c-Src and other “dasatinib-responsive” proteins.

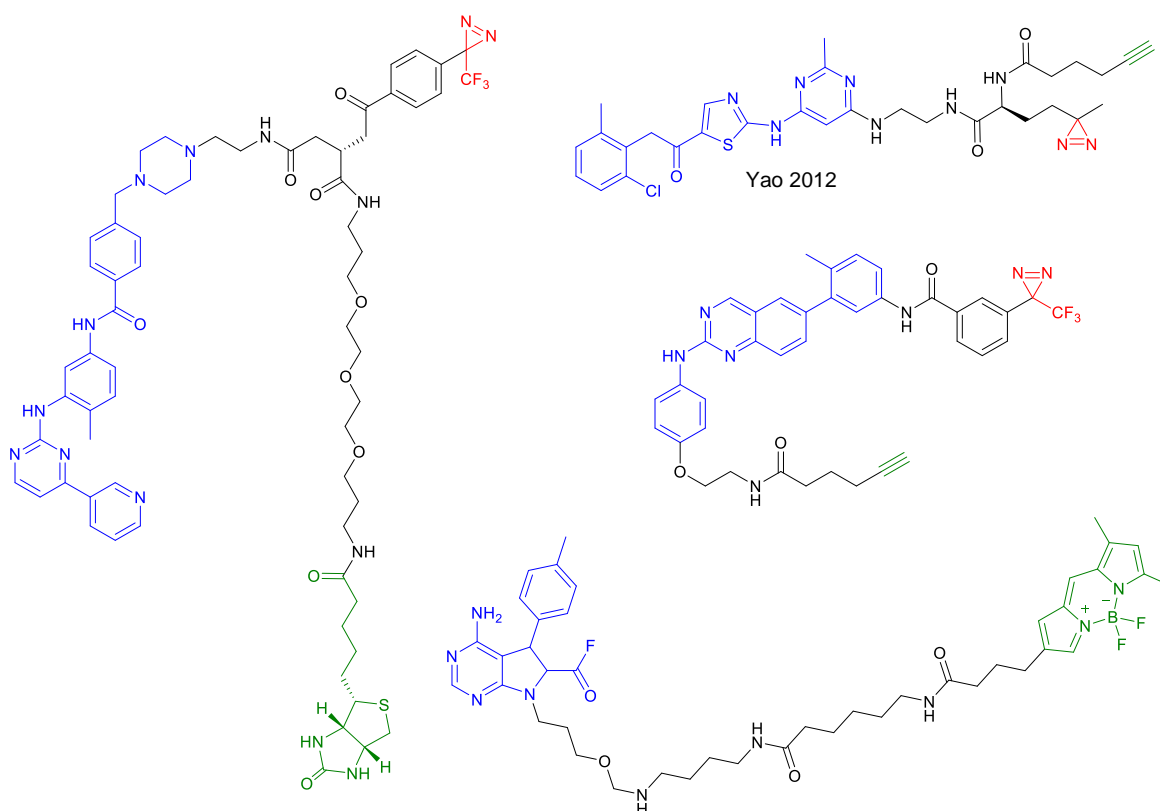


**Fig. 1.10** Structure of selected chemical probes for protein kinases.  
(Blue: binding group; green: reporter group; red: photo-reactive cross-linker)

### 1.3.2 Chemical probes for EGFR

Several chemical probes for EGFR based on 4-anilinoquinazolines have been reported (Fig. 1.11).<sup>172-175</sup> Shreder and collaborators reported the synthesis of a photoaffinity probe for EGFR bearing a TAMRA fluorophore.<sup>172</sup> Competition assays with known EGFR inhibitors demonstrated the utility of this probe for determining IC<sub>50</sub> values of inhibitors against EGFR.

Shokat and collaborators functionalized a 6-acrylamido-4-anilinoquinazoline scaffold by tethering a fluorogenic nitrobenzoxadiazole (NBD) at the C7 position through a PEG linker.<sup>174</sup> Using a competition binding assay with an analogous inhibitor, they were able to measure the fraction of EGFR active site available for signaling after inhibitor treatment, and correlated this fraction to downstream signaling events. Using the same probe, they compared the EGFR kinase-site occupancy in glioma and NSCLC cells upon erlotinib treatment.<sup>176</sup> They also showed that rapid release of erlotinib from glioma cells underlies the inefficacy of the drug in this type of cancer, and proposed the use of kinase-site occupancy might be used as a biomarker for efficacy of EGFR inhibitors.<sup>176</sup> Cravatt and coworkers modified an irreversible EGFR inhibitor with an alkynyl group suitable to react with an azide-rhodamine reporter tag in a bioorthogonal click chemistry reaction.<sup>175</sup> Combining this probe with quantitative MS, they were able to define a window of selectivity for irreversible kinase inhibitors, outside of which off-targeting and kinase-independent cytotoxicity was observed.

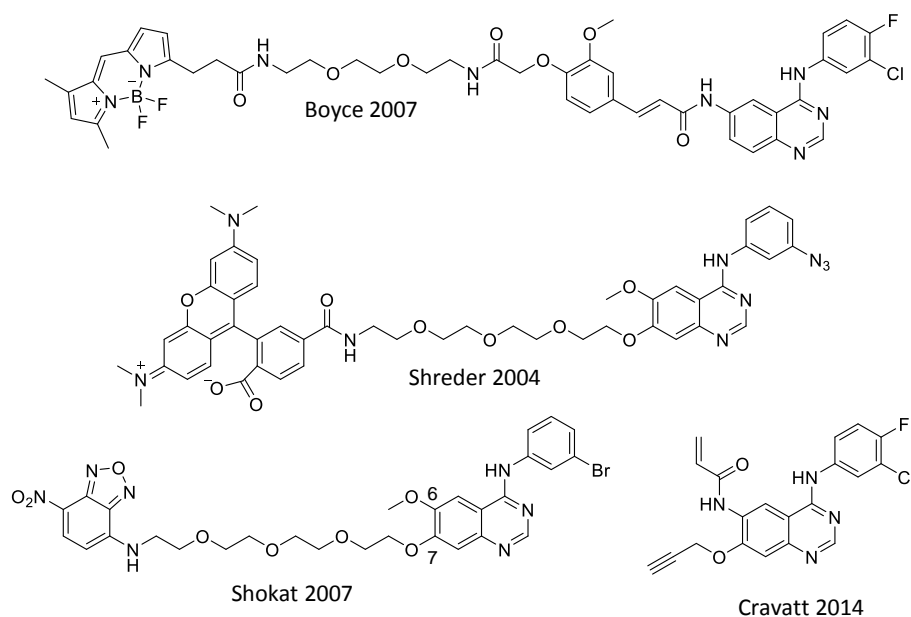


**Fig. 1.11** Structures of representative EGFR chemical probes.

## 1.4 Objectives

The clinical success of EGFR-targeted therapy, in particular against NSCLC cancers, has prompted a quest to validate the therapeutic role of EGFR inhibition in other types of cancer. Learning from the vast body of information gained from investigations on EGFR resistance mechanisms, it is clear that this task will require the understanding of the interactions of EGFR with protein partners in the context of its complex signaling network.

In an effort to contribute to the understanding of EGFR signaling specificity, we aimed to synthesize chemical probes for EGFR by biotinylating 4-phenylaminoquinazolines and determine their binding affinity for EGFR. The results obtained from the first generation EGFR probes will serve to guide the design of next generation probes with multiple tags or target groups for understanding endogenous signaling partners of EGFR.

## 2. EXPERIMENTAL SECTION

### 2.1 General information

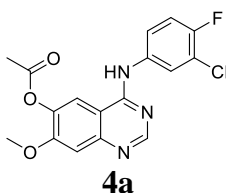
All reagents were used as received from commercial suppliers. 4-Chloro-7-methoxyquinazolin-6-yl-acetate was purchased from Pharmablock; 3-chloro-4-fluoroaniline and 3-ethynylaniline were obtained from Alfa Aesar; 4-chloro-3-fluoroaniline and ethyl 7-bromoheptanoate were purchased from Matrix; EDC·HCl was purchased from Aldrich; NHS and 5-(biotinamido)pentylamine were obtained from Pierce. All solvents were of either anhydrous or HPLC grade and used without further purification unless otherwise specified. 2-Propanol was dried with 4Å-MS. DMF was distilled from CaH<sub>2</sub> under reduce pressure and stored over 4Å-MS. All reactions were magnetically stirred and monitored by thin-layer chromatography (TLC) using Merck silica gel 60 F<sub>254</sub> pre-coated plates (0.25 mm), and TLC staining was performed with KMnO<sub>4</sub> or ninhydrin solutions. When necessary, flash column chromatography was performed on Merck silica gel 60 (0.015–0.040 mm). <sup>1</sup>H and <sup>13</sup>C NMR spectra were recorded on a Bruker Avance DPX 400 MHz at 25 °C. Chemical shifts were reported in ppm using the solvent residual signal (DMSO-*d*<sub>6</sub> δ<sub>H</sub> = 2.49, δ<sub>C</sub> = 39.5 ppm; CDCl<sub>3</sub> δ<sub>H</sub> = 7.24, δ<sub>C</sub> = 77.0 ppm) as an internal reference. 2D NMR spectroscopy was performed on a Bruker DRX600 NMR spectrometer equipped with a TXI (5 mm) Cryoprobe. High power <sup>1</sup>H (5.35 W) π/2 pulses were determined to be ~9.5 ms and <sup>13</sup>C high power π/2 pulse was 11.05 ms and a low power pulse of 65 ms was used for GARP4 decoupling. Gradient pulses were delivered along the *z*-axis using a 100 step sine program. Heteronuclear single quantum coherence (HSQC) experiments were optimised for a <sup>1</sup>JCH coupling of 145 Hz. HSQC experiments were performed using the hsqcedetgps.3 pulse program. HSQC spectra were processed (π/2 shifted sine bell squared in both dimensions) phase sensitive. IR spectra were collected on a Nicolet iS10 FT-IR Spectrometer with a smart iTR attenuated total reflectance (ATR) accessory and maximum absorption peaks were reported in cm<sup>-1</sup>. Reversed-phase HPLC was conducted on an Agilent 1260 Infinity Instrument with UV detector at 250 nm using an Alltech Nucleosil C18 column (4.6 x 250 mm, particle size 5 μm). Low-resolution mass-spectrometry was conducted on an Agilent 6130 quadrupole LC/MS system with an electrospray ionization source (ESI) using a Phenomenex Gemini C18 column (2.0 x 150 mm, particle size 3 μm); the mobile phase consisted of a gradient of 40–90% acetonitrile in water with 0.05% formic acid over 6 minutes (flow rate 0.2 mL/min, column temperature 25 °C) and the spectra were acquired in positive mode, scanning over the *m/z* range of 100–1000.

## 2.2 Synthesis and characterization

### 2.2.1 Synthesis of compounds 4a–4c

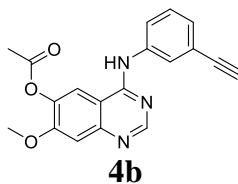
In a typical procedure, a mixture of 4-chloro-7-methoxyquinazolin-6-yl acetate (**2**) (253 mg, 1.0 mmol, 1.0 equiv) and the corresponding aniline **3a–3c** (1.2 mmol, 1.2 equiv) in 2-propanol (12 mL) was heated to reflux for 2.5 hours. The reaction mixture was cooled to room temperature and the resultant precipitate was collected by filtration, washed with 2-propanol and dried to afford the corresponding compound **4a–4c** without further purification.

#### *4-(3-chloro-4-fluorophenylamino)-7-methoxyquinazolin-6-yl acetate (4a)*



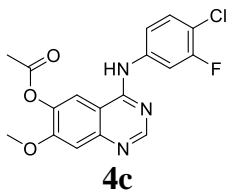
A white solid (695 mg, 97% yield) as previously described. <sup>177</sup> <sup>1</sup>H NMR (400 MHz, DMSO-*d*<sub>6</sub>) δ 11.25 (br s, 1H), 8.92 (s, 1H), 8.65 (s, 1H), 8.05 (dd, *J* = 6.8, 2.5 Hz, 1H), 7.72 (m, 1H), 7.53 (t, *J* = 9.0 Hz, 1H), 7.46 (s, 1H), 4.00 (s, 3H), 2.38 (s, 3H); <sup>13</sup>C NMR (100 MHz, DMSO-*d*<sub>6</sub>) δ 170.0, 168.5, 157.4, 151.6, 140.2, 126.0, 124.7, 118.0, 117.1, 116.9, 57.0, 20.2.

#### *4-(3-ethynylphenylamino)-7-methoxyquinazolin-6-yl acetate (4b)*



A beige solid (324 mg, 97% yield) as previously described. <sup>177</sup> <sup>1</sup>H NMR (400 MHz, DMSO-*d*<sub>6</sub>) δ 11.51 (br s, 1H), 8.92 (s, 1H), 8.82 (s, 1H), 7.90 (m, 1H), 7.76 (m, 1H), 7.54 (s, 1H), 7.48 (t, *J* = 7.8 Hz, 1H), 7.40 (m, 1H), 4.27 (s, 1H), 3.99 (s, 3H), 2.37 (s, 3H). <sup>13</sup>C NMR (100 MHz, DMSO-*d*<sub>6</sub>) 168.4, 158.8, 157.4, 151.2, 140.2, 137.2, 129.3, 127.2, 124.9, 122.1, 118.4, 107.2, 101.6, 82.9, 81.4, 57.0, 20.2.

4-(4-chloro-3-fluorophenylamino)-7-methoxyquinazolin-6-yl acetate (**4c**)

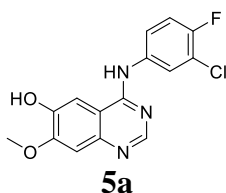


A beige solid (quantitative yield).  $^1\text{H}$  NMR (400 MHz,  $\text{DMSO-}d_6$ )  $\delta$  11.42 (br s, 1H), 8.96 (s, 1H), 8.77 (s, 1H), 7.99 (m, 1H), 7.71–7.64 (m, 2H), 7.52 (s, 1H), 4.00 (s, 3H), 2.38 (s, 3H);  $^{13}\text{C}$  NMR (100 MHz,  $\text{DMSO-}d_6$ )  $\delta$  168.4, 158.6, 157.5, 156.7 (d,  $J = 244.7$  Hz), 151.3, 140.3, 137.6, 130.5, 120.9, 118.3, 112.4 (d,  $J = 25.3$  Hz), 107.4, 101.9, 57.0, 20.2; IR (ATR): 3269 (w), 3118 (w), 3003 (w), 1767 (s), 1643 (s), 1441 (s), 1424 (s), 1364 (s), 1178 (s), 1146 (s), 1077 (m), 869 (s), 816 (m), 773 (m), 751 (m)  $\text{cm}^{-1}$ ; LC-MS (ESI):  $[\text{M} + \text{H}]^+$ ,  $m/z$  calculated for  $\text{C}_{17}\text{H}_{13}\text{ClFN}_3\text{O}_3$  362.07, found 362.1.

### 2.2.2 Synthesis of compounds **5a–5c**

In a typical procedure, a mixture of the corresponding compound **4a–4c** (0.8 mmol, 1.0 equiv) and LiOH (89 mg, 3.7 mmol, 4.6 equiv) in methanol (25 mL) and water (25 mL) was stirred at room temperature overnight. The mixture was neutralized by the addition of a stoichiometric amount of 20% aqueous acetic acid solution and stirred for one hour. The resultant precipitate was collected by filtration, washed with methanol and dried to afford the corresponding compound **5a–5c** without further purification.

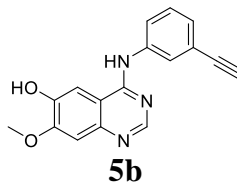
4-(3-chloro-4-fluorophenylamino)-7-methoxyquinazolin-6-ol (**5a**)



A white solid (530 mg, 92% yield) as previously described.<sup>177</sup>  $^1\text{H}$  NMR (400 MHz,  $\text{DMSO-}d_6$ )  $\delta$  9.46 (s, 1H), 8.46 (s, 1H), 8.20 (dd,  $J = 6.9, 2.6$  Hz, 1H), 7.83 (m, 1H), 7.77 (s, 1H), 7.39 (t,  $J = 9.1$  Hz, 1H), 7.20 (s, 1H), 3.97 (s, 3H);  $^{13}\text{C}$  NMR (100 MHz,  $\text{DMSO-}d_6$ )  $\delta$  155.8, 153.9, 152.8 (d,  $J = 242.2$  Hz), 151.9, 146.8, 146.2, 137.2, 122.7, 121.7 (d,  $J = 6.9$  Hz), 118.6 (d,  $J = 18.4$  Hz), 116.4 (d,  $J = 21.4$  Hz), 109.5, 107.2, 105.3, 55.9.

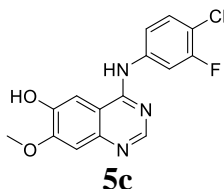


4-(3-ethynylphenylamino)-7-methoxyquinazolin-6-ol (**5b**)



A beige solid (235 mg, 93% yield) as previously described.<sup>177</sup> <sup>1</sup>H NMR (400 MHz, DMSO-*d*<sub>6</sub>) δ 9.39 (s, 1H), 8.46 (s, 1H), 8.07 (m, 1H), 7.90 (m, 1H), 7.79 (s, 1H), 7.35 (t, *J* = 7.9 Hz, 1H), 7.20 (s, 1H), 7.15 (br d, *J* = 7.6 Hz, 1H), 4.16 (s, 1H), 3.96 (s, 3H); <sup>13</sup>C NMR (100 MHz, DMSO-*d*<sub>6</sub>) δ 156.0, 153.9, 152.0, 146.8, 146.2, 140.2, 128.8, 126.0, 124.2, 122.1, 121.7, 109.7, 107.2, 105.4, 83.7, 80.4, 55.9.

4-(4-chloro-3-fluorophenylamino)-7-methoxyquinazolin-6-ol (**5c**)

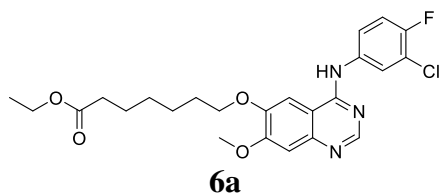


A beige solid (238 mg, 89% yield). <sup>1</sup>H NMR (400 MHz, DMSO-*d*<sub>6</sub>) δ 9.56 (s, 1H), 8.51 (s, 1H), 8.18 (dd, *J* = 12.5, 2.3 Hz, 1H), 7.79 (s, 1H), 7.73 (m, 1H), 7.52 (t, *J* = 8.7 Hz, 1H), 7.22 (s, 1H), 3.97 (s, 3H); <sup>13</sup>C NMR (100 MHz, DMSO-*d*<sub>6</sub>) δ 156.8 (d, *J* = 242.7 Hz), 155.7, 154.1, 151.8, 146.9, 146.3, 140.7 (d, *J* = 10.7 Hz), 130.0, 117.8 (d, *J* = 3.1 Hz), 112.0 (d, *J* = 17.6 Hz), 109.7, 109.0 (d, *J* = 25.7 Hz), 107.2, 105.2, 56.0. IR (ATR): 3361 (m), 1611 (m), 1576 (m), 1521 (s), 1424 (s), 1242 (s), 1207 (s), 1055 (m), 842(s) cm<sup>-1</sup>; LCMS (ESI): [M + H]<sup>+</sup>, *m/z* calculated for C<sub>15</sub>H<sub>11</sub>ClFN<sub>3</sub>O<sub>2</sub> 320.06, found 320.0.

### 2.2.3 Synthesis of compounds 6a–6c

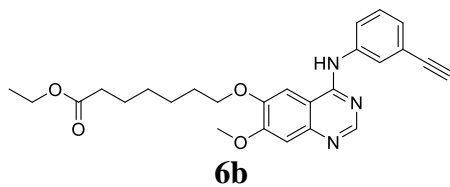
In a typical procedure, a mixture of the corresponding compound **5a–5c** (0.3 mmol, 1.0 equiv), ethyl-7-bromoheptanoate (0.07 mL, 0.33 mmol, 1.1 equiv) and K<sub>2</sub>CO<sub>3</sub> (46 mg, 0.33 mmol, 1.1 equiv) in DMF (1 mL) was stirred at 50 °C for 12 hours. Upon completion, the solvent was lyophilised and the crude product was diluted in chloroform and filtered. Chloroform was then evaporated under nitrogen. The remaining solid was washed with hexane, dried and purified by flash column chromatography (EtOAc:Hexanes 4:1) to afford the corresponding compound **6a–6c** without further purification.

*Ethyl 7-[4-(3-chloro-4-fluorophenylamino)-7-methoxyquinazolin-6-yloxy]heptanoate (6a)*



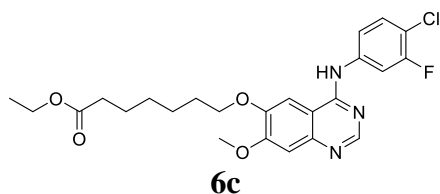
A yellow solid (61 mg, 80%) as previously described.  $^{177}$   $^1\text{H}$  NMR (400 MHz,  $\text{CDCl}_3$ )  $\delta$  8.64 (s, 1H), 7.85 (dd,  $J = 6.6, 2.7$  Hz, 1H), 7.66 (br s, 1H), 7.54 (m, 1H), 7.22 (s, 1H), 7.17 (s, 1H), 7.13 (t,  $J = 8.8$  Hz, 1H), 4.12–4.03 (m, 4H), 3.96 (s, 3H), 2.31 (t,  $J = 7.2$  Hz, 2H), 1.87 (m, 2H), 1.65 (m, 2H), 1.50–1.37 (m, 4H), 1.23 (t,  $J = 7.1$  Hz, 3H);  $^{13}\text{C}$  NMR (100 MHz,  $\text{CDCl}_3$ )  $\delta$  174.2, 156.4, 155.3, 154.7 (d,  $J = 246.3$  Hz), 153.4, 149.1, 147.4, 135.6, 124.2, 121.8 (d,  $J = 6.9$  Hz), 120.9 (d,  $J = 18.0$  Hz), 116.5 (d,  $J = 22.3$  Hz), 109.1, 107.7, 101.2, 69.2, 60.4, 56.1, 34.1, 28.5, 28.4, 25.3, 24.6, 14.2.

*Ethyl 7-[4-(3-ethynylphenylamino)-7-methoxyquinazolin-6-yloxy]heptanoate (6b)*



A beige solid (91 mg, 58% yield) as previously described.  $^{177}$   $^1\text{H}$  NMR (400 MHz,  $\text{CDCl}_3$ )  $\delta$  8.65 (s, 1H), 7.82 (m, 1H), 7.75 (m, 1H), 7.59 (br s, 1H), 7.32 (t,  $J = 7.9$  Hz, 1H), 7.26–7.23 (m, 1H), 7.22 (s, 1H), 7.16 (s, 1H), 4.08–4.04 (m, 4H), 3.96 (s, 3H), 3.06 (s, 1H), 2.30 (t,  $J = 7.3$  Hz, 2H), 1.88 (m, 2H), 1.65 (m, 2H), 1.51–1.35 (m, 4H), 1.21 (t,  $J = 7.1$  Hz, 3H);  $^{13}\text{C}$  NMR (100 MHz,  $\text{CDCl}_3$ )  $\delta$  174.1, 156.2, 155.2, 153.5, 149.1, 147.5, 138.9, 129.0, 127.7, 125.1, 122.8, 122.4, 109.1, 107.9, 100.9, 83.3, 77.4, 69.3, 60.4, 56.2, 34.2, 28.5, 25.4, 24.6, 14.2.

*Ethyl 7-[4-(4-chloro-3-fluorophenylamino)-7-methoxyquinazolin-6-yloxy]heptanoate (6c)*



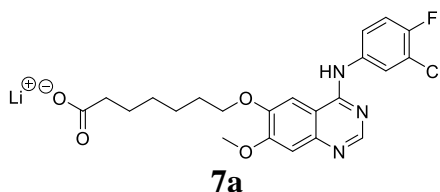
A yellow solid (92 mg, 62% yield).  $^1\text{H}$  NMR (400 MHz,  $\text{CDCl}_3$ )  $\delta$  8.67 (s, 1H), 7.87 (m, 1H), 7.75 (s, 1H), 7.43–7.31 (m, 2H), 7.23 (s, 1H), 7.16 (s, 1H), 4.09–4.02 (m, 4H), 3.96 (s, 3H), 2.31 (t,  $J = 7.2$  Hz, 2H), 1.88 (m, 2H), 1.66 (m, 2H), 1.50–1.37 (m, 4H), 1.22 (t,  $J = 7.1$  Hz, 3H);  $^{13}\text{C}$  NMR (100 MHz,  $\text{CDCl}_3$ )  $\delta$  174.3, 155.9, 155.4, 153.2, 149.2, 147.6, 130.3,

117.5, 110.0 (d,  $J = 25.7$  Hz), 107.9, 100.9, 69.3, 60.4, 56.2, 34.2, 28.4, 25.3, 24.6, 14.2. IR (ATR): 2936 (w), 2860 (w), 1731 (m), 1642 (m), 1491 (m), 1574 (s), 1426 (s), 1210 (m), 855 (m)  $\text{cm}^{-1}$ ; LC-MS (ESI):  $[\text{M} + \text{H}]^+$ ,  $m/z$  calculated for  $\text{C}_{24}\text{H}_{27}\text{ClFN}_3\text{O}_4$  476.17, found 476.2.

#### 2.2.4 Synthesis of compounds 7a–7c

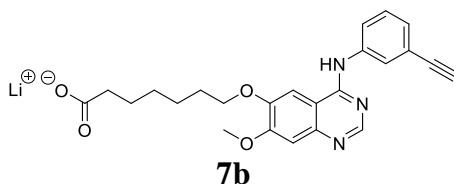
In a typical procedure, a mixture of the corresponding compound **6a–6c** (0.20 mmol, 1.0 equiv) and LiOH (22 mg, 0.92 mmol, 4.6 equiv) in methanol (6 mL) and water (6 mL) was heated to reflux for one hour. The solvent was then evaporated under reduce pressure followed by lyophilisation. The obtained solid was washed with chloroform and dried to afford the corresponding compound **7a–7c** without further purification.

##### *Lithium 7-[4-(3-chloro-4-fluorophenylamino)-7-methoxyquinazolin-6-yloxy]heptanoate (7a)*



A pale yellow solid (21 mg, 59% yield).  $^1\text{H}$  NMR (400 MHz,  $\text{DMSO}-d_6$ )  $\delta$  8.46 (s, 1H), 7.83 (s, 1H), 7.69 (dd,  $J = 7.5, 2.4$  Hz, 1H), 7.61 (s, 1H), 7.11 (m, 1H), 6.99 (t,  $J = 9.2$  Hz, 1H), 6.70 (s, 1H), 3.93 (t,  $J = 6.5$  Hz, 2H), 3.78 (s, 3H), 1.92 (t,  $J = 7.3$  Hz, 2H), 1.72 (m, 2H), 1.52–1.38 (m, 4H), 1.31 (m, 2H);  $^{13}\text{C}$  NMR (100 MHz,  $\text{DMSO}-d_6$ )  $\delta$  177.7, 159.1, 155.2, 151.7, 151.3, 150.8, 148.4, 145.9, 145.1, 123.7, 116.0, 114.9 (d,  $J = 20.3$  Hz), 106.5, 106.0, 68.1, 55.2, 38.3, 29.2, 29.0, 26.3, 25.7. IR (ATR) 2939 (w), 2853 (w), 1621 (m), 1575 (m), 1496 (s), 1473 (m), 1421 (s), 1214 (m), 860 (m)  $\text{cm}^{-1}$ ; LC-MS (ESI):  $[\text{M} + 2\text{H}]^+$ ,  $m/z$  calculated for  $\text{C}_{22}\text{H}_{22}\text{ClFN}_3\text{O}_4$  448.13, found 448.1.

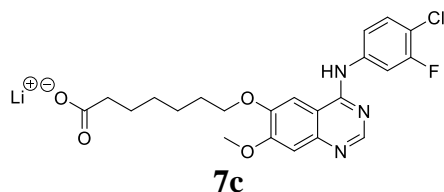
##### *Lithium 7-[4-(3-ethynylphenylamino)-7-methoxyquinazolin-6-yloxy]heptanoate (7b)*



A pale yellow solid (quantitative yield).  $^1\text{H}$  NMR (400 MHz,  $\text{DMSO}-d_6$ )  $\delta$  7.78 (s, 1H), 7.60 (s, 1H), 7.43 (m, 1H), 7.20 (m, 1H), 7.02 (t,  $J = 7.7$  Hz, 1H), 6.67 (m, 2H), 3.93 (t,  $J = 6.5$  Hz, 2H), 3.86 (s, H), 3.78 (s, 1H), 1.92 (t,  $J = 7.2$  Hz, 2H), 1.72 (m, 2H), 1.51–1.37 (m, 4H),

1.34–1.30 (m, 2H).  $^{13}\text{C}$  NMR (100 MHz, DMSO- $d_6$ )  $\delta$  177.6, 758.9, 155.3, 151.6, 146.0, 145.0, 127.7, 126.8, 125.1, 120.5, 116.0, 106.6, 106.0, 85.6, 78.1, 68.1, 55.2, 38.1, 29.2, 29.0, 26.4, 25.7. IR (ATR) 2942 (w), 1622 (w), 1559 (m), 1506 (m), 1472 (m), 1424 (s), 1244 (m), 862 (m)  $\text{cm}^{-1}$ ; LC-MS (ESI):  $[\text{M} + 2\text{H}]^+$ ,  $m/z$  calculated for  $\text{C}_{24}\text{H}_{24}\text{N}_3\text{O}_4$  420.18, found 420.2

**Lithium** 7-[4-(4-chloro-3-fluorophenylamino)-7-methoxyquinazolin-6-yloxy]heptanoate (**7c**)

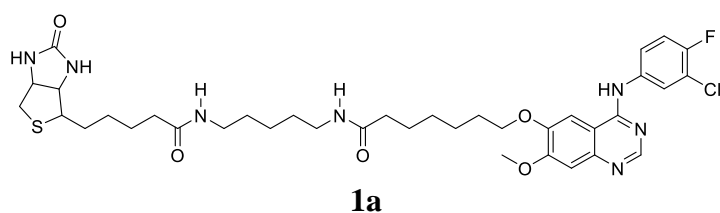


A yellow solid (quantitative yield).  $^1\text{H}$  NMR (400 MHz, DMSO- $d_6$ )  $\delta$  7.94 (br s, 1H), 7.72–7.67 (m, 2H), 7.09 (m, 2H), 6.75 (br s, 1H), 3.95 (m, 2H), 3.80 (s, 3H), 1.91 (t,  $J = 7.2$  Hz, 2H), 1.72 (m, 2H), 1.51–1.38 (m, 4H), 1.34 (m, 2H);  $^{13}\text{C}$  NMR (100 MHz, DMSO- $d_6$ )  $\delta$  128.1, 121.5, 110.0, 106.1, 68.1, 55.2, 38.4, 29.2, 29.0, 26.4, 25.7; IR (ATR) 2939 (w), 1617 (w), 1559 (m), 1506 (s), 1472 (s), 1419 (s), 1244 (m), 1211 (m), 806 (m)  $\text{cm}^{-1}$ ; LC-MS (ESI):  $[\text{M} + 2\text{H}]^+$ ,  $m/z$  calculated for  $\text{C}_{22}\text{H}_{22}\text{ClFN}_3\text{O}_4$  448.13, found 448.1.

### 2.2.5 Synthesis of probes 1a–1c

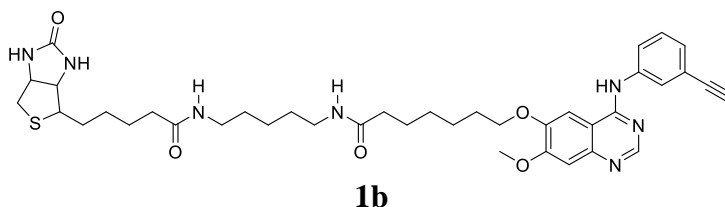
In a typical procedure, a mixture of the corresponding compound **7a–7c** (0.09 mmol, 1 equiv), NHS (15 mg, 0.13 mmol, 1.4 equiv) and EDC·HCl (20 mg, 0.10 mmol, 1.1 equiv) in DMF (0.9 mL) was stirred at room temperature overnight. The solvent was lyophilised and the remaining crude product was dissolved in chloroform and filtered. Chloroform was then removed under nitrogen. To the crude product were added 5-(biotinamido)pentylamine (8 mg, 0.02 mmol, 0.2 equiv) and DMF (0.2 mL). The mixture was stirred at 40 °C overnight. After lyophilisation of the solvent, the crude product was purified by flash column chromatography (EtOH:EtOAc 2:3) to afford the corresponding probe **1a–1c**. A fraction of each probe (1 mg) was further purified by reverse-phase HPLC (Section 2.3).

#### Probe 1a



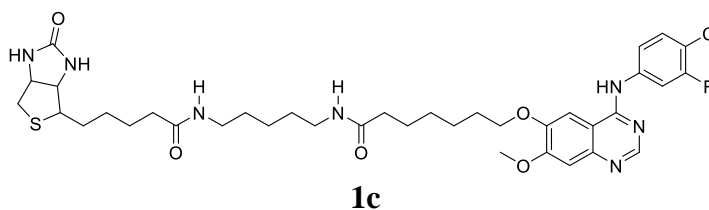
A yellow solid (10 mg, 29% yield over two steps).  $^1\text{H}$  NMR (400 MHz,  $\text{DMSO-}d_6$ )  $\delta$  10.67 (br s, 1H), 8.65 (s, 1H), 8.15 (s, 1H), 8.10 (dd,  $J = 6.8, 2.5$  Hz, 1H), 7.83–7.79 (m, 3H), 7.47 (t,  $J = 9.1$  Hz, 1H), 7.28 (s, 1H), 6.40 (s, 1H), 6.35 (s, 1H), 4.28 (m, 1H), 4.18 (t,  $J = 6.5$  Hz, 2H), 4.11 (m, 1H), 3.95 (s, 3H), 3.07 (m, 1H), 2.98 (m, 4H), 2.78 (dd,  $J = 12.5, 5.0$  Hz, 1H), 2.53 (m, 1H), 2.04 (m, 4H), 1.79 (m, 2H), 1.51–1.16 (m, 18H);  $^{13}\text{C}$  NMR (100 MHz,  $\text{DMSO-}d_6$ )  $\delta$  171.9, 162.7, 157.1, 157.5, 149.0, 135.6, 125.1, 123.8, 119.0, 116.6 (d,  $J = 21.9$  Hz), 108.1, 103.7, 69.2, 61.0, 59.2, 56.2, 55.4, 38.3, 35.4, 35.2, 28.8, 28.4, 28.2, 28.0, 25.3, 23.8; IR (ATR) 3281 (br m), 2930 (m), 2857 (m), 1698 (m), 1635 (w), 1515 (m), 1498 (s), 1438 (s), 1204 (s), 1162 (s), 1043 (s), 1023 (s), 998 (s), 775 (m)  $\text{cm}^{-1}$ ; LC-MS (ESI):  $[\text{M} + \text{H}]^+$ ,  $m/z$  calculated for  $\text{C}_{37}\text{H}_{49}\text{ClFN}_7\text{O}_5\text{S}$  758.32, found 758.3

### Probe 1b



A yellow solid (8 mg, 14% yield over two steps).  $^1\text{H}$  NMR (400 MHz,  $\text{DMSO-}d_6$ )  $\delta$  8.48 (s, 1H), 7.99 (m, 1H), 7.90 (m, 1H), 7.86 (s, 1H), 7.75–7.70 (m, 2H), 7.39 (t,  $J = 7.9$  Hz, 1H), 7.20–7.18 (m, 2H), 6.40 (s, 1H), 6.34 (s, 1H), 4.27 (m, 1H), 4.18 (s, 1H), 4.15–4.11 (m, 3H), 3.93 (s, 1H), 3.06 (m, 1H), 2.98 (m, 4H), 2.80 (dd,  $J = 12.4, 5.0$  Hz, 1H), 2.56 (m, 1H), 2.03 (m, 4H), 1.81 (m, 2H), 1.56–1.16 (m, 18H);  $^{13}\text{C}$  NMR (100 MHz,  $\text{DMSO-}d_6$ )  $\delta$  171.9, 171.8, 162.7, 156.1, 154.4, 152.6, 148.4, 146.9, 139.8, 128.8, 124.8, 122.6, 121.7, 108.9, 107.2, 102.6, 83.5, 80.5, 68.8, 61.0, 59.2, 55.8, 55.4, 38.3, 35.4, 35.2, 28.8, 28.5, 28.2, 28.0, 25.4, 25.3, 23.8; IR (ATR) 3281 (br m), 2928 (m), 2855 (m), 1703 (s), 1636 (m), 1624 (m), 1428 (s), 1243 (s), 1211 (m), 1023 (s), 951 (m), 855 (m)  $\text{cm}^{-1}$ ; LC-MS (ESI):  $[\text{M} + \text{H}]^+$ ,  $m/z$  calculated for  $\text{C}_{39}\text{H}_{51}\text{N}_7\text{O}_5\text{S}$  730.37, found 730.4.

### Probe 1c



A yellow solid (7 mg, 20% yield over two steps).  $^1\text{H}$  NMR (400 MHz,  $\text{DMSO-}d_6$ )  $\delta$  9.80 (s, 1H), 8.53 (s, 1H), 8.17 (dd,  $J = 12.3, 2.3$  Hz, 1H), 7.92 (s, 1H), 7.75–7.71 (m, 3H), 7.56 (t,  $J = 8.7$  Hz, 1H), 7.20 (s, 1H), 6.40 (s, 1H), 6.34 (s, 1H), 4.28 (m, 1H), 4.15 (t,  $J = 6.4$  Hz, 2H), 4.10 (m, 1H), 3.93 (s, 3H), 3.07 (s, 1H), 2.98 (m, 4H), 2.80 (dd,  $J = 12.3, 5.0$  Hz, 1H), 2.57 (s, 1H), 2.04 (m, 4H), 1.80 (m, 2H), 1.55–1.15 (m, 18H);  $^{13}\text{C}$  NMR (100 MHz,  $\text{DMSO-}d_6$ )  $\delta$  171.9, 171.8, 162.7, 129.3, 126.5, 107.2, 61.0, 59.2, 55.9, 55.4, 38.3, 35.4, 35.2, 28.8, 28.5, 28.4, 28.2, 28.0, 25.4, 25.3, 23.8; IR (ATR) 3284 (br m), 2929 (m), 2856 (w), 1700 (s), 1635 (s), 1580 (m), 1428 (s), 1245 (m), 1213 (m), 1154 (m), 1022 (s), 857 (m)  $\text{cm}^{-1}$ ; LC-MS (ESI):  $[\text{M} + \text{H}]^+$ ,  $m/z$  calculated for  $\text{C}_{37}\text{H}_{49}\text{ClFN}_7\text{O}_5\text{S}$  758.32, found 758.3.

### 2.3 Purification of chemical probes

Compounds **1a–1c** were purified by reversed-phase HPLC using an Alltech Nucleosil C18 column (4.6 x 250 mm, particle size 5  $\mu\text{m}$ ). The mobile phase consisted of a gradient of 40–90% acetonitrile (B) in water with 0.1% TFA (A) over 9 minutes, followed by 9 minutes isocratic 90% B and then a gradient of 90–40% B in 3 minutes. The flow rate was 1.0 mL/min and the column compartment was kept at 25  $^\circ\text{C}$ . The fractions were then collected and lyophilised. Purity was confirmed by  $^1\text{H}$  NMR spectroscopy.

### 2.4 KINOMEscan<sup>TM</sup> binding assay

KINOMEscan<sup>TM</sup>  $K_d$  determination of chemical probes **1a–1c** for EGFR were performed by DiscoverX, San Diego, CA.<sup>178</sup> EGFR-tagged T7 phage strains were prepared in an *E. coli* host derived from the BL21 strain. *E. coli* were grown to log-phase, infected with T7 phage and incubated with shaking at 32 $^\circ\text{C}$  until lysis. The lysates were centrifuged and filtered to remove cell debris. Streptavidin-coated magnetic beads were treated with biotinylated small-molecule ATP mimics for 30 minutes at room temperature to generate affinity resins for the binding assay. The liganded beads were blocked with excess biotin and washed with blocking buffer (SeaBlock (Pierce), 1% BSA, 0.05% Tween 20, 1 mM DTT) to remove unbound ligand and to reduce non-specific binding. Binding reactions were assembled by combining the target kinase (EGFR), liganded affinity beads, and test compound (**1a–1c** and **6b**) in 1x binding buffer (20% SeaBlock, 0.17x PBS, 0.05% Tween 20, 6 mM DTT). All reactions were performed in polystyrene 96-well plates in a final volume of 0.135 ml. The assay plates were incubated at room temperature with shaking for 1 hour and the affinity beads were washed with wash buffer (1x PBS, 0.05% Tween 20). The beads were then re-suspended in elution buffer (1x PBS, 0.05% Tween 20, 0.5  $\mu\text{M}$  non-biotinylated affinity ligand) and incubated at room temperature with shaking for 30 minutes. The kinase

concentration in the eluates was measured by qPCR. All test were done in duplicates. Binding constants ( $K_d$ 's) were calculated with a standard dose-response curve using the Hill equation:

$$\text{Response} = \text{Background} + \frac{\text{Signal} - \text{Background}}{1 + \left( \frac{K_d^{\text{Hill slope}}}{\text{Dose}^{\text{Hill slope}}} \right)}$$

The Hill Slope was set to -1. Curves were fitted using a non-linear least square fit with the Levenberg-Marquardt algorithm.

### 3. RESULTS AND DISCUSSION

#### 3.1 EGFR Probes design

The identification of synergistic effects of combination therapy has inspired the quest of multitargeted inhibitors for EGFR. In 2010, Cai and coworkers reported the synthesis of a dual-probe directed against EGFR/ErbB2 and histone deacetylases (HDACs).<sup>177</sup> The strategy was to tether a 4-anilinoquinazoline moiety (targeting EGFR/ErbB2) and a hydroxamic acid (targeting HDACs) with a linker of appropriate length for dual inhibition of both EGFR/ErbB2 and HDACs. Crystal structures of 4-anilinoquinazolines bound to EGFR showed that position C6 and C7 of the 4-anilinoquinazoline core may be in the more solvent exposed region (Fig. 3.1).<sup>119</sup> Moreover, substituents at these C6 and C7 positions in the 4-anilinoquinazoline core of gefitinib and erlotinib have been found to improve drug pharmacodynamics.<sup>118</sup> Therefore, these positions were predicted to be suitable for the introduction of a linker.

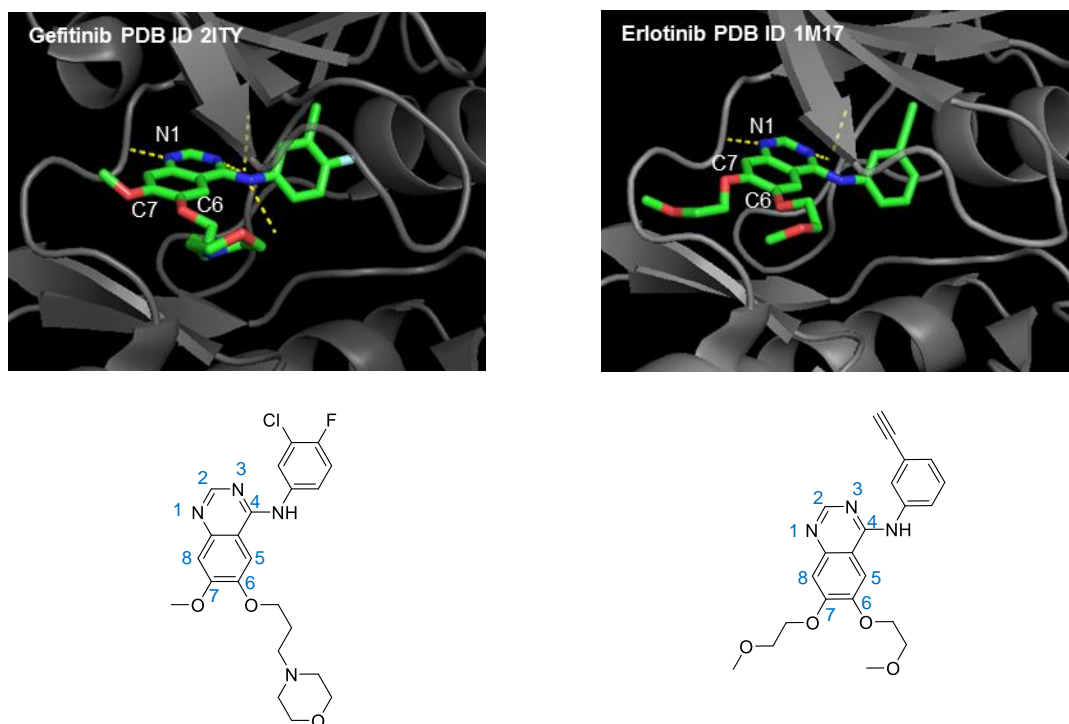


**Fig. 3.1** Crystal structures of gefitinib and erlotinib bound to the EGFR ATP site.  
(Images created by PyMOL from indicated PDB files)

IC<sub>50</sub> values of these dual inhibitors against EGFR in vitro (entries 3, 4, 5, 6, 7 and 8 in Table 3.1) were lower than those of erlotinib (entry 1). SAR studies showed that EGFR inhibition was largely unaffected by the change in linker length and substitution on the aniline core, but the optimal IC<sub>50</sub> value was observed with a heptanoate linker (entries 5 and 6). Changing this heptanoate linker from C6 to C7 (entries 7 and 8) produced a slight 2–3-fold increase in



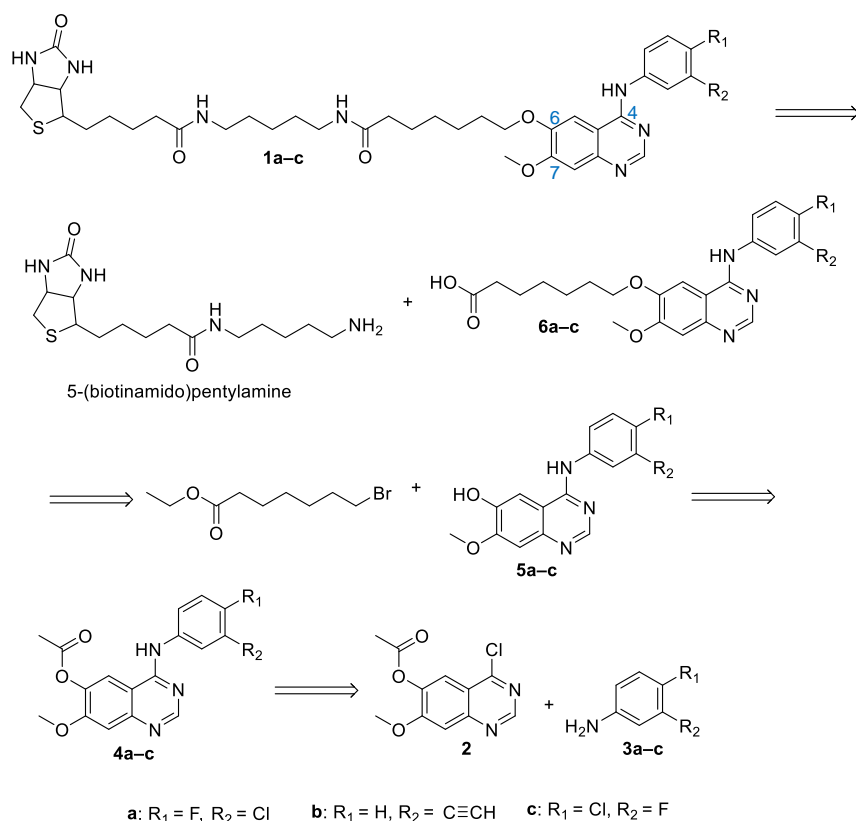
IC<sub>50</sub>, thus position C6 was preferred over C7 for linker attachment. This is consistent with the crystallographic structural data that indicated potentially improved accessibility at the C6 position (Figure 3.1). In another instance, Boyce and coworkers reported the synthesis of an irreversible EGFR probe bearing a BODIPY fluorophore tag attached to C6 through a PEG linker (entry 10).<sup>173</sup> Compared to the parent 4-anilinoquinazoline (entry 9), the probe showed only a 2.8-fold increase in IC<sub>50</sub> values.

**Table 3.1** SAR studies of previously reported EGFR probes.<sup>173, 177</sup>

Entry	Structure	IC <sub>50</sub> (nM)	Ref.
1		48.0	177
2		7.1	177
3	R <sub>1</sub> = F, R <sub>2</sub> = Cl 	9.4	177
4	R <sub>1</sub> = H, R <sub>2</sub> = C≡CH 	15.0	177
5	R <sub>1</sub> = F, R <sub>2</sub> = Cl 	3.1	177
6	R <sub>1</sub> = H, R <sub>2</sub> = C≡CH 	2.4	177
7	R <sub>1</sub> = F, R <sub>2</sub> = Cl 	7.0	177
8	R <sub>1</sub> = H, R <sub>2</sub> = C≡CH 	8.2	177
9		29	173
10		80	173

Encouraged by these results, for our first-generation EGFR probes, we aimed to modify 4-anilinoquinazolines with an affinity tag through a heptanoate linker in position C6 (Compounds **1a–1c** in Scheme 3.1) in order to test first if the C6 position would be amenable

to extended linker sizes without substantial loss of affinity. Biotin, as the most common affinity tag, with strong binding to avidin/streptavidin/neutravidin ( $K_d \approx 10^{-14}$ – $10^{-15}$  M) and low interference with the function of modified molecules, was chosen for the first-generation probes.<sup>160</sup> In some cases, biotinylated probes can be used in live cells, allowing for identification of target proteins in an endogenous environment.<sup>179</sup>



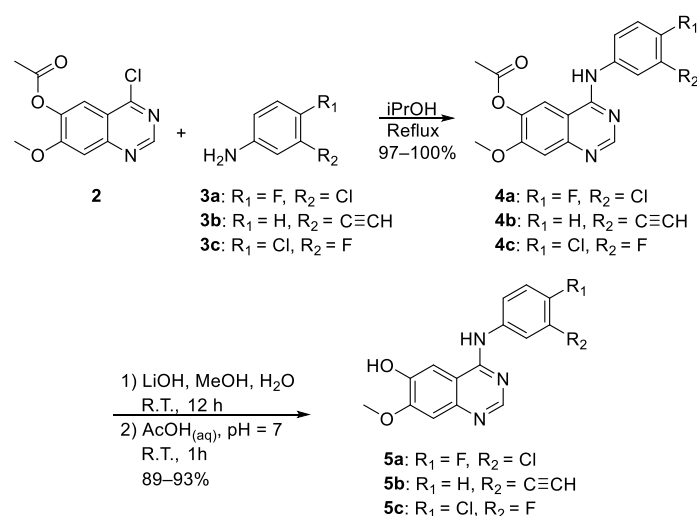
**Scheme 3.1** Design and retrosynthetic analysis of first-generation EGFR probes **1a–1c**.

The retrosynthetic analysis of the first-generation EGFR probes **1a–1c** is shown in Scheme 3.1. The biotin affinity tag could be readily introduced from commercially available 5-(biotinamido)pentylamine through an amidation reaction. The synthetic approach of 4-anilinoquinazolines has been reported and usually involves a  $S_NAr$  reaction between 4-chloroquinazoline and an aniline.<sup>118</sup> The synthesis of 4-anilinoquinazolines **5a–5c** follows the methods reported by Cai and coworkers.<sup>177</sup> To maintain the core structures of erlotinib and gefitinib, which bind EGFR with high affinity ( $K_d = 0.67$  nM and 1.0 nM respectively) with known selectivity profiles,<sup>115</sup> we selected 3-chloro-4-fluoroaniline (**3a**) and 3-ethynylaniline (**3b**) as starting anilines for the  $S_NAr$  reaction with 4-chloroquinazoline. 4-Chloro-3-fluoroaniline (**3c**), an aniline similar to **3a**, was also used to interrogate the effect of the halogen positions on binding affinity, as future derivatisation reactions could be enabled at these halogenated positions via cross-coupling reactions.<sup>180</sup> The 4-

anilinoquinazolines **4a–4c** could be prepared readily from commercially available 4-chloro-7-methoxyquinazolin-6-yl acetate (**2**) as the quinazoline core. Upon formation of the 4-anilinoquinazoline scaffolds **4a–c**, the acetyl group would then be removed to afford the anilinoquinazolin-6-ols **5a–c**, which are suitable for alkylation with a heptanoate linker through an S<sub>N</sub>2 reaction as previously reported.<sup>177</sup> Once prepared, these probes would be tested in binding assays to inform on the feasibility of obtaining next generation multifunctional probes through the C6 position.

## 3.2 Probes synthesis

### 3.2.1 Synthesis of 4-anilinoquinazoline binding groups



**Scheme 3.2** Synthesis of 4-anilinoquinazoline binding groups.

Compounds **5a–c** were synthesized following reported methods with modifications (Scheme 3.2).<sup>118, 177</sup> Coupling of 4-chloro-7-methoxyquinazolin-6-yl acetate (**2**) with anilines **3a–c** afforded the corresponding 6-acetyloxy protected 4-anilinoquinazolines **4a–c** with excellent yields, and the precipitated products were used without the need for further purification. Hydrolysis of compounds **4a–c** with LiOH followed by protonation with diluted acetic acid provided the corresponding 4-anilinoquinazolin-6-ols **5a–c** in good yields. The addition of acetic acid was carefully controlled, as the reported synthesis of **5a** with excess of acid afforded two products as indicated by TLC. From <sup>1</sup>H NMR spectroscopy, the two products were assigned as the expected product **5a** and its corresponding quinazolonium salt (Fig. 3.2). Protonation of **5a** at acidic pH is expected to occur at the N1 position, which is the most basic nitrogen due to the resonance stabilization of the conjugate acid. When only one equiv of acetic acid was used, protonation of **5a** was not observed. Compounds **4a–4b** and **5a–5b**

had been previously reported, however without their full structural characterisation. Here these compounds were obtained with higher or comparable yields respectively.<sup>177</sup>

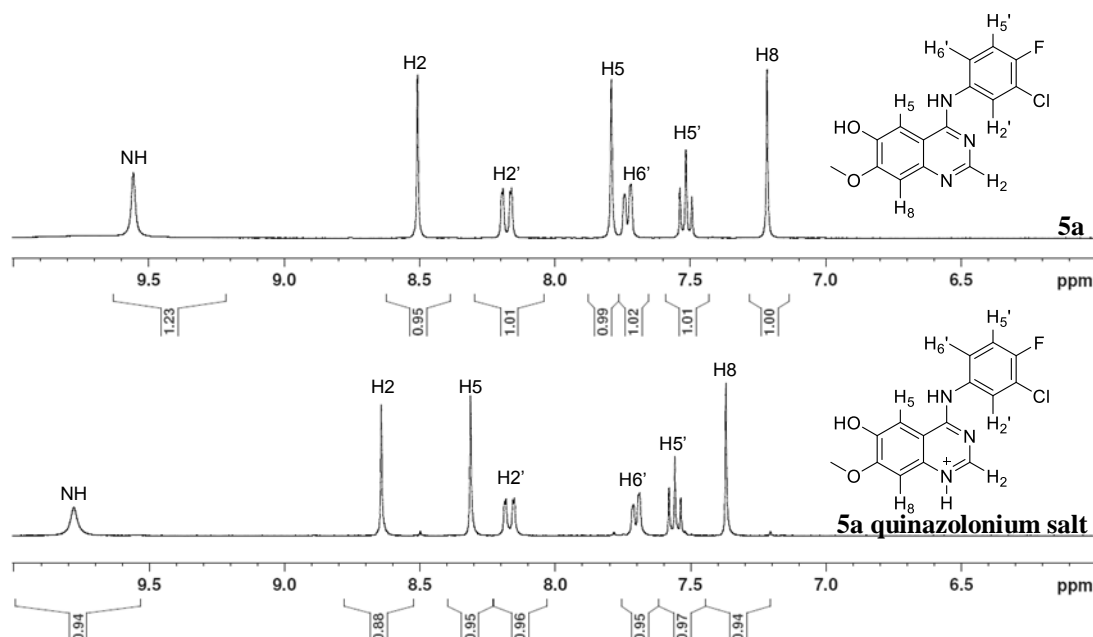


**Fig. 3.2**  $^1\text{H}$  NMR spectrum of compound **5a** and its corresponding quinazolonium salt.

Compounds **4c** and **5c** have not been previously reported, and NMR characterisation ( $^1\text{H}$ ,  $^{13}\text{C}$  and HSQC spectroscopy) was conducted to ensure correct structural assignments (Fig. 3.3).  $^1\text{H}$  NMR spectrum indicated the expected total of 11 protons (Fig. 3.3 a). The three singlets at 8.51, 7.79 and 7.22 ppm correspond to protons H2, H5 and H8 of the quinazoline, and their chemical shifts are similar to those reported for compounds **5a** and **5b**.<sup>177</sup> The differences in the  $^1\text{H}$  NMR spectrum of **5c** compared to its structural isomer **5a** arose from the signals corresponding to the aniline core. The multiplets corresponding to the aniline core in **5c** at 8.18 ( $J_{\text{H2}'\text{-F}} = 12.5$  Hz,  $J_{\text{H2}'\text{-H6}'} = 2.3$  Hz), 7.73 and 7.52 ( $J_{\text{H5}'\text{-F}} = J_{\text{H5}'\text{-H6}'} = 8.7$  Hz) ppm were assigned according to their H-H and H-F coupling constants.  $^{13}\text{C}$  NMR spectrum indicated the expected total of 15 carbons (Fig. 3.3 b). The carbon signals at 156.8 ( $J_{\text{C3}'\text{-F}} = 242.7$  Hz), 109.0 ( $J_{\text{C2}'\text{-F}} = 25.7$  Hz), 112.0 ( $J_{\text{C4}'\text{-F}} = 17.6$  Hz), 140.7 ( $J_{\text{C1}'\text{-F}} = 10.7$  Hz) and 117.8 ( $J_{\text{C6}'\text{-F}} = 3.1$  Hz) ppm were correlated to the aniline core according to their C-F coupling constants. These assignments are confirmed by H-C correlations in the HSQC spectrum (Fig. 3.3 c). As an example, the signals corresponding to C2'/H2', C5'/H5' and C6'/H6' correlations in the HSQC spectrum were in agreement with H-F and C-F coupling constants observed in  $^1\text{H}$  and  $^{13}\text{C}$  NMR spectra. The spectroscopic data for compound **5c** was used as a reference for the structural characterisation of compounds **1c**, **4c**, **6c** and **7c** derivative of the same aniline structure.

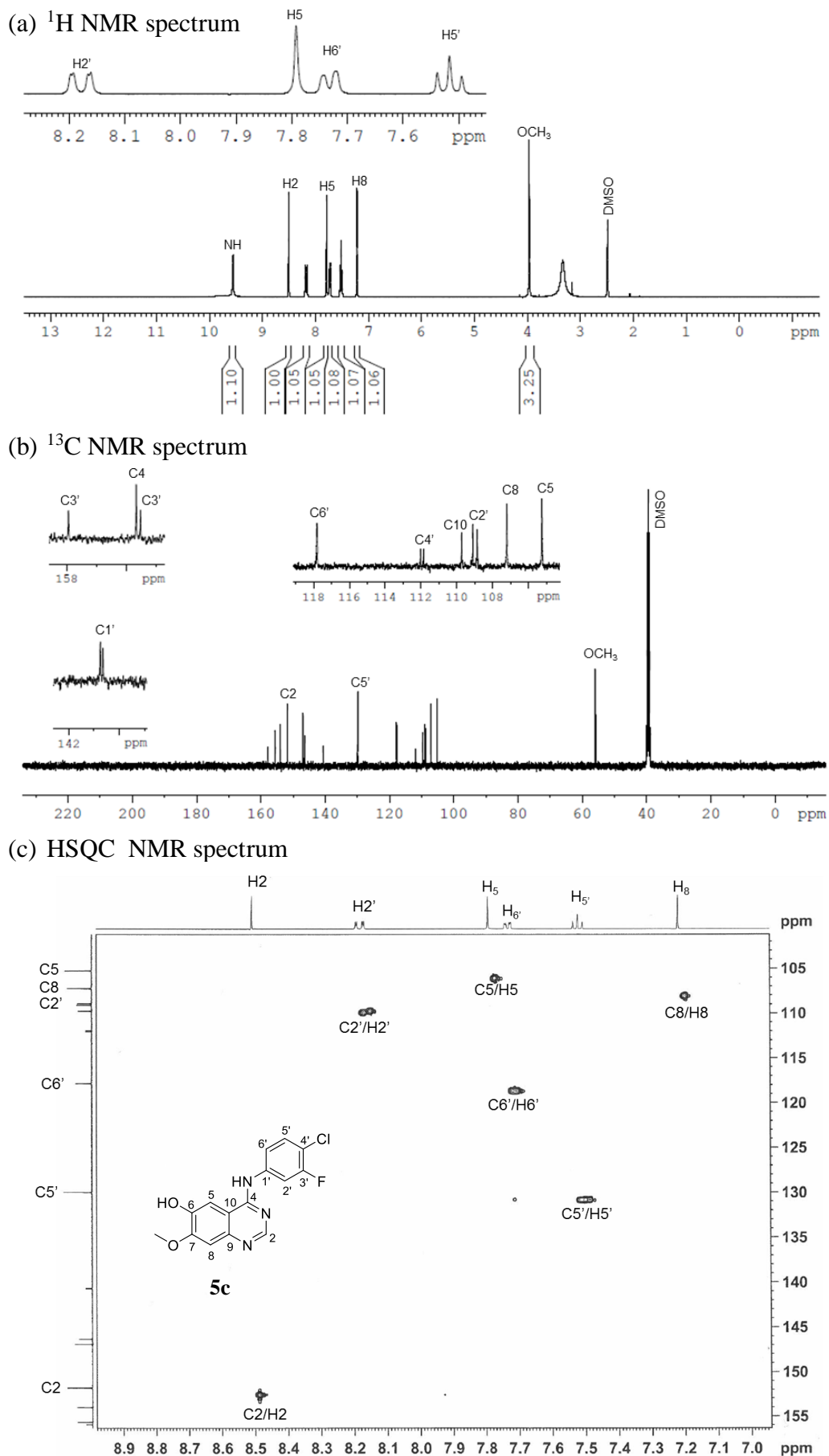
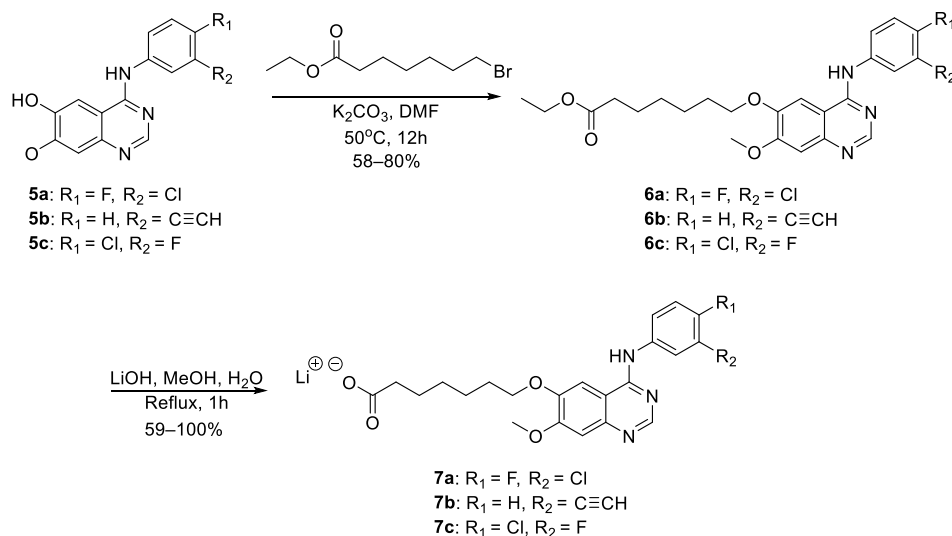


**Fig. 3.3**  $^1\text{H}$ ,  $^{13}\text{C}$  and HSQC NMR spectra of compound **5c**.

### 3.2.2 Linker attachment at the C6 position



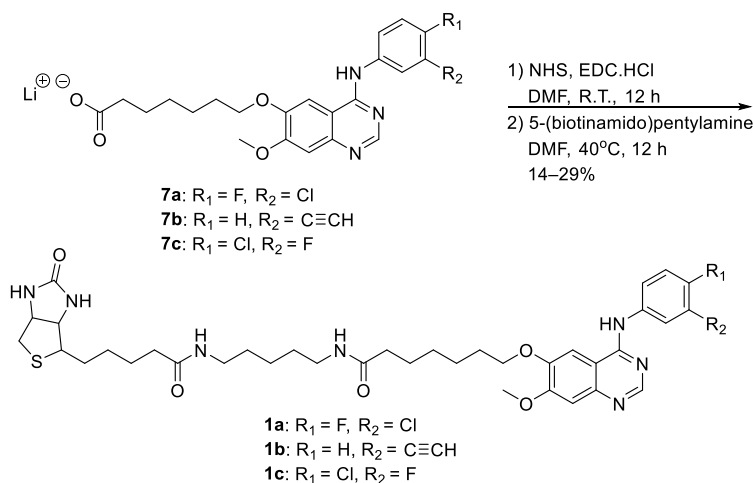
**Scheme 3.3** Attachment of the heptanoate linker to the C6 position of the 4-anilinoquinazoline core.

The alkylation  $S_N2$  reaction of compound **5a** with ethyl 7-bromoheptanoate in the presence of  $K_2CO_3$  to furnish compound **6a** has been previously reported in moderate yield (53%).<sup>177</sup> The reproduction of these reported conditions (1.0 equiv **5a**, 1.1 equiv ethyl 7-bromoheptanoate, 2.4 equiv  $K_2CO_3$ ,  $40^\circ C$ , 3h) for compound **6a** afforded this compound in low yield (~35%). Reduction in the molar ratio of carbonate base (1.1 equiv) was then applied because excess base may generate adventitious hydroxide with moisture and hydrolyse ethyl 7-bromoheptanoate prematurely. To compensate for the reduction of the base equivalence that may slow down the reaction, temperature was raised from 40 to  $50^\circ C$  and time extended from 3 to 12h. This modified procedure improved the yield to up to 80% for all alkylation products **6a–6c** (Scheme 3.3). After flash column chromatography purification, compounds **6a–c** were hydrolysed with  $LiOH$  to obtain the corresponding carboxylate salts **7a–7c** in moderate to excellent yields (Scheme 3.3). The conversion to these carboxylates was readily verified by the loss of ethoxy signals in the  $^1H$  (4.09–4.02 and 1.22 ppm) and  $^{13}C$  NMR (60.4 and 14.2 ppm) spectra.

### 3.2.3 Attachment of the biotin affinity tag

To attach the amine-terminal biotin tag, the carboxylate salts **7a–7c** were first converted to their corresponding activated succinimidyl esters through EDC coupling (Scheme 3.4). Upon confirmation of product formation by TLC the activated esters were isolated by precipitating by-products in chloroform followed by filtration and lyophilisation. The isolated activated esters were then used without further purification in the amidation reaction

with 5-(biotinamido)pentylamine, which afforded the corresponding biotinylated probes **1a–1c**. After flash column chromatography purification, probes **1a–1c** were obtained in unoptimised yields (14–29%) over two steps.



**Scheme 3.4** Attachment of biotin tag to carboxylate salts **7a–7c**.

### 3.3 Probes purification and characterization

The structural characterisation of the chemical probes **1a–1c** was performed via <sup>1</sup>H and <sup>13</sup>C NMR spectroscopy as well as IR spectroscopy and LC-MS. The characterization of probe **1c** is discussed here as a typical sample. Complete spectra for probes **1a–1c** are located in the Appendix A1. In the <sup>1</sup>H NMR spectrum of **1c**, the multiplicity and chemical shifts of the signals in the region of 8.53–7.20 ppm corresponding to the 4-anilinoquinazoline core were comparable to those described for the precursor **5c** in Section 3.2.1. The presence of the biotin tag was confirmed by its characteristic signals, including the protons marked as H<sub>a</sub> and H<sub>b</sub> at 6.40 and 6.35 ppm, protons H<sub>c</sub> and H<sub>d</sub> at 4.28 and 4.11 and proton H<sub>e1</sub> at 2.81 respectively (Fig. 3.4). In the <sup>13</sup>C NMR spectrum, some characteristic signals of the biotin tag included the carbonyl carbons of amides at 171.9 and 171.8 ppm, the biotin carbonyl at 162.7, and carbons C<sub>d</sub> and C<sub>c</sub> at 61.0 and 59.2 ppm respectively (Fig. 3.4).

IR spectroscopic data are consistent with the NMR evidence, showing the N-H stretching vibration at 3284 cm<sup>-1</sup> for the biotin N-H groups. Compared to the starting material, the intensity of methylene C-H stretching at 2929 cm<sup>-1</sup> and 2856 cm<sup>-1</sup> is higher due to the methylene groups in both the heptanoate linker and the 5-(biotinamido)pentylamine tag. The presence of two carbonyl groups of different nature is also observed in the region between 1600 cm<sup>-1</sup> and 1700 cm<sup>-1</sup>. The C=O stretching vibration at lower frequency (1635 cm<sup>-1</sup>) is characteristic of secondary amides, present both in the biotin tag and the newly formed amide

bond, while the peak at higher frequency ( $1700\text{ cm}^{-1}$ ) is typically observed in the biotin moiety. LC-MS analysis of **1c** showed the presence of a single compound with a  $m/z$  of 758.3 ( $[M + H]^+$   $m/z$  calculated for  $C_{37}H_{49}ClFN_7O_5S$  758.32), corresponding to monoprotonated **1c**. All probes (**1a–1c**) analysed by LC-MS produced the expected  $m/z$  ratios.

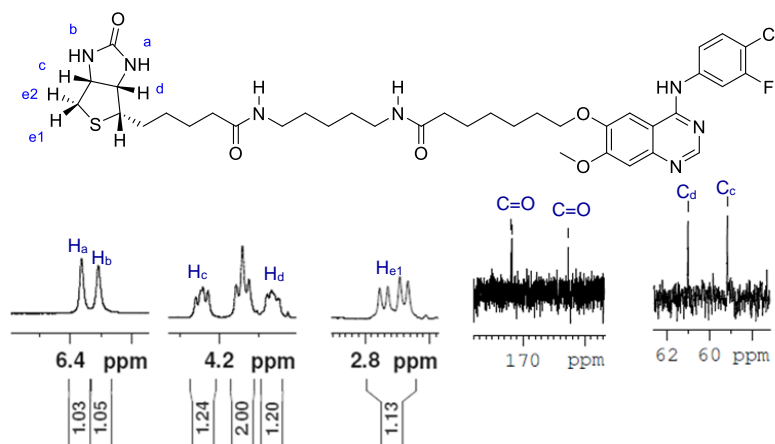


**Fig. 3.4** Selected regions of  $^1\text{H}$  and  $^{13}\text{C}$  NMR spectra of probe **1c** showing characteristic signals of the biotin tag.

All biotinylated probes were purified by HPLC before biological testing. A representative chromatogram from the purification of chemical probe **1b** is shown in Fig. 3.5, typically from runs using a gradient of 40–90% acetonitrile in water with 0.1% TFA over 9 minutes at 1.0 mL/min. After lyophilisation, the purified probes were analysed again by  $^1\text{H}$  NMR to confirm probe purity.

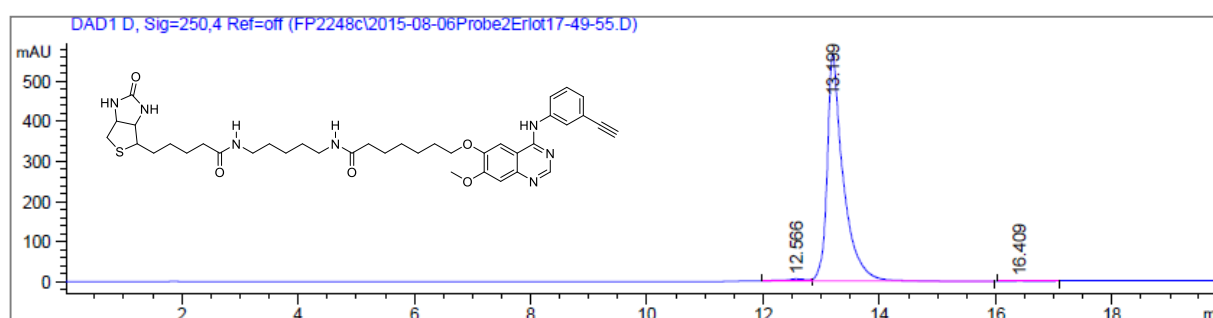


**Fig. 3.5** A representative chromatogram from compound **1b** purification.

### 3.4 Binding assays

To evaluate probes **1a–1c** binding affinity against EGFR,  $K_d$  values were determined by KINOMEScan<sup>TM</sup> assay (performed by DiscoverX, San Diego, CA, detailed results in appendix A2). Briefly, the molecules to test (probes **1a–1c**) compete for binding between a DNA-tagged kinase of interest (EGFR in this case) and a known ligand immobilized in solid



beads (Fig. 3.6). Non-binding compounds have no effect on the amount of kinase captured. Binding compounds prevent kinase binding to the immobilized ligands, reducing the amount of kinase captured on beads. Compounds of interest are tested at different concentrations, and the amount of kinase captured on beads with or without a binding compound is measured by qPCR that detects the associated DNA label. Binding KINOMEScan™ assays have several advantages over in vitro enzymatic assays.<sup>178</sup> Unlike IC<sub>50</sub> determinations, KINOMEScan™ assays do not require ATP or a substrate, and they report a measure of direct binding affinity rather than activity. As these results are not dependant on ATP or on the specific choice of a substrate, the binding affinity values allow a more direct comparison of experimental results. Thus, although  $K_d$  and IC<sub>50</sub> values may correlate, they may not be directly comparable. Erlotinib, for example, has a strong affinity for EGFR (entry 1 in Table 3.2,  $K_d$  = 0.67 nM), but its IC<sub>50</sub> presents a 72-fold difference (entry 1 in Table 3.1, IC<sub>50</sub> = 48 nM).

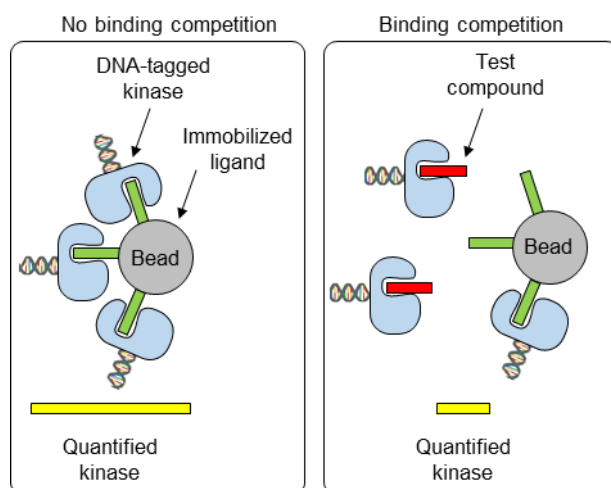


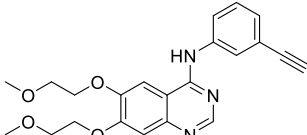
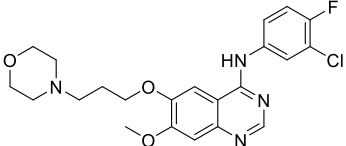
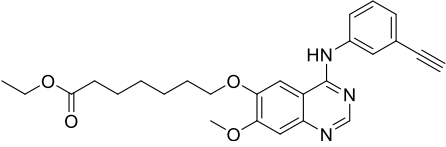
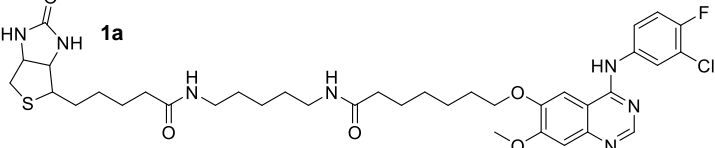
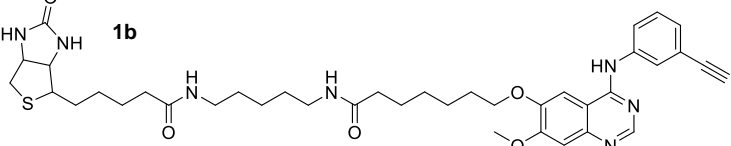
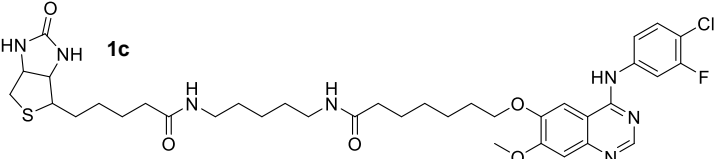
**Fig. 3.6** Schematic representation of the KINOMEScan™ binding assays.

To assess the effect of biotin tag attachment on binding potency against EGFR, the  $K_d$  of compound **6b**, precursor of probe **1b** was also evaluated, along with **1a–1c**. The  $K_d$  values are reported in Table 3.2. As a reference, the reported  $K_d$  values of erlotinib and gefitinib determined with the same methodology are included as well (entries 1 and 2 respectively).

The non-biotinylated compound **6b** with a short linker but without the biotin tag showed high binding affinity for EGFR (entry 3,  $K_d$  = 1.5 nM). The core structure of **6b** is identical to erlotinib (entry 1), and their  $K_d$  values are in close proximity (1.5 vs 0.67 nM) with only a 2-fold difference. This  $K_d$  value for **6b** also correlates with the reported IC<sub>50</sub> of compound **6** in Table 3.1 (IC<sub>50</sub> = 2.4 nM)<sup>177</sup>, which differs only in the terminal group next to the

carbonyl (hydroxylamine instead of ethoxy). The high binding affinity of **6b** confirms the efficiency of this 4-anilinoquinazoline scaffold for accessing effective EGFR inhibitors or probes, and supports previous observations that position C6 is suitable for various linker attachments.

**Table 3.2** Binding affinity of chemical probes **1a–1c** and selected reference compounds against EGFR.

Entry	Compound	$K_d$ (nM)
1	Erlotinib 	0.67 <sup>115</sup>
2	Gefitinib 	1.0 <sup>115</sup>
3	<b>6b</b> 	1.5
4	<b>1a</b> 	23
5	<b>1b</b> 	34
6	<b>1c</b> 	41

The introduction of the biotin tag in compound **1b** was accompanied with a 23-fold increase in its  $K_d$  (entry 5,  $K_d = 34$  nM) compared to the non-biotinylated precursor **6b** (entry 3,  $K_d = 1.5$  nM) and a 51-fold difference with the analogous drug erlotinib (entry 1,  $K_d = 0.67$  nM). The binding affinity of **1b**, however, remains in the low nM concentration. Likewise, the biotinylated probe **1a** presents a  $K_d$  in the low nM concentration (entry 4,  $K_d = 23$  nM), with a 23-fold increase compared to the analogous drug gefitinib (entry 2,  $K_d = 1.0$  nM). This data

suggest that the linker length in probes **1a** and **1b**, while resulting in binding affinity loss, is acceptable, as the binding affinities of these probes (**1a** and **1b**) for EGFR are still maintained well below 100 nM.

As seen from the  $K_d$  values of probes **1a–1c** in Table 3.2, the different substitution patterns in the aniline scaffold do not significantly impact on the binding affinity of the probes. This data was consistent with previous SAR studies, as the substituents in the aniline ring are usually well tolerated.<sup>118, 177</sup> The  $K_d$  value of the compound **1c** was also well below the 100 nM limit recommended for high-quality probes, confirming the utility of these chemical probes. Taken together, these data demonstrate that chemical probes for EGFR with good binding affinity can be rapidly accessed through the modification of 4-anilinoquinazolines at the C6 position with an appropriate linker length (heptanoate).

Based on the retention of binding affinity observed for the biotinylated chemical probes **1a–1c**, these structures stand as promising candidates for further modification into high-quality multifunctional chemical probes. Recently, some EGFR inhibitors have been modified with other chemical structures aiming to obtain dual TKIs, for example EGFR/MET and EGFR/Src inhibitors (Fig. 3.7).<sup>181, 182</sup> The introduction of these multi-targeting approaches in our reported biotinylated probes might be a starting point to the development of multifunctional EGFR probes.

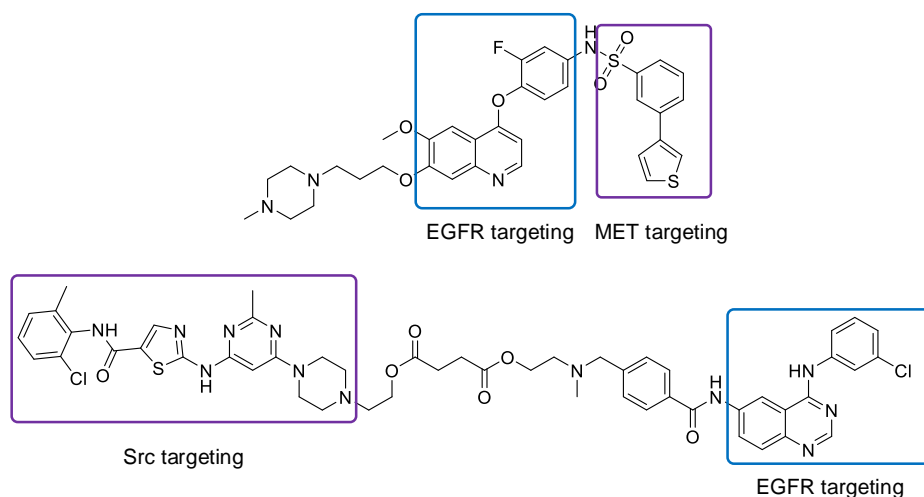


**Fig. 3.7** Structure of some recently reported dual EGFR inhibitors.<sup>181, 182</sup>

#### 4. CONCLUSIONS AND FUTURE DIRECTIONS

EGFR is a canonical RTPK, and EGFR signalling activity remains a highlight of protein kinase chemistry in general. EGFR activity is highly dependent on its conformational state, which is regulated by PTMs and interaction with protein partners. In addition to the complex protein characteristics of EGFR itself, the different signaling pathways triggered by EGFR integrate into highly interconnected networks. Although the redundant and robust characteristics of this network are essential for homeostasis, the same features are harnessed in malignancies.

EGFR was one of the first RTPKs to be linked to human cancers, prompting the development of EGFR targeted therapies. Many EGFR inhibitors based on 4-anilinoquinazolines have been developed. Currently, five EGFR inhibitors have received FDA approval. However, successful EGFR-targeted therapies have been limited in some cancers due to EGFR mutations, especially for NSCLC. Furthermore resistance is a challenge to overcome in EGFR-targeted therapy. Numerous studies have highlighted the role of other signaling proteins conferring resistance to EGFR-targeted therapies.

Recent studies have shown the utility of combination therapies in overcoming reprogramming resistance mechanisms, as well as the identification of new mechanisms.<sup>183, 184</sup> They have also shown that genetic analyses alone are insufficient to configure tumor specific combination therapies. This highlights the importance of interrogating protein interactions, especially EGFR, in their endogenous environment. Understanding endogenous EGFR signaling networks may be aided by the development of molecular tools that shed light on endogenous protein interactions. EGFR probes have already demonstrated utility in determining active site occupancy, IC<sub>50</sub> values of EGFR inhibitors, and windows of selectivity for irreversible inhibitors.

In this work, we synthesized biotinylated chemical probes targeting EGFR based on 4-anilinoquinazolines modified at the C6 position, which is a less explored attachment site in A/BPs. Through the proper selection of linker length (heptanoate), the probes retained  $K_d$  values well below 100 nM recommended for high-quality probes. These first generation probes will be further modified with other linkers of various length and branching points, other reporter groups and other cross-linking groups to obtain next-generation multifunctional chemical probes (Fig. 4.1).

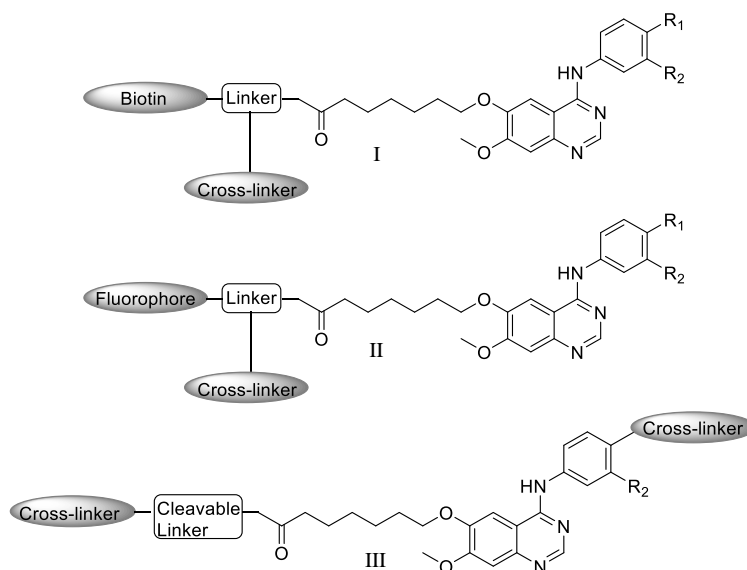


**Fig. 4.1** Schematic representation of potential second-generation EGFR chemical probes.

For example, a photo-reactive group could be attached to the biotinylated probes to covalently modify EGFR (I, Fig. 4.1). Labelled EGFR proteins could then be enriched and analysed by MS to confirm EGFR identity, PTMs and also potential off-targets. This approach has been explored with other PK inhibitors and allowed identification of off-targets.<sup>167</sup> In another approach, the 4-anilinoquinazoline scaffold could be modified with an electrophilic “warhead” or other reactive group and a fluorophore to obtain an imaging probe for EGFR visualization (II, Fig. 4.1). Such imaging probes for EGFR have shown success using a resorcinol acid derivative scaffold.<sup>185</sup> If the probe size needs to be limited to ensure cell permeability, a “click” handle may also be installed for attaching the reporter groups after the capturing step in cell lysates.<sup>168</sup> In yet another approach, these probes could be modified with two cross-linkers spaced with a cleavable linker to covalently modify both EGFR and proximal protein partners (III, Fig. 4.1). The identity of cross-linked proteins could then be determined by MS.<sup>186</sup> Thus, this strategy might potentially elucidate the nature of endogenous EGFR signaling complexes. The characterization of these signaling complexes might shed light on the resistance mechanisms in malignant cells and provide potentially new combination targets to improve on existing EGFR-based therapeutics.

## REFERENCES

1. Manning, G.; Whyte, D. B.; Martinez, R.; Hunter, T., *Science* **2002**, 298, 1912-1934.
2. Hunter, T.; Manning, G., The Eukaryotic Protein Kinase Superfamily and the Emergence of Receptor Tyrosine Kinases In *Receptor Tyrosine Kinases: Structure, Functions, and Role in Human Disease.*, Wheeler, D. L.; Yarden, Y., Eds. Humana Press: 2014; pp 1-16.
3. Endicott, J. A.; Noble, M. E.; Johnson, L. N., *Annu. Rev. Biochem.* **2012**, 81, 587-613.
4. Johnson, L. N.; Lewis, R. J., *Chem. Rev.* **2001**, 101, 2209-2242.
5. Cohen, P., *Nat. Cell Biol.* **2002**, 4, E127-E130.
6. Kobe, B.; Kemp, B. E., Principles of kinase regulation. In *Handbook of Cell Signaling*, 1 ed.; Dennis, E. A.; Bradshaw, R. A., Eds. Academic Press: 2003; Vol. 2.
7. Endres, N. F.; Barros, T.; Cantor, A. J.; Kuriyan, J., *Trends Biochem. Sci.* **2014**, 39, 437-446.
8. Huse, M.; Kuriyan, J., *Cell* **2002**, 109, 275-282.
9. Tong, M.; Seeliger, M. A., *ACS Chem. Biol.* **2015**, 10, 190-200.
10. Jura, N.; Zhang, X.; Endres, N. F.; Seeliger, M. A.; Schindler, T.; Kuriyan, J., *Mol. Cell* **2011**, 42, 9-22.
11. Taylor, S. S.; Keshwani, M. M.; Steichen, J. M.; Kornev, A. P., *Philos. Trans. R. Soc., B* **2012**, 367, 2517-2528.
12. Taylor, S. S.; Kornev, A. P., *Trends Biochem. Sci.* **2011**, 36, 65-77.
13. Kornev, A. P.; Taylor, S. S., *Biochim. Biophys. Acta* **2010**, 1804, 440-444.
14. Endicott, J. A.; Noble, M. E. M.; Johnson, L. N., *Annu. Rev. Biochem.* **2012**, 81, 587-613.
15. Blume-Jensen, P.; Hunter, T., *Nature* **2001**, 411, 355-365.
16. Hanahan, D.; Weinberg, R. A., *Cell* **2011**, 144, 646-674.
17. Patterson, H.; Nibbs, R.; McInnes, I.; Siebert, S., *Clin. Exp. Immunol.* **2014**, 176, 1-10.
18. Chico, L. K.; Van Eldik, L. J.; Watterson, D. M., *Nat. Rev. Drug Discov.* **2009**, 8, 892-909.
19. Dorn, G. W.; Force, T., *J. Clin. Invest.* **2005**, 115, 527-537.
20. Wang, Y., *Circulation* **2007**, 116, 1413-1423.
21. Cohen, P., *Nat. Rev. Drug Discov.* **2002**, 1, 309-315.
22. Cohen, P.; Alessi, D. R., *ACS Chem. Biol.* **2013**, 8, 96-104.
23. Rask-Andersen, M.; Zhang, J.; Fabbro, D.; Schioth, H. B., *Trends Pharmacol. Sci.* **2014**, 35, 604-620.
24. Zhang, J.; Yang, P. L.; Gray, N. S., *Nat. Rev. Cancer* **2009**, 9, 28-39.
25. Rask-Andersen, M.; Masuram, S.; Schioth, H. B., *Annu. Rev. Pharmacol. Toxicol.* **2014**, 54, 9-26.
26. Imai, K.; Takaoka, A., *Nat. Rev. Cancer* **2006**, 6, 714-727.
27. Fabbro, D.; Cowan-Jacob, S. W.; Mobitz, H.; Martiny-Baron, G., Targeting cancer with small-molecular-weight kinase inhibitors. In *Kinase inhibitors: methods and protocols*, Kuster, B., Ed. 2012; Vol. 795.
28. Liu, Q.; Sabnis, Y.; Zhao, Z.; Zhang, T.; Buhrlage, S. J.; Jones, L. H.; Gray, N. S., *Chem. Biol.* **2013**, 20, 146-159.
29. van Linden, O. P.; Kooistra, A. J.; Leurs, R.; de Esch, I. J.; de Graaf, C., *J. Med. Chem.* **2014**, 57, 249-277.
30. Traxler, P.; Furet, P., *Pharmacol. Ther.* **1999**, 82, 195-206.
31. Liao, J. J.-L., *J. Med. Chem.* **2007**, 50, 409-424.
32. Zuccotto, F.; Ardini, E.; Casale, E.; Angiolini, M., *J. Med. Chem.* **2010**, 53, 2681-2694.

33. Liu, Y.; Gray, N. S., *Nat. Chem. Biol.* **2006**, *2*, 358-364.
34. Zhao, Z.; Wu, H.; Wang, L.; Liu, Y.; Knapp, S.; Liu, Q.; Gray, N. S., *ACS Chem. Biol.* **2014**, *9*, 1230-41.
35. Foda, Z. H.; Seeliger, M. A., *Nat. Chem. Biol.* **2014**, *10*, 796-797.
36. Cox, K. J.; Shomin, C. D.; Ghosh, I., *Future Med. Chem.* **2011**, *3*, 29-43.
37. Lamba, V.; Ghosh, I., *Curr. Pharm. Des.* **2012**, *18*, 2936-2945.
38. Capdeville, R.; Buchdunger, E.; Zimmermann, J.; Matter, A., *Nat. Rev. Drug Discov.* **2002**, *1*, 493-502.
39. Wu, P.; Nielsen, T. E.; Clausen, M. H., *Trends Pharmacol. Sci.* **2015**, *36*, 422-439.
40. Fabbro, D.; Cowan-Jacob, S. W.; Moebitz, H., *Br. J. Pharmacol.* **2015**, *172*, 2675-2700.
41. Weinstein, I. B.; Joe, A. K., *Nat. Clin. Pract. Oncol.* **2006**, *3*, 448-457.
42. Torti, D.; Trusolino, L., *EMBO Mol. Med.* **2011**, *3*, 623-636.
43. Schlessinger, J., *Cold Spring Harbor Perspect. Biol.* **2014**, *6*, a008912.
44. Yarden, Y.; Pines, G., *Nat. Rev. Cancer* **2012**, *12*, 553-563.
45. Burgess, A. W., *Growth Factors* **2008**, *26*, 263-274.
46. Normanno, N.; De Luca, A.; Bianco, C.; Strizzi, L.; Mancino, M.; Maiello, M. R.; Carotenuto, A.; De Feo, G.; Caponigro, F.; Salomon, D. S., *Gene* **2006**, *366*, 2-16.
47. Roskoski, R., Jr., *Pharmacol Res* **2014**, *79*, 34-74.
48. Holbro, T.; Hynes, N. E., *Annu. Rev. Pharmacol. Toxicol.* **2004**, *44*, 195-217.
49. Shi, F.; Telesco, S. E.; Liu, Y.; Radhakrishnan, R.; Lemmon, M. A., *Proc. Natl. Acad. Sci. U.S.A.* **2010**, *107*, 7692-7697.
50. Harris, R. C.; Chung, E.; Coffey, R. J., *Exp. Cell. Res.* **2003**, *284*, 2-13.
51. Schneider, M. R.; Wolf, E., *J. Cell Physiol.* **2009**, *218*, 460-466.
52. Ullrich, A.; Schlessinger, J., *Cell* **1990**, *61*, 203-212.
53. Schlessinger, J., *Cell* **2000**, *103*, 211-225.
54. Lemmon, M. A.; Schlessinger, J., *Cell* **2010**, *141*, 1117-1134.
55. Lemmon, M. A.; Schlessinger, J.; Ferguson, K. M., *Cold Spring Harbor Perspect. Biol.* **2014**, *6*, a020768.
56. Bessman, N. J.; Freed, D. M.; Lemmon, M. A., *Curr. Opin. Struct. Biol.* **2014**, *29*, 95-101.
57. Kovacs, E.; Zorn, J. A.; Huang, Y.; Barros, T.; Kuriyan, J., *Annu. Rev. Biochem.* **2015**, *84*, 739-764.
58. Ferguson, K. M.; Berger, M. B.; Mendrola, J. M.; Cho, H.-S.; Leahy, D. J.; Lemmon, M. A., *Mol. Cell* **2003**, *11*, 507-517.
59. Burgess, A. W.; Cho, H.-S.; Eigenbrot, C.; Ferguson, K. M.; Garrett, T. P. J.; Leahy, D. J.; Lemmon, M. A.; Sliwkowski, M. X.; Ward, C. W.; Yokoyama, S., *Mol. Cell* **2003**, *12*, 541-552.
60. Cho, H.-S.; Leahy, D. J., *Science* **2002**, *297*, 1330-1333.
61. Bouyain, S.; Longo, P. A.; Li, S.; Ferguson, K. M.; Leahy, D. J., *Proc. Natl. Acad. Sci. USA* **2005**, *102*, 15024-15029.
62. Garrett, T. P. J.; McKern, N. M.; Lou, M.; Elleman, T. C.; Adams, T. E.; Lovrecz, G. O.; Kofler, M.; Jorissen, R. N.; Nice, E. C.; Burgess, A. W.; Ward, C. W., *Mol. Cell* **2003**, *11*, 495-505.
63. Zhang, X.; Gureasko, J.; Shen, K.; Cole, P. A.; Kuriyan, J., *Cell* **2006**, *125*, 1137-1149.
64. Endres, N. F.; Das, R.; Smith, A. W.; Arkhipov, A.; Kovacs, E.; Huang, Y.; Pelton, J. G.; Shan, Y.; Shaw, D. E.; Wemmer, D. E.; Groves, J. T.; Kuriyan, J., *Cell* **2013**, *152*, 543-556.
65. Arkhipov, A.; Shan, Y.; Das, R.; Endres, N. F.; Eastwood, M. P.; Wemmer, D. E.; Kuriyan, J.; Shaw, D. E., *Cell* **2013**, *152*, 557-569.

66. Ogiso, H.; Ishitani, R.; Nureki, O.; Fukai, S.; Yamanaka, M.; Kim, J.-H.; Saito, K.; Sakamoto, A.; Inoue, M.; Shirouzu, M.; Yokoyama, S., *Cell* **2002**, *110*, 775-787.
67. Garrett, T. P. J.; McKern, N. M.; Lou, M.; Elleman, T. C.; Adams, T. E.; Lovrecz, G. O.; Zhu, H.-J.; Walker, F.; Frenkel, M. J.; Hoyne, P. A.; Jorissen, R. N.; Nice, E. C.; Burgess, A. W.; Ward, C. W., *Cell* **2002**, *110*, 763-773.
68. Lemmon, M. A., *Exp. Cell Res.* **2009**, *315*, 638-648.
69. Matsushita, C.; Tamagaki, H.; Miyazawa, Y.; Aimoto, S.; Smith, S. O.; Sato, T., *Proc. Natl. Acad. Sci. U.S.A.* **2012**, *110*, 1646-1651.
70. Qiu, C.; Tarrant, M. K.; Choi, S. H.; Sathyamurthy, A.; Bose, R.; Banjade, S.; Pal, A.; Bornmann, W. G.; Lemmon, M. A.; Cole, P. A.; Leahy, D. J., *Structure* **2008**, *16*, 460-467.
71. Jura, N.; Shan, Y.; Cao, X.; Shaw, D. E.; Kuriyan, J., *Proc. Natl. Acad. Sci. U.S.A.* **2009**, *106*, 21608-21613.
72. Jura, N.; Endres, N. F.; Engel, K.; Deindl, S.; Das, R.; Lamers, M. H.; Wemmer, D. E.; Zhang, X.; Kuriyan, J., *Cell* **2009**, *137*, 1293-1307.
73. Red Brewer, M.; Choi, S. H.; Alvarado, D.; Moravcevic, K.; Pozzi, A.; Lemmon, M. A.; Carpenter, G., *Mol. Cell* **2009**, *34*, 641-651.
74. Thiel, K. W.; Carpenter, G., *Proc. Natl. Acad. Sci. U.S.A.* **2007**, *104*, 19238-19243.
75. Gajiwala, K. S., *Protein Sci.* **2013**, *22*, 995-999.
76. Kovacs, E.; Das, R.; Wang, Q.; Collier, T. S.; Cantor, A.; Huang, Y.; Wong, K.; Mirza, A.; Barros, T.; Grob, P.; Jura, N.; Bose, R.; Kuriyan, J., *Mol Cell Biol* **2015**, *35*, 3083-3102.
77. Sebastian, S.; Settleman, J.; Reshkin, S. J.; Azzariti, A.; Bellizzi, A.; Paradiso, A., *Biochim. Biophys. Acta* **2006**, *1766*, 120-139.
78. Arteaga, C. L.; Engelman, J. A., *Cancer Cell* **2014**, *25*, 282-303.
79. Reardon, D. A.; Wen, P. Y.; Mellinghoff, I. K., *Neuro. Oncol.* **2014**, *16 Suppl 8*, viii7-viii13.
80. Schlessinger, J.; Lemmon, M. A., *Sci. Signaling* **2003**, *2003*, Re12.
81. Pawson, T., *Cell* **2004**, *116*, 191-203.
82. Morandell, S.; Stasyk, T.; Skvortsov, S.; Ascher, S.; Huber, L. A., *Proteomics* **2008**, *8*, 4383-4401.
83. Wilson, K. J.; Gilmore, J. L.; Foley, J.; Lemmon, M. A.; Riese, D. J., 2nd, *Pharmacol. Ther.* **2009**, *122*, 1-8.
84. Henson, E. S.; Gibson, S. B., *Cell Signal* **2006**, *18*, 2089-2097.
85. Jorissen, R.; Walker, F.; Pouliot, N.; Garrett, T. P. J.; Ward, C. W.; Burgess, A. W., *Exp. Cell. Res.* **2003**, *284*, 31-53.
86. Yarden, Y.; Sliwkowski, M. X., *Nat. Rev. Mol. Cell. Biol.* **2001**, *2*, 127-137.
87. Oda, K.; Matsuoka, Y.; Funahashi, A.; Kitano, H., *Mol. Syst. Biol.* **2005**, *1*, 2005.0010.
88. Citri, A.; Yarden, Y., *Nat. Rev. Mol. Cell. Biol.* **2006**, *7*, 505-516.
89. Freeman, M., *Nature* **2000**, *408*, 313-319.
90. Avraham, R.; Yarden, Y., *Nat. Rev. Mol. Cell Biol.* **2011**, *12*, 104-117.
91. Volinsky, N.; Kholodenko, B. N., *Cold Spring Harb. Perspect. Biol.* **2013**, *5*, a009043.
92. Sorkin, A.; Goh, L. K., *Exp. Cell. Res.* **2009**, *315*, 683-696.
93. Zwang, Y.; Yarden, Y., *Traffic* **2009**, *10*, 349-363.
94. Dougherty, M. K.; Muller, J.; Ritt, D. A.; Zhou, M.; Zhou, X. Z.; Copeland, T. D.; Conrads, T. P.; Veenstra, T. D.; Lu, K. P.; Morrison, D. K., *Mol. Cell* **2005**, *17*, 215-224.
95. Schulze, A.; Lehmann, K.; Jefferies, H. B. J.; McMahon, M.; Downward, J., *Genes Dev.* **2001**, *15*, 981-994.
96. Mason, J. M.; Morrison, D. J.; Basson, M. A.; Licht, J. D., *Trends Cell Biol.* **2006**, *16*, 45-54.



97. Gur, G.; Rubin, C.; Katz, M.; Amit, I.; Citri, A.; Nilsson, J.; Amariglio, N.; Henriksson, R.; Rechavi, G.; Hedman, H.; Wides, R.; Yarden, Y., *EMBO J.* **2004**, *23*, 3270-3281.
98. Anastasi, S.; Fiorentino, L.; Fiorini, M.; Fraioli, R.; Sala, G.; Castellani, L.; Alema, S.; Alimandi, M.; Segatto, O., *Oncogene* **2003**, *22*, 4221-4234.
99. Gotoh, N., *Int. J. Biochem. Cell Biol.* **2009**, *41*, 511-515.
100. Olayioye, M.; Neve, R. M.; Lane, H. A.; Hynes, N. E., *EMBO J.* **2000**, *19*, 3159-3167.
101. Kholodenko, B. N., *Nat. Rev. Mol. Cell Biol.* **2006**, *7*, 165-176.
102. Kholodenko, B. N.; Hancock, J. F.; Kolch, W., *Nat. Rev. Mol. Cell Biol.* **2010**, *11*, 414-426.
103. Marshall, C. J., *Cell* **1995**, *80*, 179-185.
104. Santos, S. D.; Verveer, P. J.; Bastiaens, P. I., *Nat. Cell Biol.* **2007**, *9*, 324-330.
105. von Kriegsheim, A.; Baiocchi, D.; Birtwistle, M.; Sumpton, D.; Bienvenut, W.; Morrice, N.; Yamada, K.; Lamond, A.; Kalna, G.; Orton, R.; Gilbert, D.; Kolch, W., *Nat. Cell Biol.* **2009**, *11*, 1458-1464.
106. Bennett, H. L.; Brummer, T.; Timpson, P.; Patterson, K. I.; Daly, R. J., Signaling by the EGF receptor in human cancers: accentuate the positive, eliminate the negative. . In *Cancer Drug Discovery and Development: EGFR Signaling Networks in Cancer Therapy*, 1st ed.; Haley, J. D.; Gullick, W. J., Eds. Humana Press: 2008.
107. Giancotti, F. G., *FEBS Lett.* **2014**, *588*, 2558-2570.
108. Lynch, T. J.; Bell, D. W.; Sordella, R.; Gurubhagavatula, S.; Okimoto, R. A.; Brannigan, B. W.; Harris, P. L.; Haserlat, S. M.; Supko, J. G.; Haluska, F. G.; Louis, D. N.; Christiani, D. C.; Settleman, J. E.; Haber, D. A., *N. Engl. J. Med.* **2004**, *350*, 2129-2139.
109. Red Brewer, M.; Yun, C. H.; Lai, D.; Lemmon, M. A.; Eck, M. J.; Pao, W., *Proc. Natl. Acad. Sci. U.S.A.* **2013**, *110*, E3595-E3604.
110. Shtiegman, K.; Kochupurakkal, B. S.; Zwang, Y.; Pines, G.; Starr, A.; Vexler, A.; Citri, A.; Katz, M.; Lavi, S.; Ben-Basat, Y.; Benjamin, S.; Corso, S.; Gan, J.; Yosef, R. B.; Giordano, S.; Yarden, Y., *Oncogene* **2007**, *26*, 6968-6978.
111. Klinger, B.; Bluthgen, N., *Biochem. Soc. Trans.* **2014**, *42*, 770-775.
112. Hopkins, A. L., *Nat. Chem. Biol.* **2008**, *4*, 682-690.
113. Csermely, P.; Korcsmaros, T.; Kiss, H. J.; London, G.; Nussinov, R., *Pharmacol. Ther.* **2013**, *138*, 333-408.
114. Dorel, M.; Barillot, E.; Zinovyev, A.; Kuperstein, I., *Biochem. Biophys. Res. Commun.* **2015**, *464*, 386-391.
115. Davis, M. I.; Hunt, J. P.; Herrgard, S.; Ciceri, P.; Wodicka, L. M.; Pallares, G.; Hocker, M.; Treiber, D. K.; Zarrinkar, P. P., *Nat. Biotechnol.* **2011**, *29*, 1046-1051.
116. Roskoski, R., Jr., *Pharmacol Res* **2014**, *87*, 42-59.
117. Rewcastle, G. W.; Denny, W. A.; Bridges, A. J.; Zhou, H.; Cody, D. R.; McMichael, A.; Fry, D. W., *J. Med. Chem.* **1995**, *38*, 3482-3487.
118. Barker, A. J.; Gibson, K. H.; Grundy, W.; Godfrey, A. A. B.; Jeffrey J. ; Healy, M. P.; Woodburn, J. R.; Ashton, S. E.; Curry, B. J.; Scarlett, L.; Henthorn, L.; Richards, L., *Bioorg. Med. Chem. Lett.* **2001**, *11*, 1911-1914.
119. Johnson, L. N., *Q. Rev. Biophys.* **2009**, *42*, 1-40.
120. Stamos, J.; Sliwkowski, M. X.; Eigenbrot, C., *J. Biol. Chem.* **2002**, *277*, 46265-46272.
121. Wood, E. R.; Truesdale, A. T.; McDonald, O. B.; Yuan, D.; Hassell, A.; Dickerson, S. H.; Ellis, B.; Pennisi, C.; Horne, E.; Lackey, K.; Alligood, K. J.; Rusnak, D. W.; Gilmer, T. M.; Shewchuk, L., *Cancer Res* **2004**, *64*, 6652-6659.
122. Yun, C. H.; Boggon, T. J.; Li, Y.; Woo, M. S.; Greulich, H.; Meyerson, M.; Eck, M. J., *Cancer Cell* **2007**, *11*, 217-27.
123. Eck, M. J.; Yun, C. H., *Biochim. Biophys. Acta* **2010**, *1804*, 559-566.

124. Perez, R.; Crombet, T.; de Leon, J.; Moreno, E., *Front Pharmacol* **2013**, *4*, 53.
125. Holohan, C.; Van Schaeybroeck, S.; Longley, D. B.; Johnston, P. G., *Nat. Rev. Cancer* **2013**, *13*, 714-726.
126. Pao, W.; Miller, V. A.; Politi, K. A.; Riely, G. J.; Somwar, R.; Zakowski, M. F.; Kris, M. G.; Varmus, H., *PLoS Med.* **2005**, *2*, e73.
127. Kobayashi, S.; Boggon, T. J.; Dayaram, T.; Janne, P. A.; Kocher, O.; Meyerson, M.; Johnson, B. E.; Eck, M. J.; Tenen, D. G.; Halmos, B., *N. Engl. J. Med.* **2005**, *352*, 786-792.
128. Yun, C. H.; Mengwasser, K. E.; Toms, A. V.; Woo, M. S.; Greulich, H.; Wong, K. K.; Meyerson, M.; Eck, M. J., *Proc. Natl. Acad. Sci. U.S.A.* **2008**, *105*, 2070-2075.
129. Yoshikawa, S.; Kukimoto-Niino, M.; Parker, L.; Handa, N.; Terada, T.; Fujimoto, T.; Terazawa, Y.; Wakiyama, M.; Sato, M.; Sano, S.; Kobayashi, T.; Tanaka, T.; Chen, L.; Liu, Z. J.; Wang, B. C.; Shirouzu, M.; Kawa, S.; Semba, K.; Yamamoto, T.; Yokoyama, S., *Oncogene* **2013**, *32*, 27-38.
130. Yu, H. A.; Riely, G. J., *J. Natl. Compr. Canc. Netw.* **2013**, *11*.
131. Nelson, V.; Ziehr, J.; Agulnik, M.; Johnson, M., *Onco. Targets Ther.* **2013**, *6*, 135-143.
132. Keating, G. M., *Drugs* **2014**, *74*, 207-221.
133. Steuer, C. E.; Khuri, F. R.; Ramalingam, S. S., *Cancer* **2015**, *121*, E1-6.
134. Niederst, M. J.; Engelman, J. A., *Sci. Signaling* **2013**, *6*, re6.
135. Engelman, J. A.; Zejnullahu, K.; Mitsudomi, T.; Song, Y.; Hyland, C.; Park, J. O.; Lindeman, N.; Gale, C. M.; Zhao, X.; Christensen, J.; Kosaka, T.; Holmes, A. J.; Rogers, A. M.; F, C.; Mok, T.; Lee, C.; Johnson, B. E.; Cantley, L., C.; Janne, P. A., *Science* **2007**, *316*, 1039-1043.
136. Bean, J.; Brennan, C.; Shih, J. Y.; Riely, G.; Viale, A.; Wang, L.; Chitale, D.; Motoi, N.; Szoke, J.; Broderick, S.; Balak, M.; Chang, W. C.; Yu, C. J.; Gazdar, A.; Pass, H.; Rusch, V.; Gerald, W.; Huang, S. F.; Yang, P. C.; Miller, V.; Ladanyi, M.; Yang, C. H.; Pao, W., *Proc. Natl. Acad. Sci. USA* **2007**, *104*, 20932-20937.
137. Yano, S.; Wang, W.; Li, Q.; Matsumoto, K.; Sakurama, H.; Nakamura, T.; Ogino, H.; Kakiuchi, S.; Hanibuchi, M.; Nishioka, Y.; Uehara, H.; Mitsudomi, T.; Yatabe, Y.; Nakamura, T.; Sone, S., *Cancer Res.* **2008**, *68*, 9479-9487.
138. Turke, A. B.; Zejnullahu, K.; Wu, Y. L.; Song, Y.; Dias-Santagata, D.; Lifshits, E.; Toschi, L.; Rogers, A.; Mok, T.; Sequist, L.; Lindeman, N. I.; Murphy, C.; Akhavanfard, S.; Yeap, B. Y.; Xiao, Y.; Capelletti, M.; Iafrate, A. J.; Lee, C.; Christensen, J. G.; Engelman, J. A.; Janne, P. A., *Cancer Cell* **2010**, *17*, 77-88.
139. Yonesaka, K.; Zejnullahu, K.; Okamoto, I.; Satoh, T.; Cappuzzo, F.; Souglakos, J.; Ercan, D.; Rogers, A.; Roncalli, M.; Takeda, M.; Fujisaka, Y.; Philips, J.; Shimizu, T.; Maenishi, O.; Cho, Y.; Sun, J.; Destro, A.; Taira, K.; Takeda, K.; Okabe, T.; Swanson, J.; Itoh, H.; Takada, M.; Lifshits, E.; Okuno, K.; Engelman, J. A.; Shivdasani, R. A.; Nishio, K.; Fukuoka, M.; Varella-Garcia, M.; Nakagawa, K.; Janne, P. A., *Sci. Transl. Med.* **2011**, *3*, 99ra86.
140. Guix, M.; Faber, A. C.; Wang, S. E.; Olivares, M. G.; Song, Y.; Qu, S.; Rinehart, C.; Seidel, B.; Yee, D.; Arteaga, C. L.; Engelman, J. A., *J. Clin. Invest.* **2008**, *118*, 2609-2619.
141. Cortot, A. B.; Repellin, C. E.; Shimamura, T.; Capelletti, M.; Zejnullahu, K.; Ercan, D.; Christensen, J. G.; Wong, K. K.; Gray, N. S.; Janne, P. A., *Cancer Res.* **2013**, *73*, 834-843.
142. Zhang, Z.; Lee, J. C.; Lin, L.; Olivas, V.; Au, V.; LaFramboise, T.; Abdel-Rahman, M.; Wang, X.; Levine, A. D.; Rho, J. K.; Choi, Y. J.; Choi, C. M.; Kim, S. W.; Jang, S. J.; Park, Y. S.; Kim, W. S.; Lee, D. H.; Lee, J. S.; Miller, V. A.; Arcila, M.; Ladanyi, M.; Moonsamy, P.; Sawyers, C.; Boggon, T. J.; Ma, P. C.; Costa, C.; Taron, M.; Rosell, R.; Halmos, B.; Bivona, T. G., *Nat. Genet.* **2012**, *44*, 852-860.
143. Meyer, A. S.; Miller, M. A.; Gertler, F. B.; Lauffenburger, D. A., *Sci. Signal.* **2013**, *6*, ra66.

144. Sequist, L. V.; Waltman, B. A.; Dias-Santagata, D.; Digumarthy, S.; Turke, A. B.; Fidias, P.; Bergethon, K.; Shaw, A. T.; Gettinger, S.; Cosper, A. K.; Akhavanfard, S.; Heist, R. S.; Temel, J.; Christensen, J. G.; Wain, J. C.; Lynch, T. J.; Vernovsky, K.; Mark, E. J.; Lanuti, M.; Lafrate, A. J.; Mino-Kenudson, M.; Engelman, J. A., *Sci. Transl. Med.* **2011**, *3*, 75ra26.
145. Sos, M. L.; Koker, M.; Weir, B. A.; Heynck, S.; Rabinovsky, R.; Zander, T.; Seeger, J. M.; Weiss, J.; Fischer, F.; Frommolt, P.; Michel, K.; Peifer, M.; Mermel, C.; Girard, L.; Peyton, M.; Gazdar, A. F.; Minna, J. D.; Garraway, L. A.; Kashkar, H.; Pao, W.; Meyerson, M.; Thomas, R. K., *Cancer Res.* **2009**, *69*, 3256-3261.
146. Ohashi, K.; Sequist, L. V.; Arcila, M. E.; Moran, T.; Chmielecki, J.; Lin, Y. L.; Pan, Y.; Wang, L.; de Stanchina, E.; Shien, K.; Aoe, K.; Toyooka, S.; Kiura, K.; Fernandez-Cuesta, L.; Fidias, P.; Yang, J. C.; Miller, V. A.; Riely, G. J.; Kris, M. G.; Engelman, J. A.; Vnencak-Jones, C. L.; Dias-Santagata, D.; Ladanyi, M.; Pao, W., *Proc. Natl. Acad. Sci. U.S.A.* **2012**, *109*, E2127-E2133.
147. Ercan, D.; Xu, C.; Yanagita, M.; Monast, C. S.; Pratilas, C. A.; Montero, J.; Butaney, M.; Shimamura, T.; Sholl, L.; Ivanova, E. V.; Tadi, M.; Rogers, A.; Repellin, C.; Capelletti, M.; Maertens, O.; Goetz, E. M.; Letai, A.; Garraway, L. A.; Lazzara, M. J.; Rosen, N.; Gray, N. S.; Wong, K. K.; Janne, P. A., *Cancer Discov.* **2012**, *2*, 934-947.
148. Misale, S.; Yaeger, R.; Hobor, S.; Scala, E.; Janakiraman, M.; Liska, D.; Valtorta, E.; Schiavo, R.; Buscarino, M.; Siravegna, G.; Bencardino, K.; Cercek, A.; Chen, C. T.; Veronese, S.; Zanon, C.; Sartore-Bianchi, A.; Gambacorta, M.; Gallicchio, M.; Vakiani, E.; Boscaro, V.; Medico, E.; Weiser, M.; Siena, S.; Di Nicolantonio, F.; Solit, D.; Bardelli, A., *Nature* **2012**, *486*, 532-536.
149. Prahallad, A.; Sun, C.; Huang, S.; Di Nicolantonio, F.; Salazar, R.; Zecchin, D.; Beijersbergen, R. L.; Bardelli, A.; Bernards, R., *Nature* **2012**, *483*, 100-104.
150. Corcoran, R. B.; Ebi, H.; Turke, A. B.; Coffee, E. M.; Nishino, M.; Cogdill, A. P.; Brown, R. D.; Della Pelle, P.; Dias-Santagata, D.; Hung, K. E.; Flaherty, K. T.; Piris, A.; Wargo, J. A.; Settleman, J.; Mino-Kenudson, M.; Engelman, J. A., *Cancer Discov.* **2012**, *2*, 227-235.
151. Arrowsmith, C. H.; Audia, J. E.; Austin, C.; Baell, J.; Bennett, J.; Blagg, J.; Bountra, C.; Brennan, P. E.; Brown, P. J.; Bunnage, M. E.; Buser-Doepner, C.; Campbell, R. M.; Carter, A. J.; Cohen, P.; Copeland, R. A.; Cravatt, B.; Dahlin, J. L.; Dhanak, D.; Edwards, A. M.; Frye, S. V.; Gray, N.; Grimshaw, C. E.; Hepworth, D.; Howe, T.; Huber, K. V.; Jin, J.; Knapp, S.; Kotz, J. D.; Kruger, R. G.; Lowe, D.; Mader, M. M.; Marsden, B.; Mueller-Fahrnow, A.; Muller, S.; O'Hagan, R. C.; Overington, J. P.; Owen, D. R.; Rosenberg, S. H.; Roth, B.; Ross, R.; Schapira, M.; Schreiber, S. L.; Shoichet, B.; Sundstrom, M.; Superti-Furga, G.; Taunton, J.; Toledo-Sherman, L.; Walpole, C.; Walters, M. A.; Willson, T. M.; Workman, P.; Young, R. N.; Zuercher, W. J., *Nat. Chem. Biol.* **2015**, *11*, 536-541.
152. Alaimo, P. J.; Shogren-Knaak, M. A.; Shokat, K. M., *Curr. Opin. Cell Biol.* **2001**, *5*, 360-367.
153. Weiss, W. A.; Taylor, S. S.; Shokat, K. M., *Nat. Chem. Biol.* **2007**, *3*, 739-744.
154. Bunnage, M. E.; Chekler, E. L.; Jones, L. H., *Nat. Chem. Biol.* **2013**, *9*, 195-199.
155. Schreiber, S. L., *Chem. Eng. News* **2003**, *81*, 51-61.
156. Chan, J.; Dodani, S. C.; Chang, C. J., *Nat. Chem.* **2012**, *4*, 973-984.
157. Cravatt, B. F.; Wright, A. T.; Kozarich, J. W., *Annu. Rev. Biochem.* **2008**, *77*, 383-414.
158. Heal, W. P.; Dang, T. H.; Tate, E. W., *Chem. Soc. Rev.* **2011**, *40*, 246-257.
159. Jeffery, D. A.; Bogyo, M., *Curr. Opin. Biotechnol.* **2003**, *14*, 87-95.
160. Ziegler, S.; Pries, V.; Hedberg, C.; Waldmann, H., *Angew. Chem. Int. Ed. Engl.* **2013**, *52*, 2744-2792.
161. Sadaghiani, A. M.; Verhelst, S. H.; Bogyo, M., *Curr. Opin. Chem. Biol.* **2007**, *11*, 20-28.

162. Frye, S. V., *Nat. Chem. Biol.* **2010**, *6*, 159-161.
163. Workman, P.; Collins, I., *Chem. Biol.* **2010**, *17*, 561-577.
164. Cohen, P., *Biochem. J.* **2010**, *425*, 53-54.
165. Knapp, S.; Arruda, P.; Blagg, J.; Burley, S.; Drewry, D. H.; Edwards, A.; Fabbro, D.; Gillespie, P.; Gray, N. S.; Kuster, B.; Lackey, K. E.; Mazzafera, P.; Tomkinson, N. C.; Willson, T. M.; Workman, P.; Zuercher, W. J., *Nat. Chem. Biol.* **2013**, *9*, 3-6.
166. Garcia-Serna, R.; Mestres, J., *Drug Discov. Today* **2011**, *16*, 99-106.
167. Fischer, J. J.; Dalhoff, C.; Schrey, A. K.; Graebner, O. Y.; Michaelis, S.; Andrich, K.; Glinski, M.; Kroll, F.; Sefkow, M.; Dreger, M.; Koester, H., *J. Proteomics* **2011**, *75*, 160-168.
168. Shi, H.; Zhang, C. J.; Chen, G. Y.; Yao, S. Q., *J. Am. Chem. Soc.* **2012**, *134*, 3001-3014.
169. Ranjitkar, P.; Perera, B. G.; Swaney, D. L.; Hari, S. B.; Larson, E. T.; Krishnamurty, R.; Merritt, E. A.; Villen, J.; Maly, D. J., *J. Am. Chem. Soc.* **2012**, *134*, 19017-19025.
170. Cohen, M. S.; Hadjivassiliou, H.; Taunton, J., *Nat. Chem. Biol.* **2007**, *3*, 156-160.
171. Daub, H., *ACS Chem. Biol.* **2015**, *10*, 201-212.
172. Shreder, K.; Wong, M. S.; Nomanbhoy, T.; Leventhal, P. S.; Fuller, S. R., *Org. Lett.* **2004**, *6*, 3715-3718.
173. Boyce, J. P.; Brown, M. E.; Fitzner, J. N.; Kowski, T. J. Kinase-directed, activity-based probes. US 2007/0009977 A1, Jan 11 2007, 2007.
174. Blair, J. A.; Rauh, D.; Kung, C.; Yun, C. H.; Fan, Q. W.; Rode, H.; Zhang, C.; Eck, M. J.; Weiss, W. A.; Shokat, K. M., *Nat. Chem. Biol.* **2007**, *3*, 229-238.
175. Lanning, B. R.; Whitby, L. R.; Dix, M. M.; Douhan, J.; Gilbert, A. M.; Hett, E. C.; Johnson, T. O.; Joslyn, C.; Kath, J. C.; Niessen, S.; Roberts, L. R.; Schnute, M. E.; Wang, C.; Hulse, J. J.; Wei, B.; Whiteley, L. O.; Hayward, M. M.; Cravatt, B. F., *Nat. Chem. Biol.* **2014**, *10*, 760-767.
176. Barkovich, K. J.; Hariono, S.; Garske, A. L.; Zhang, J.; Blair, J. A.; Fan, Q. W.; Shokat, K. M.; Nicolaides, T.; Weiss, W. A., *Cancer Discov.* **2012**, *2*, 450-457.
177. Cai, X.; Zhai, H. X.; Wang, J.; Forrester, J.; Qu, H.; Yin, L.; Lai, C. J.; Bao, R.; Qian, C., *J. Med. Chem.* **2010**, *53*, 2000-9.
178. Fabian, M. A.; Biggs, W. H., 3rd; Treiber, D. K.; Atteridge, C. E.; Azimioara, M. D.; Benedetti, M. G.; Carter, T. A.; Ciceri, P.; Edeen, P. T.; Floyd, M.; Ford, J. M.; Galvin, M.; Gerlach, J. L.; Grotzfeld, R. M.; Herrgard, S.; Insko, D. E.; Insko, M. A.; Lai, A. G.; Lelias, J. M.; Mehta, S. A.; Milanov, Z. V.; Velasco, A. M.; Wodicka, L. M.; Patel, H. K.; Zarrinkar, P. P.; Lockhart, D. J., *Nat. Biotechnol.* **2005**, *23*, 329-336.
179. Leslie, B. J.; Hergenrother, P. J., *Chem. Soc. Rev.* **2008**, *37*, 1347-1360.
180. Khan, I.; Ibrar, A.; Ahmed, W.; Saeed, A., *Eur. J. Med. Chem.* **2015**, *90*, 124-169.
181. Szokol, B.; Gyulavari, P.; Kurko, I.; Baska, F.; Szantai-Kis, C.; Greff, Z.; Orfi, Z.; Petak, I.; Penzes, K.; Torka, R.; Ullrich, A.; Orfi, L.; Vantus, T.; Keri, G., *ACS Med. Chem. Lett.* **2014**, *5*, 298-303.
182. Rao, S.; Larroque-Lombard, A. L.; Peyrard, L.; Thauvin, C.; Rachid, Z.; Williams, C.; Jean-Claude, B. J., *PLoS One* **2015**, *10*, e0117215.
183. Crystal, A. S.; Shaw, A. T.; Sequist, L. V.; Friboulet, L.; Niederst, M. J.; Lockerman, E. L.; Frias, R. L.; Gainor, J. F.; Amzallag, A.; Greninger, P.; Lee, D.; Kalsy, A.; Gomez-Caraballo, M.; Elamine, L.; Howe, E.; Hur, W.; Awad, M. M.; Ramaswamy, S.; Mino-Kenudson, M.; Iafrate, A. J.; Benes, C. H.; Engelman, J. A., *Science* **2014**, *346*, 1480-1486.
184. Leto, S. M.; Sassi, F.; Catalano, I.; Torri, V.; Migliardi, G.; E.R., Z.; Throsby, M.; Bertotti, A.; Trusolino, L., *Clin. Cancer Res.* **2015**, In press.
185. Zambaldo, C.; Sadhu, K. K.; Karthikeyan, G.; Barluenga, S.; Daguer, J.-P.; Winssinger, N., *Chem. Sci.* **2013**, *4*, 2088-2092.
186. Liu, F.; Rijkers, D. T.; Post, H.; Heck, A. J., *Nat. Methods* **2015**, In press.

## APPENDICES

### Table of contents

Appendix A1	Full spectroscopic characterization of new compounds <b>1a–1c, 4c, 6c, 7a–7c</b> .	A2
Appendix A2	Curve images from KINOMEscan <sup>TM</sup> binding assays.	A11

## APPENDIX A1

Full spectroscopic characterization of new compounds **1a–1c**, **4c**, **6c**, **7a–7c**.

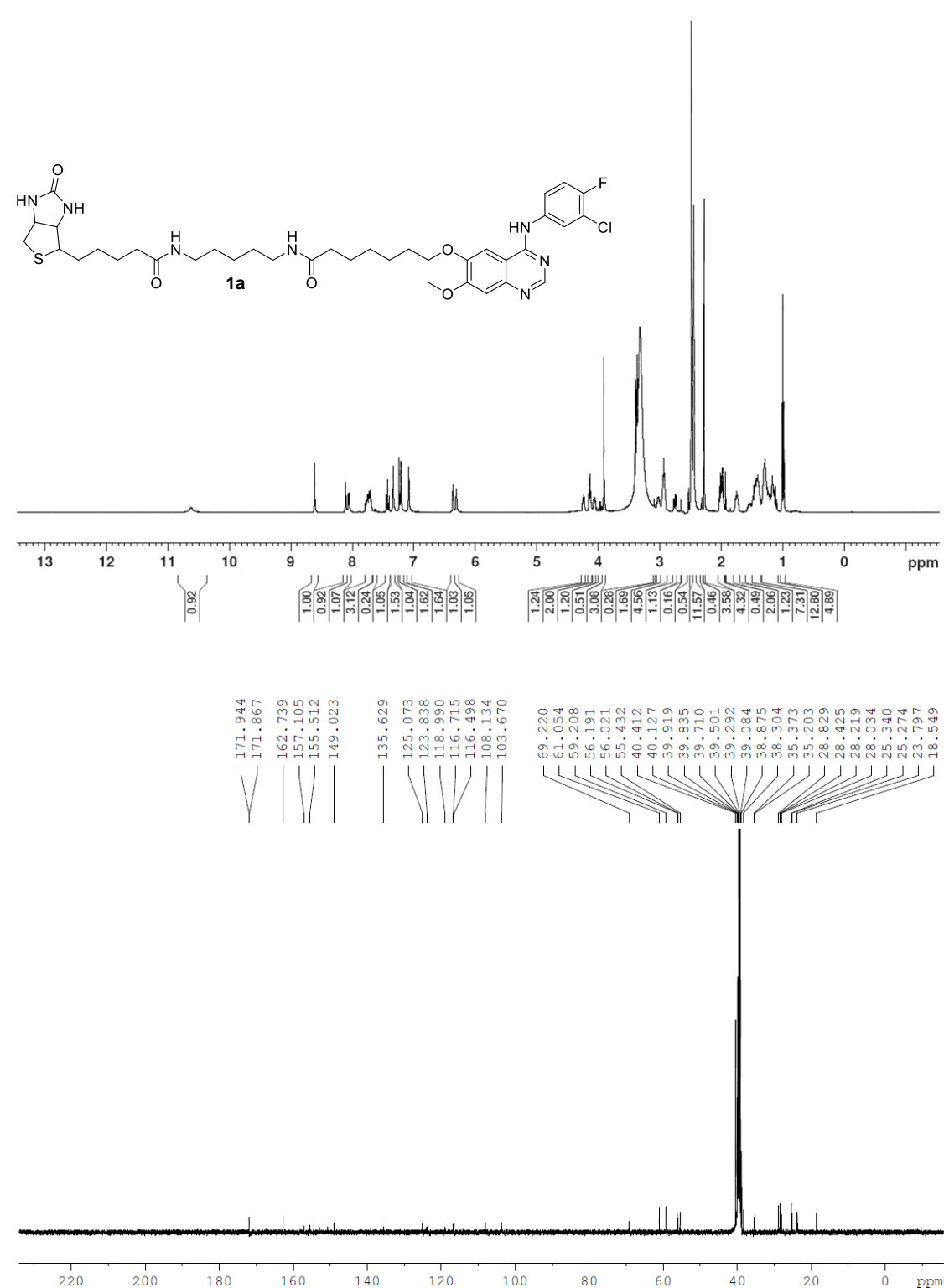


**Fig. A1.**  $^1\text{H}$  and  $^{13}\text{C}$  NMR spectra of probe **1a**.



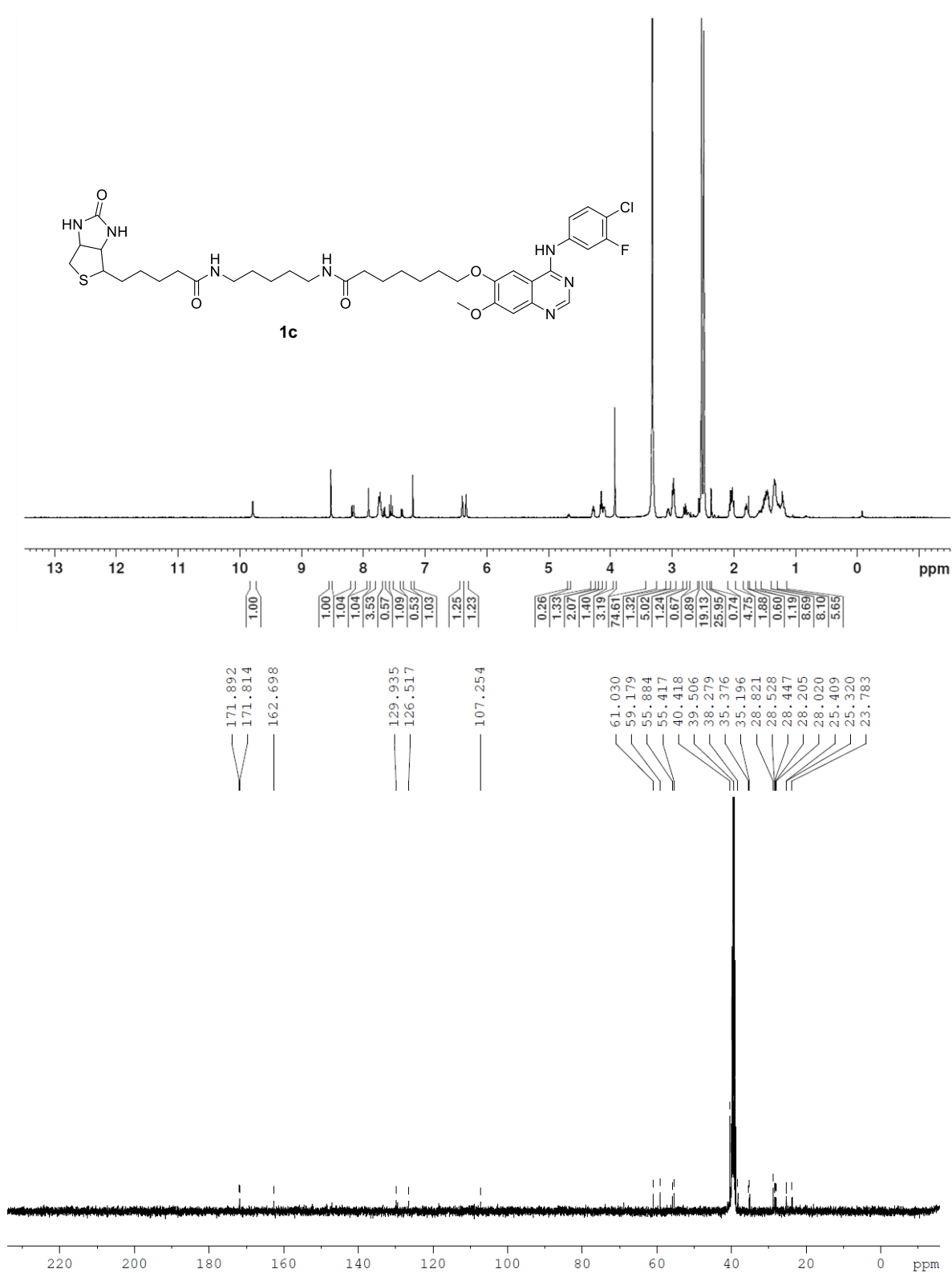


**Fig. A3.**  $^1\text{H}$  and  $^{13}\text{C}$  NMR spectra of probe **1c**.



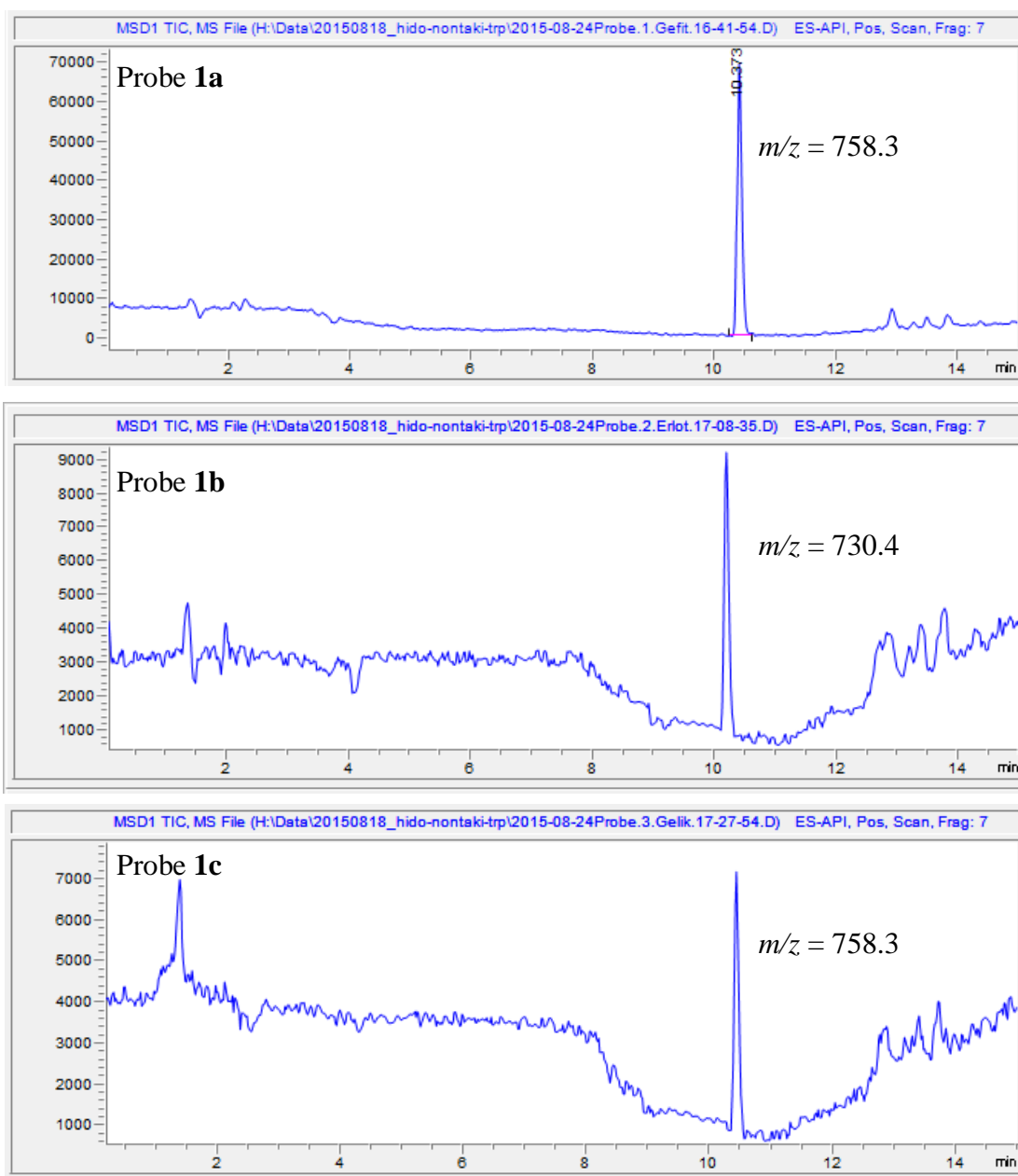


**Fig. A4.** Total Ion Chromatogram of probes **1a–1c**.

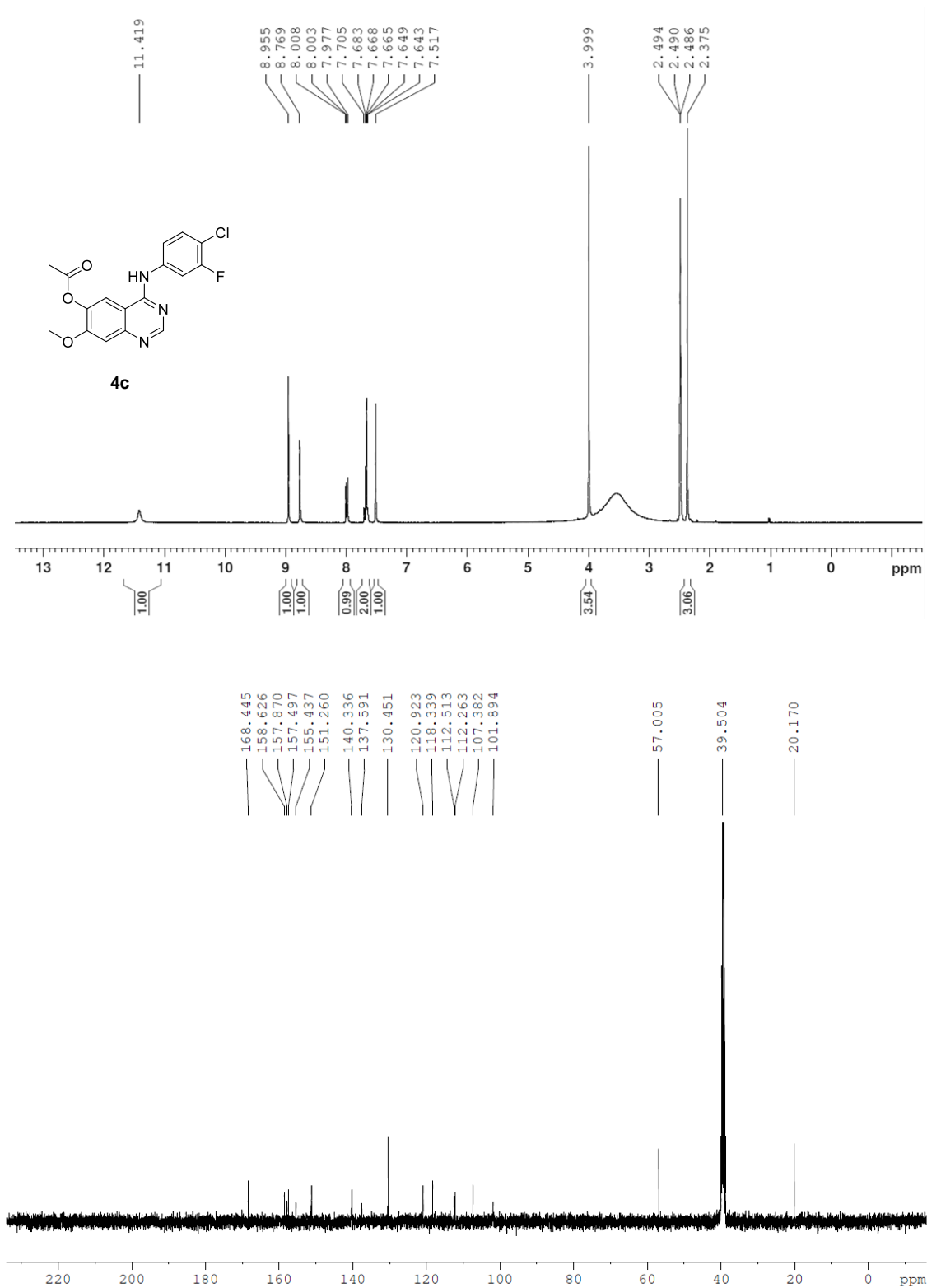


**Fig. A5.** <sup>1</sup>H and <sup>13</sup>C NMR spectra of compound **4c**.

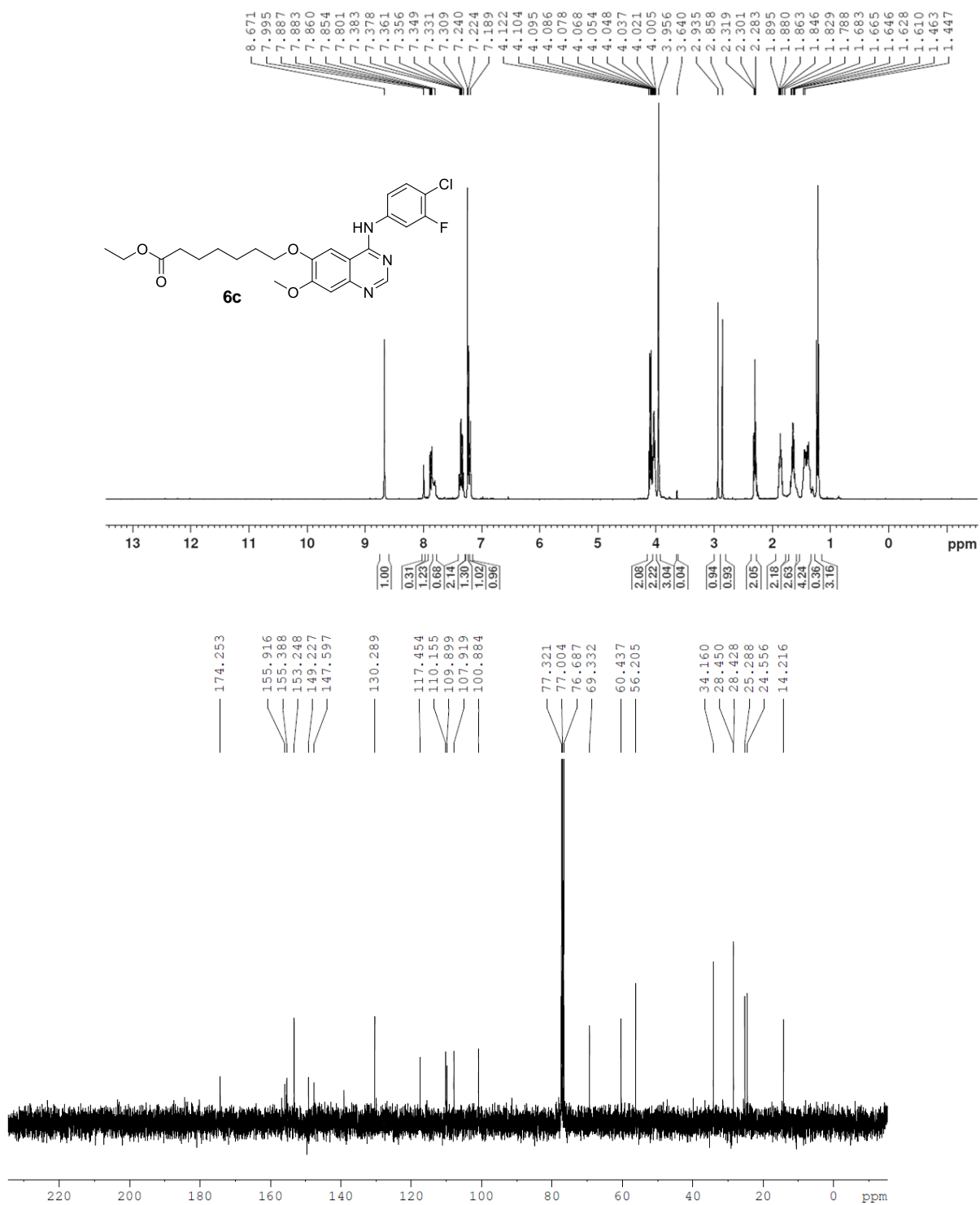


**Fig. A6.** <sup>1</sup>H and <sup>13</sup>C NMR spectra of compound **6c**.

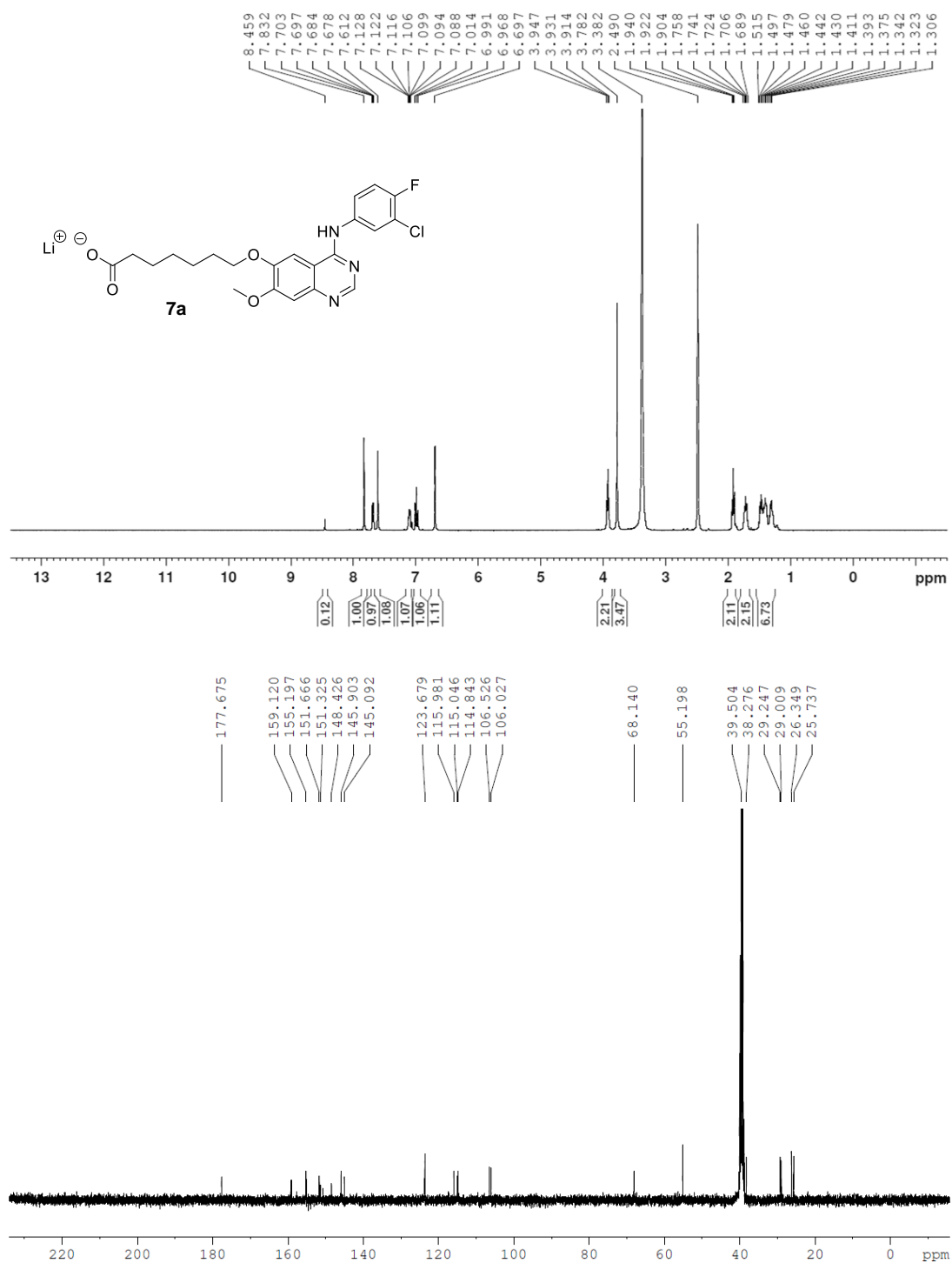


**Fig. A7.** <sup>1</sup>H and <sup>13</sup>C NMR spectra of compound **7a**.

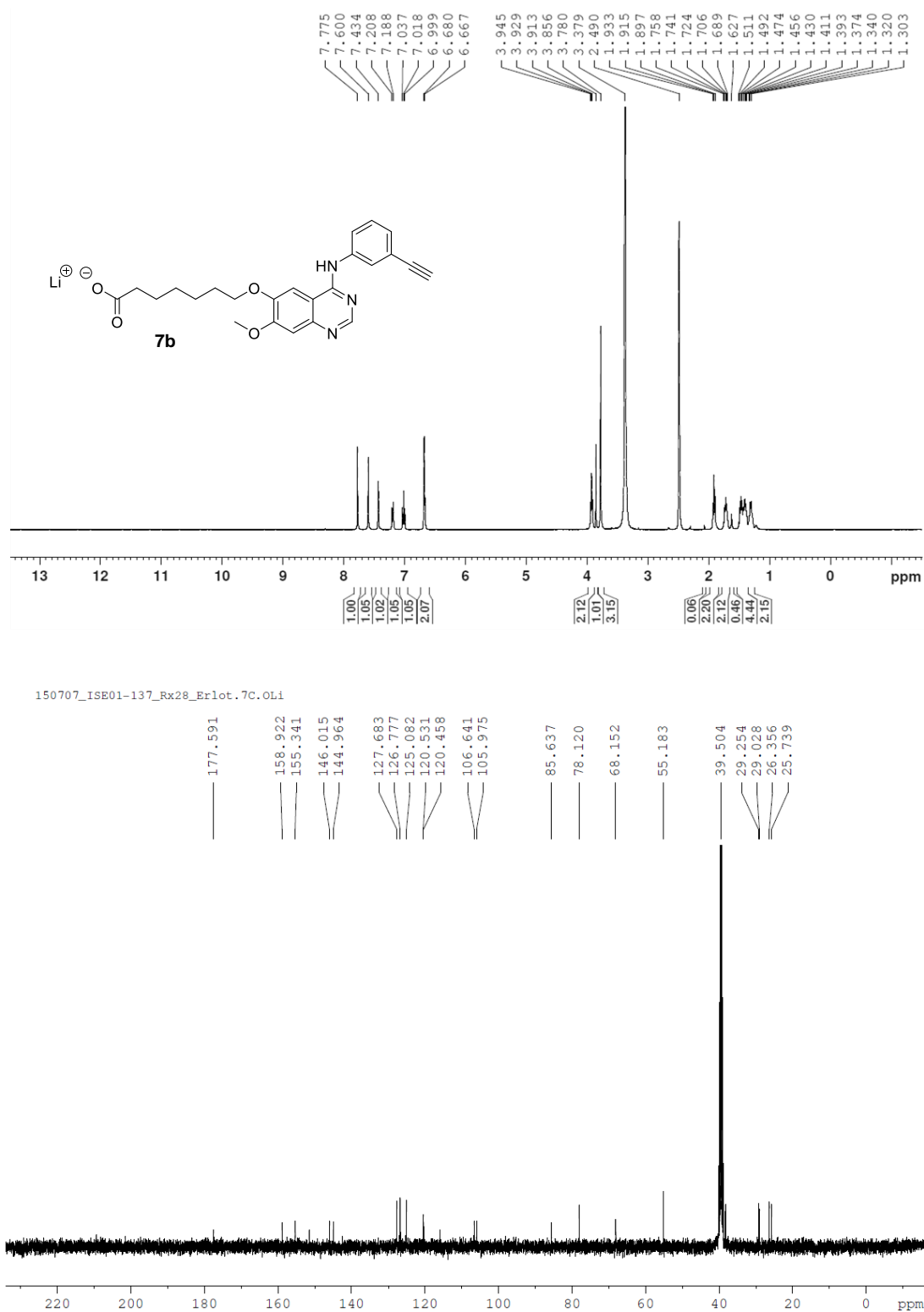


**Fig. A8.**  $^1\text{H}$  and  $^{13}\text{C}$  NMR spectra of compound **7b**.

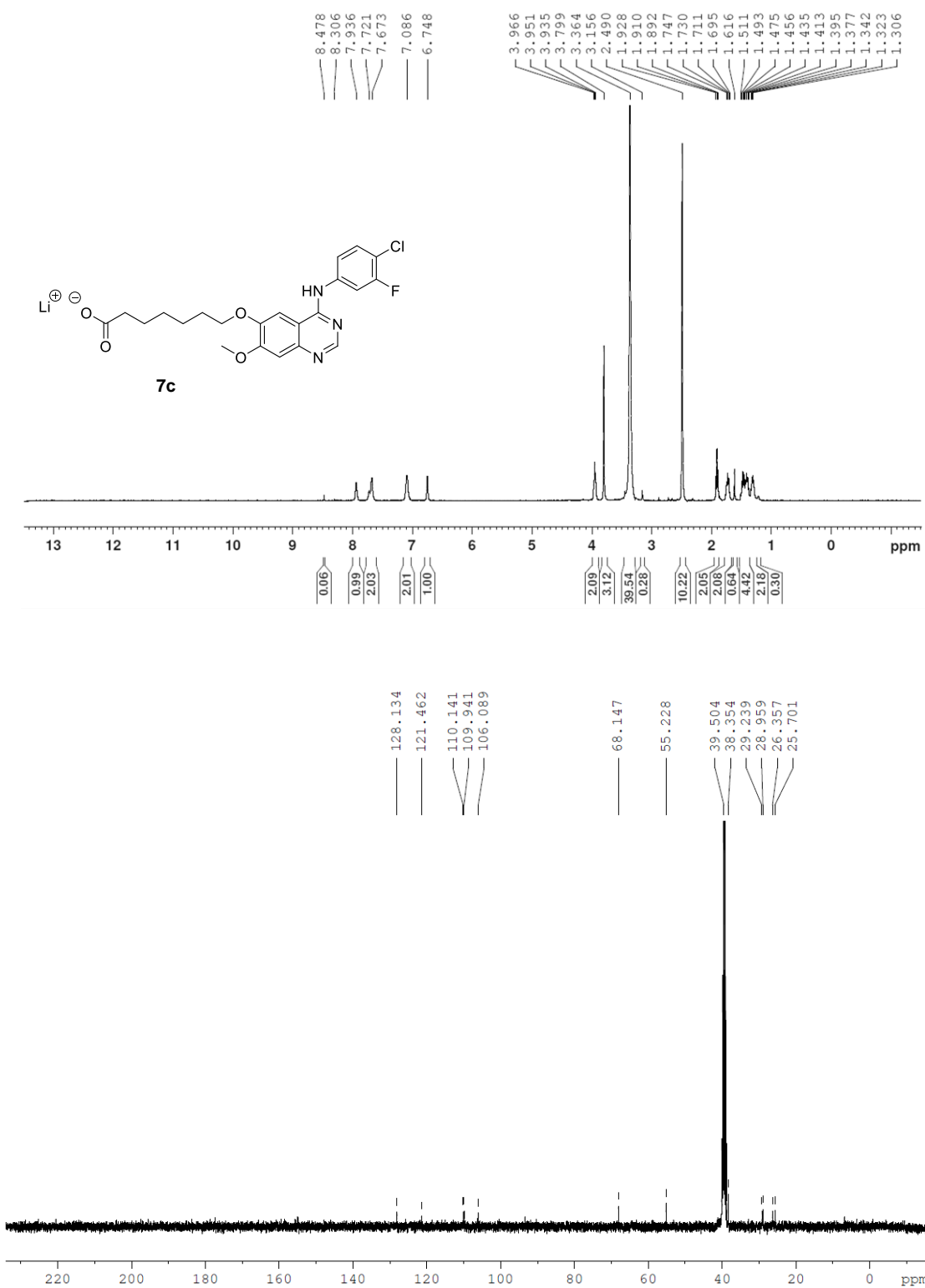


**Fig. A9.** <sup>1</sup>H and <sup>13</sup>C NMR spectra of compound **7c**.

## APPENDIX A2

Curve images from KINOMEscan™ binding assays.

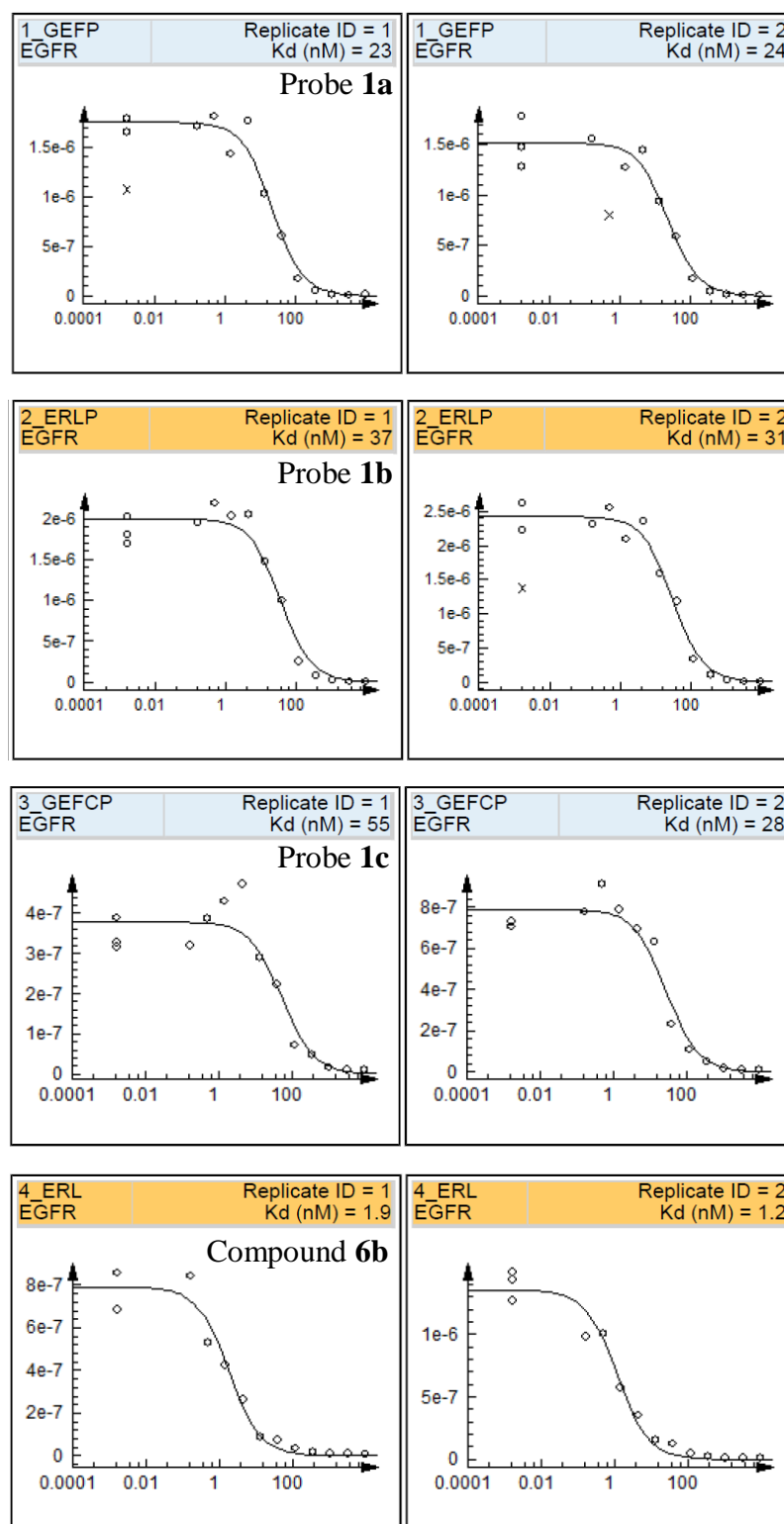


**Fig. A10.** Curve images from KINOMEscan™ binding assays.

The amount of EGFR measured by qPCR (signal; y-axis) is plotted against the corresponding compound concentration in nM in log10 scale (x-axis). Data points marked with an “x” were not used for  $K_d$  determination.